Biological response of *Chlorella vulgaris* to pulsed electric field treatment for improvement of protein extraction

Zur Erlangung des akademischen Grades einer

DOKTORIN DER NATURWISSENSCHAFTEN

(Dr. rer. nat.)

von der KIT-Fakultät für Chemie und Biowissenschaften

des Karlsruher Instituts für Technologie (KIT)

genehmigte

DISSERTATION

von

M. Sc. Damaris Krust

1. Referent: Prof. Dr. Peter Nick

2. Referent: Prof. Dr. Tilman Lamparter

Tag der mündlichen Prüfung: 27.04.2022

Die zentralen Teile dieser Arbeit wurden veröffentlicht:

Krust, Damaris; Gusbeth, Christian; Müller, Alexander S.K.; Scherer, Daniel; Müller, Georg; Frey, Wolfgang; Nick, Peter (2022): Biological signalling supports biotechnology – Pulsed electric fields extract a cell-death inducing factor from Chlorella vulgaris. In *Bioelectrochemistry* 143, p. 107991. Available online at https://doi.org/10.1016/j.bioelechem.2021.107991.

Akaberi, Sahar; **Krust, Damaris**; Müller, Georg; Frey, Wolfgang; Gusbeth, Christian (2020): Impact of incubation conditions on protein and C-Phycocyanin recovery from Arthrospira platensis post-pulsed electric field treatment. In *Bioresource technology* 306, p. 123099. Available online at https://doi.org/10.1016/j.biortech.2020.123099

Zusammenfassung

Angesichts des Klimawandels und einer stetig wachsenden Weltbevölkerung können Mikroalgen eine wichtige Rolle als nachhaltige Energie- und Nahrungsquelle der Zukunft spielen. Zur Extraktion wertvoller Inhalts- und Nährstoffe ist ein Zellaufschluss notwendig. Die Elektroimpulsbehandlung (EIB) bietet eine energieeffiziente und schonende Alternative im Vergleich zu mechanischen Zellaufschlussmethoden. Jedoch sind die biologischen Prozesse und zellulären Mechanismen hinter dem Zelltod nach EIB noch wenig untersucht. Aus diesem Grund wurden die einzellige grüne Mikroalge *Chlorella vulgaris* und das Cyanobakterium Spirulina als Modellorganismen verwendet, um die Wirkung von EIB auf biologische Zellen zu untersuchen. Dafür wurde eine Methode zur Überwachung der Viabilität nach EIB unter Verwendung von Fluoresceindiacetat (FDA) in *C. vulgaris* etabliert. Im Anschluss wurden die experimentellen EIB-Parameter so eingestellt, dass ein fixes Verhältnis von Zellen nach der Behandlung abstirbt, während der andere Teil überlebt. Mit diesen Werkzeugen war eine quantitative Analyse des Zelltodes nach EIB möglich. Basierend auf den Analyseergebnissen wurde die EIB-Extraktion von Proteinen und dem wertvollen blauen Farbstoff Phycocyanin aus Spirulina unter verschiedenen post-EIB Inkubationsbedingungen untersucht.

Zur Optimierung der Elektroextraktionseffizienz in Spirulina wurden die Einflüsse des pH des externen Mediums, der Biomassekonzentration, der Zellaggregation sowie der Energiereduktion untersucht. Das optimierte Elektroextraktionsprotokoll mit höherer Biomassekonzentration und geringerer Behandlungsenergie erfordert eine post-EIB-Inkubation unter kontrollierten Bedingungen (Raumtemperatur, pH 6 oder 8, homogene Suspension), die für die Freisetzung und Stabilität von Phycocyanin entscheidend sind. Mit diesem Wissen besteht eine mögliche biotechnologische Anwendung darin, schonende EIB mit niedrigstem Energieeintrag durchzuführen, was zu einer effizienten Protein- und Phycocyanin-Gewinnung führt.

An *C. vulgaris* konnte gezeigt werden, dass EIB mit niedrigem Energieeintrag auch als abiotisches Stresssignal wirken kann. Dies wurde sichtbar in Form einer gestörten Redox-Homöostase, bei der sowohl die Freisetzung von Wasserstoffperoxid als auch Lipidoxidation gemessen werden konnten. Die Hemmung von Prozessen, die mit dem programmierten Zelltod (PCD) zusammenhängen, zeigten, dass höchstwahrscheinlich Ca-Signalwege, Aktindynamik und Membranversteifung keine notwendige Rolle beim EIB-induzierten Zelltod spielen. Die Freisetzung von Cytochrom f konnte nur im Hochdruckhomogenisations (HPH) Extrakt und nicht nach EIB nachgewiesen werden. Zellsuspensionen mit hoher Zelldichte, die an der Überlebensschwelle gepulst wurden, zeigten nur eine langsame Manifestation des Zelltods. Dies führte zur Entdeckung

eines Zelltod-induzierenden Faktors (CDIF). Es konnte nachgewiesen werden, dass durch EIB und HPH-Behandlung der CDIF aus *C. vulgaris* extrahiert werden kann. Wasserlöslicher Extrakt, der diesen CDIF enthielt, führte zum Absterben von unbehandelten Mikroalgen (insbesondere nur bei *C. vulgaris*). Weitere Experimente zeigten die Entstehung des CDIF in der stationären Wachstumsphase, Hitzelabilität und Dosisabhängigkeit. Ebenso wie die Empfindlichkeit gegenüber direkter EIB hing die Empfindlichkeit der Empfängerzellen gegenüber dem CDIF vom Zellzyklusstadium ab. Untersuchungen zur Extraktionseffizienz von Proteinen aus *C. vulgaris* führten zu dem Ergebnis, dass die erforderliche spezifische Energie für maximalen Ertrag der zuvor bestimmten Behandlungsenergie an der Überlebensschwelle entspricht. Alle experimentellen Ergebnisse weisen darauf hin, dass der EIB-induzierte Zelltod und die damit verbundene hohe Extraktionseffizienz nicht nur auf rein physikalische Phänomene zurückzuführen sind, sondern einen biologischen Prozess beinhalten müssen. Das Arbeitsmodell bezüglich des CDIF beinhaltet, dass der Faktor aus zellwandabbauenden Enzymen wie Chitinasen besteht. EIB bei sehr geringem Energieeintrag wirkt als abiotisches Stresssignal. In Kombination mit einer beschädigten Zellintegrität aufgrund von Poren in der Zellmembran führen PCD-Prozesse zu einer enzymatischen Autolyse, bei der der CDIF (Chitinasen) freigesetzt wird. Die Zellwand wird durch den CDIF geschwächt. Wird der CDIF-haltige Extrakt unbehandelten Empfängerzellen zugesetzt, zeigt er zunächst über den Zellwandabbau eine äußere Wirkung. Nach Internalisierung kann der CDIF als internes Signal fungieren, das PCD auslöst.

Abstract

In the face of climate change and a constantly growing world population, microalgae can play a major role as future sustainable energy and food source. For the extraction of valuable components and nutrients, a cell disruption step is necessary. Pulsed electric field (PEF) treatment provides an energy-efficient and gentle alternative compared to mechanical cell disruption methods. However, biological processes and cellular mechanisms behind cell death are still poorly understood. For this purpose, the unicellular green microalgae *Chlorella vulgaris* and the cyanobacterium Spirulina were used as model organisms to investigate the effect of PEF treatment on a biological cell. A method was established to monitor cell viability after PEF treatment in *C. vulgaris* by using cell sorting based on fluorescein diacetate (FDA). Next, the experimental parameters of PEF treatment were calibrated to a point, where a set ratio of cells undergoes cell death after treatment while the other part stays viable. With these tools in hand, quantitative analysis of the cell death response to PEF treatment was possible. Furthermore, electroextraction of proteins and the valuable blue pigment C-phycocyanin from fresh Spirulina biomass was investigated under the influence of post-PEF incubation conditions.

For optimization of biotechnological electroextraction efficiency in Spirulina, the influences of pH of the external medium, biomass concentration, cell aggregation as well as lower energy input were studied. The optimized electroextraction protocol with higher biomass concentration and lower treatment energy requires post-PEF incubation at controlled conditions (room temperature, pH 6 or 8, homogenous suspension) that are crucial for C-phycocyanin liberation and stability. Taking advantage of this knowledge, a possible biotechnological application consists of administering gentle PEF treatment at the determined lowest specific energy resulting in efficient protein and C-phycocyanin recovery.

It could be shown that PEF treatment of *C. vulgaris* at lower energy input, while physically inflicting damage, could also act as an abiotic stress signal. This manifests in the form of a perturbed redox homeostasis, where both the release of hydrogen peroxide at the survival threshold as well as lipid oxidation at higher energies could be measured. When inhibiting various programmed cell death (PCD) connected processes, the results showed that most likely calcium signaling, actin remodeling and membrane rigidifying do not play necessary roles in PEF induced cell death. Cytochrome f release could only be verified in high-pressure homogenization (HPH) extract and not at various post-PEF conditions. The fact that high cell density suspensions pulsed at the survival threshold showed only slow manifestation of cell death led to the discovery of a cell-death inducing factor (CDIF). It could be verified that in response to PEF and HPH treatment, a CDIF can be extracted

from *C. vulgaris.* The water-soluble extract containing this CDIF caused recipient microalgae (specifically only *C. vulgaris*) to die, even though the recipient cells had not been subjected to direct PEF treatment. Further studies showed the generation of the CDIF in the stationary phase, heat-lability, and dose-dependency. Same as sensitivity to direct PEF treatment, the responsiveness of recipient cells to the CDIF depended on the cell cycle stage. When checking protein recovery efficiency in *C. vulgaris* for varied low energy inputs, the required specific energy for maximum yield was at the previously determined survival threshold. All experimental results point toward the assumption that cell death and extraction efficiency following PEF treatment cannot be a merely physical phenomenon but must involve a biological process. The working model regarding the CDIF proposes that the factor consists of cell wall degrading enzymes such as chitinases. PEF treatment at very low energy input acts as an abiotic stress signal. In combination with damaged cell integrity due to pores in the cell membrane, PCD processes result in enzymatic autolysis releasing the CDIF (chitinases). The cell wall is weakened due to the work of the CDIF. When the water-soluble extract containing CDIF is added to viable recipient cells, it first causes an external effect via cell wall degradation. Secondly, after internalization, the CDIF can act as an internal signal triggering PCD.

Abbreviations

BA	benzyl alcohol
BSA	bovine serum albumin
CDIF	cell-death inducing factor
CDW	cell dry weight
C-PC	phycocyanin obtained from cyanobacteria
CTRL	control
C.v. cont	*Chlorella vulgaris* cultivated under continuous light
C.v. syn	*Chlorella vulgaris* cultivated as a synchronized culture
cyt c	cytochrome c
cyt f	cytochrome f
DMSO	dimethylsulphoxide
dpi	days post inoculation
DPI	diphenyleneiodonium chloride
EF-Tu	elongation factor tu
ER	endoplasmatic reticulum
fw	fresh weight
FDA	fluorescein diacetate
GLV	green leave volatile
GRAS	generally recognized as safe
HPH	high-pressure homogenization
HR	hypersensitive response
Hsp	heat shock protein
IB	initial buffer
LatB	latrunculin B

MALDI-TOF	matrix assisted laser desorption/ionization, time-of-flight
MDA	malondialdehyde
MS	mass spectroscopy
MW	molecular weight
OD_{750}	optical density at 750 nm
PA	phosphatidic acid
PAR	photosynthetically active radiation
PBS	phosphate buffer saline
PC	phycocyanin
PCD	programmed cell death
PEF	pulsed electric field
PI	protease inhibitor
PLD	phospholipase D
Q_{10}	temperature coefficient
RboH	respiratory burst oxidase homologue
ROS	reactive oxygen species
R-PC	phycocyanin obtained from red algae
RuBisCO	ribulose-1,5-bisphosphate carboxylase oxygenase
SAG	Sammlung von Algenkulturen der Universität Göttingen
SDS-PAGE	sodium dodecyl sulfate polyacrylamide gel electrophoresis
SEC	size-exclusion chromatography
SN	supernatant
TAP	tris acetate phosphate

Physical variables

variable	unit	description
A	-	absorbance
a	m	cell radius
α	°	angle
CDW	$kg \cdot l^{-1}$	cell dry weight
c	% CDW	normalized concentration
C_m	F	membrane capacitance per area
E_{ext}	$V \cdot m^{-1}$	electric field strength
f	Hz	frequency
k	s	time constant
λ	nm	wavelength
light (PAR)	$mol \cdot m^{-2} \cdot s^{-1}$	photosynthetic photon flux density
m	kg	mass
MW	Da	molecular weight
N	-	number of pulses
p	-	volume fraction
Q	$l \cdot s^{-1}$	flow rate
ρ	$kg \cdot l^{-1}$	density
$\Delta\Phi_0$	V	resting potential difference of a living cell
$\Delta\Phi_m$	V	induced transmembrane potential difference
σ	$S \cdot m^{-1}$	conductivity
T	°C	temperature
Δt	s	duration of the pulse
τ	s	duration of the cell cycle
τ_c	s	time constant of membrane charging
V	l	volume
ΔW_{spec}	$J \cdot ml^{-1}$	specific energy delivered to PEF treated samples

Contents

List of figures

Preface

The usual workflow of research spans from making interesting observations to constructing a hypothesis as the final product of induction, questioning and inference. The implications of the hypothesis then need to be transformed into cautiously planned experiments and the compiled data tested for significance. Depending on the results, the hypothesis can be validated or needs to be revised. This scheme can be applied to almost any subject area. However, science unfortunately is not always linear and straightforward and model organisms, even on a laboratory scale, are not easily understood and sometimes unsuitable to generate simple hypotheses to validate or reject. Often, experimental systems are subject to complex modulation by partially unknown or uncontrollable variables. In these cases, the advantages of interdisciplinary study can benefit research by seeing one project from different angles to identify and, when possible, control those variables. The biological cell to the physicist is a model of fluid space contained by a membrane, the engineer wants to optimize extraction efficiency, the biochemist sees a bag full of enzymes and the biologist recognizes the whole system with its compartments enabling complex interplay over time and space. Combining these views should lead to a holistic model and the opportunity to create superior hypotheses to work with. The following work focuses on the observation of a biological phenomenon that can support biotechnology while including the disciplines of biology, biochemistry, biophysics, and bioengineering.

1. Motivation

Apart from the ongoing pandemic, our planet faces many challenges including most urgently climate change as well as the steadily growing world population that needs to be fed. Microalgae can play a major role in the future as a new sustainable source for energy and food. The phytoplankton in the world's oceans is already responsible for half of the carbon dioxide annually fixated by photosynthesis by converting it into oxygen (Borowitzka *et al,* 2016, p. 5). Additionally, algae cultivation offers a rapidly growing and renewable resource that does not compete with food crops for fertile arable land. Why not use this resource? Depending on species and cultivation system, microalgae are rich in proteins, lipids, antioxidants as well as other valuable components and, therefore, harbor potential for numerous applications.

For example, the green microalgae *Auxenochlorella protothecoides* contains high amounts of lipids and is currently researched as a source for biofuel (Silve *et al,* 2018b; Silve *et al,* 2018a). Another quite interesting candidate is the cyanobacterium *Arthrospira platensis* (more commonly known as Spirulina) that has gained attention for its nutraceutical properties (Fernández-Rojas *et al,* 2014). Spirulina also produces high amounts of phycocyanin, the only natural source for blue food colorants, and has been certified as GRAS (generally recognized as safe), the food industry standard. Lastly, the green microalgae *Chlorella vulgaris* contains valuable components (omega-3 fatty acids, vitamins, antioxidants) and a high protein content of approx. 50-60 % of dry weight in addition to also possessing GRAS status (Safi *et al,* 2014). This has attracted great interest in using *C. vulgaris* as a dietary supplement as part of a protein-rich diet.

However, due to its rigid cell wall, unprocessed microalgae biomass would simply pass through the human digestive system and valuable nutrients would not be absorbed (Gille *et al,* 2015). Cell disruption is necessary for the extraction of intracellular components and physical methods are preferable because chemical extraction techniques often prevent subsequent use in the food industry. This is where electroporation via pulsed electric field (PEF) treatment comes into play: cell disruption via PEF treatment offers an energy-efficient and gentle alternative. One advantage lies in the direct processing of the biomass without an additional energy-intensive drying step. PEF treatment usually leads to irreversible electroporation of the cell membrane, while the cell wall remains intact. The cells die due to irreversible pores in the cell membrane, soluble intracellular components such as proteins begin to leak out and then accumulate in the supernatant through mere incubation. Since PEF treatment does not cause small cell debris in comparison to mechanical disruption methods, the separation of proteins by filtration or centrifugation is easy to achieve. In addition, the remaining sediment contains lipid components such as intracellular oil

droplets, which are then easily accessible for solvent extraction. Furthermore, the remaining biomass can also be used for thermochemical conversion or anaerobic fermentation. Thus, PEF treatment as an extraction method offers a promising technology for the sequential extraction of proteins for food, lipids for biodiesel and biogas (**Figure 1**).

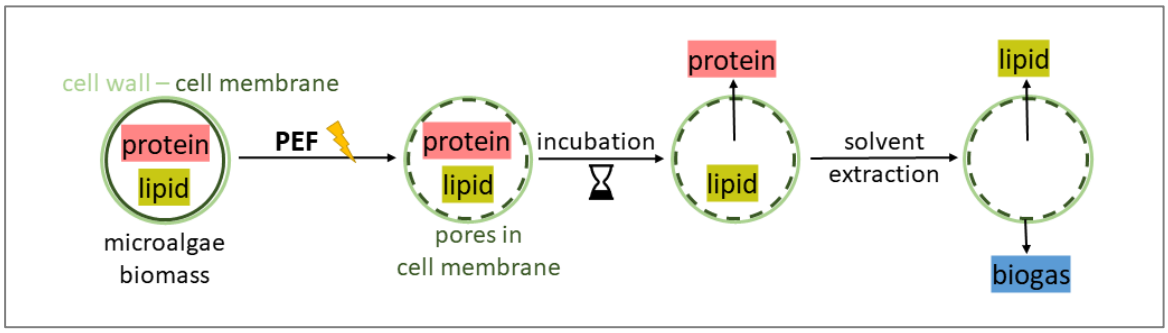

Figure 1 Biorefinery concept based on PEF technology showing valorization of multiple components in cascade process.

It is not exactly known which cellular processes that are triggered by PEF treatment ultimately lead to the release of valuable components – apart from the physical aspect of cell membrane electroporation. The type of cell death induced by PEF treatment influences the efficiency of protein extraction. Therefore, a better understanding of cell death in response to PEF treatment could lead to possible improvements in protein extraction efficiency. A biotechnological strategy could be to use PEF treatment with a very low energy input as a biological signal for the induction of cell death. This could optimize cell disruption via PEF treatment in terms of energy efficiency since the high specific energies used so far are designed to irreversibly permeabilize the membranes of as many cells as possible. The biological aspects of PEF treatment could thus contribute to an energy-efficient extraction of proteins and other ingredients.

2. Background theory

To understand the biological aspects of PEF treatment for the improvement of protein extraction in microalgae, first and foremost it is necessary to intrinsically understand the study subject. Therefore, in the first subchapter, an overview of microalgae in general and their applications as renewable resources will be given. This is followed by detailed descriptions of the model organisms used in this work: *C. vulgaris* and *A. platensis* (Spirulina). The next subchapter focuses on the extraction method of PEF treatment which is an electroporation-based technology. State of the art theoretical considerations of electroporation help to understand the physical aspects of this method while giving a short overview of possible applications including the extraction of biomolecules. Lastly, but most importantly, comes an introduction to the subject of cell death in plants, focusing on programmed cell death in unicellular phytoplankton and cell death due to electroporation.

2.1. Microalgae

Algae are assigned to the thallophytes, which are plants lacking roots, stems, and leaves. Furthermore, eukaryotic algae can be broadly defined as single- or multicellular photosynthetic organisms with chlorophyll *a* as the primary photosynthetic pigment living in aquatic environments (Kadereit *et al,* 2021, p. 723). Cyanobacteria are commonly called blue-green algae and perform oxygenic photosynthesis as well; however, they are prokaryotic organisms. The most common habitats of algae are fresh water, brackish water, and saline water but they can also be found growing in snow (Hoham & Remias, 2020), desert soil (Lewis & Lewis, 2005) or hot springs (Lee, 2018; pp. 58-59). Algae often constitute the first trophic level of the aquatic ecosystem, by providing organic material from carbon dioxide, water, and sunlight through photosynthesis. The ability to grow purely from light energy and convert it into chemical energy is called photoautotrophism and is restricted to plants including eukaryotic algae and cyanobacteria. Through fusion of a heterotrophic eukaryotic cell with a photoautotrophic prokaryotic cyanobacteria, a process well known in literature as endosymbiosis, the first plant cell was formed. The term “eukaryotic algae” is not a monophyletic group and there exist eukaryotic algae with more complex chloroplast structures due to secondary endosymbiosis events. Examples of algae surrounded by one or two membranes of chloroplast endoplasmic reticulum (ER) are dinoflagellates (one membrane) or diatoms (two membranes) (Lee, 2018; p. 26). The general evolutionary context including primary and secondary endosymbiosis is shown in **Figure 2**.

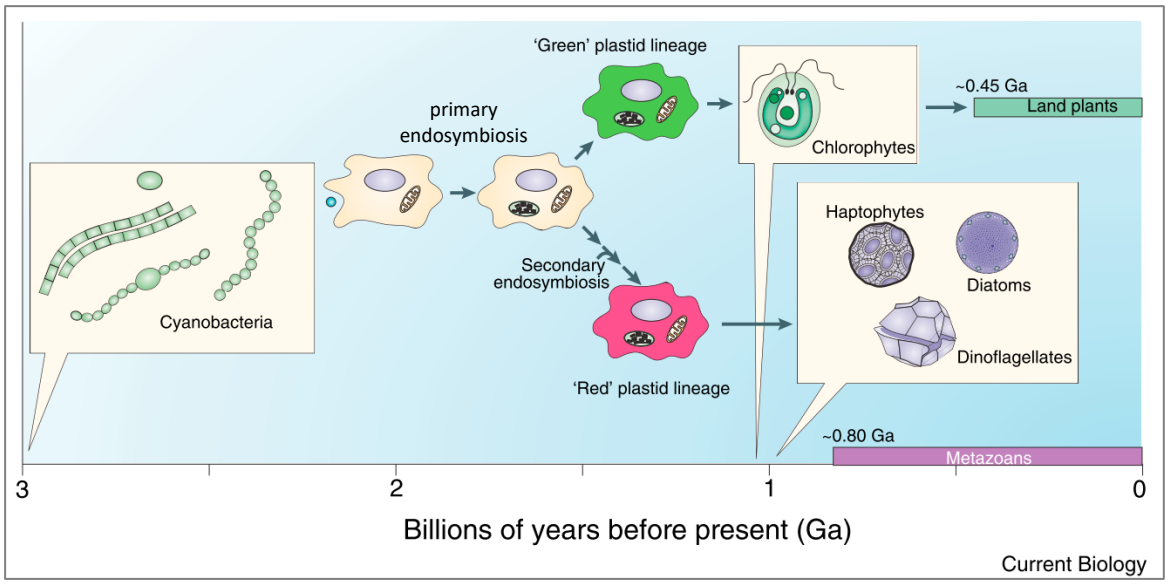

Figure 2 Evolutionary context of microalgae, copied from Bidle, 2016.

Microalgae as a renewable resource

Microalgae are broadly defined as microscopically small algae and can assume different organization forms, such as unicellular, colonial, or filamentous. The number of identified species lies in the range of 40,000 to 60,000, however, estimations go from 200,000 to almost one million species. This immensely high biodiversity promises many possible applications as renewable resource (Rosello Sastre & Posten, 2010). In contrast to terrestrial crop plants in conventional agriculture, the advantages of microalgae cultivation lie in not competing for arable land, less water usage, and no need for insecticides and pesticides. Furthermore, the whole biomass can be used because of the simple morphology of the cells. All this taken together leads to 3-5 times higher productivity of microalgae compared with conventional terrestrial crop plants, relative to used area (Schenk *et al,* 2008). Microalgae harbor many valuable components, leading to numerous applications, in the most part as health or food supplement. Around one third of the production is already used for animal feed, most importantly in aquaculture since microalgae constitute the first trophic level of the aquatic ecosystem (Ahmad et al. 2020). Microalgal biomass can also be used as fertilizer to reduce the usage of nitrogen fertilizers and improve soil quality. Another promising application is the production of biofuel, biogas or hydrogen for the energy sector. Lately, the interest for algal metabolites as a substitute for antibiotics has arisen and could provide a solution to increasing antibiotic resistances (Bhowmick *et al,* 2020).

Depending on the application purpose, the cultivation of microalgae can take place in open pond systems or closed photobioreactors. Open pond cultivation brings the advantages of low investment costs and almost no technical complexity, however, the disadvantage is low

productivity (relative to area used), which in the case of open pond cultivation does not necessarily exceed the productivity of conventional crop plants. Closed photobioreactor systems bring up to 10 times higher productivity and are in addition GMP (Good Manufacturing Practice) certifiable if required for the product. However, this cultivation type is costly and technically more complex (Rosello Sastre & Posten, 2010). The challenge to using microalgae as a renewable resource mainly lies in lowering the costs for microalgae cultivation. In addition, it would be helpful to provide more research in the optimization of cultivation, processing, and further applications including customer evaluations, especially for use in the food sector. Combining more than one application by cascade processing would further promote sustainability as well.

2.1.1. *Chlorella vulgaris* as model organism

The unicellular, non-mobile green eukaryotic microalga *C. vulgaris* was discovered in 1890 by Martinus Willem Beijerinck, a Dutch researcher (Beijerinck, 1890). The name *Chlorella* is derived from the Greek word *chloros* (Χλωρός, green) and the Latin suffix *ella* refers to its microscopic size (Safi *et al,* 2014). The classification is the following: Superkingdom: *Eukaryota,* Kingdom*: Viridiplantae,* Phylum*: Chlorophyta,* Class*: Trebouxiophyceae,* Order*: Chlorellales,* Family*: Chlorellaceae,* Genus*: Chlorella,* Specie*: Chlorella vulgaris. C. vulgaris* was used as a historical model organism to study photosynthesis and carbon dioxide assimilation. The habitat of this species is in freshwater and soil, and it can be found in symbiosis with some ciliates (Kodama & Sumita, 2022), lower animals (*Hydra*) or lichen (Kessler, 1992).

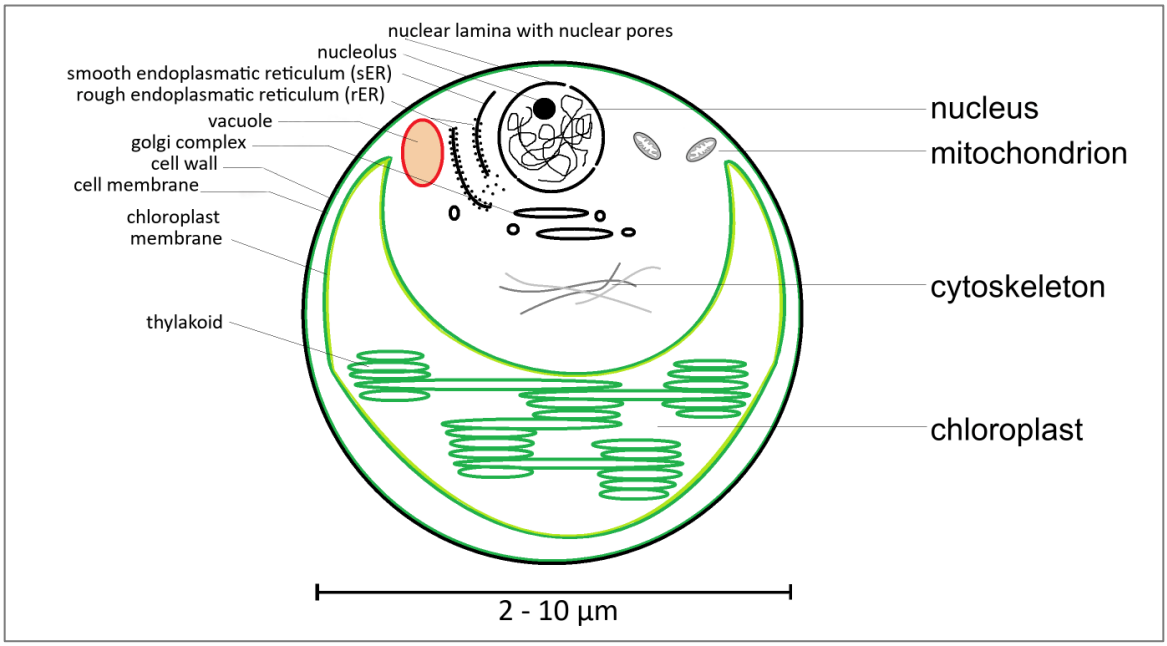

Figure 3 Schematic ultrastructure of *C. vulgaris* showing different organelles, size proportions not precise (author's own, taken from Krust, 2018).

Morphologically, *C. vulgaris* cultures are comprised of spherical cells with sizes ranging from 2 to 10 µm in diameter (**Figure 3**). A thick and rigid cell wall preserves cell integrity, provides protection against invaders and harsh environmental conditions, and can reach 17-21 nm after maturation. However, composition and thickness both vary according to growth phase. The rigidity can partly be attributed to the existence of a chitin-like glycan that can be digested with chitinases releasing *N*-acetylglucosamine (Kapaun & Reisser, 1995; Gerken *et al,* 2013). Chitin in microalgae cell walls is quite unexpected, however, sequencing of the related species *Chlorella variabilis* showed the existence of genes from the chitin metabolism likely acquired by horizontal gene transfer from algal viruses (Blanc *et al,* 2010). The single chloroplast is cup-shaped and located peripherally, the nucleus is situated close to the cell membrane with the ER and the Golgi complex located next to it. *C. vulgaris* contains several mitochondria, closely associated with the chloroplast, as well as several vacuoles surrounded by a single-layer membrane (Safi *et al,* 2014). The reproduction of *C. vulgaris* is through asexual autosporulation (mitosis). One mature mother cell can form 2-16 autospores and after the division of the chloroplast and nucleus, daughter cells develop their own cell wall and are consequently released by rupture of the mother cell wall (Yamamoto *et al,* 2004, **Figure 4**).

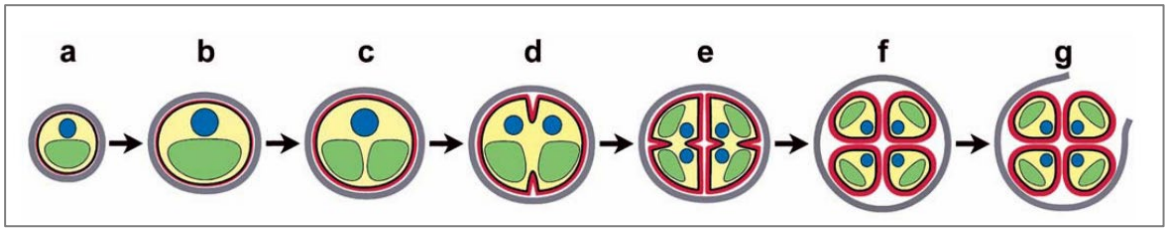

Figure 4 Schematic drawings summarizing the timing and portion of daughter cell-wall synthesis in *C. vulgaris*. **a** Early cell-growth phase. **b** Late cell-growth phase. **c** Chloroplast-dividing phase. **d** First protoplast-dividing phase. **e** Second protoplast-dividing phase. **f** Autospore maturing phase. **g** Hatching phase. Gray line: mother cell wall, red line: daughter cell wall. Copied from Yamamoto *et al,* 2004.

C. vulgaris can be cultivated under three different conditions: (1) autotrophic with light and carbon dioxide plus nutrients like nitrogen and trace elements, (2) mixotrophic with light and carbon dioxide as well as an additional organic carbon source or (3) heterotrophic with no light and only an organic carbon source. The supplementation with an organic carbon source increases biomass and lipid productivity, however, it also increases the cost of cultivation. Harvesting of *C. vulgaris* biomass can be executed by centrifugation, flocculation or ultrafiltration (Safi *et al,* 2014). The choice of disruption method also determines the quality of the extracted compounds.

When looking at the biochemical composition from a biotechnological point of view, *C. vulgaris* contains in the most part protein with 40-60 % of dry weight, however, this percentage varies

greatly according to growth conditions. The amino acid profile compares favorably to the standard profile for human nutrition (*World Health Organization, WHO*) and is mostly comparable to egg protein (Scherer, 2019). *C. vulgaris* protein contains essential and non-essential amino acids and provides an excellent capacity for emulsification. Under normal growth conditions, the lipid content is quite low, but especially nitrogen starvation can boost the lipid content to reach over 50 % which can be suitable for different applications depending on the fatty acid profile (nutrition or biodiesel). The most abundant of carbohydrates is starch in the chloroplast followed by cellulose and β1→3 glucan in the cell wall. Important pigments are mostly chlorophyll and carotenoids. A high vitamin content and strong antioxidant activity through radical scavengers complement the favorable composition. These factors lead to applications in human nutrition as well as animal feed. However, also wastewater treatment and agrochemical application as fertilizer play increasingly bigger roles (Safi *et al,* 2014).

For a better understanding of the biological processes in the cell and in order to establish genetic tools for biotechnological manipulation, the genetic information of the species is very important. A little over two years ago the scaffolded genome assembly and annotation was published (Cecchin *et al,* 2019). Unfortunately, the protein database (uniprot.org; date: 2021-12-20) still only contains scarce information about proteins in *C. vulgaris* (90 reviewed; 506 unreviewed) in comparison with the closely related species C*hlamydomonas reinhardtii* (366 reviewed; 30,946 unreviewed).

2.1.2. *Arthrospira platensis* (Spirulina) as model organism

A. platensis is a filamentous, non-heterocystous oxygenic photosynthetic cyanobacterium. The classification is the following: Superkingdom: *Bacteria*, Phylum: *Cyanobacteria*, Order: *Oscillatoriales*, Family: *Microcoleaceae*, Genus: *Arthrospira*, Species: *Arthrospira platensis.* It has already historically been used as food: (1) in the 9th century in Africa in the region around Lake Chad as "*dihe*" or "*die*", small cakes made of Spirulina and (2) in the 16th century in South America by the Aztecs as "*tecuitlatl*" meaning stone's excrement (Ali & Saleh, 2012).

The habitat of Spirulina are water bodies with high carbonate/bicarbonate content, elevated pH, and salinity (tropical or subtropical). Morphologically, the filaments are composed of multicellular trichomes, a hair-like structure of single-file connected cyanobacterial cells. Cylindrical trichomes of Spirulina form an open left-hand helix with a helix diameter of 30-70 µm and trichome length of up to 0.5 mm (**Figure 5**). Under the light microscope, one can see transverse cross-walls of the single cells in the solitary, free-floating trichomes. When looking at the cell envelope, the whole trichome is surrounded by a thin sheath with a thickness of about 0.5 µm. Each cell has a Gram-negative type envelope (40-60 nm), also called cell wall, which is made of four layers. Thylakoid

bundles appear transversely to cross-walls with the neighboring cell. Thylakoid-free areas contain ribosomes, DNA fibrils as well as gas vacuoles for free floating of the trichomes. Cell division takes place via binary fission. Trichomes are elongated by multiple intercalary cell divisions all along the filament. Multiplication of trichomes is executed by fragmentation. Trichome breakage is initiated by the destruction of an intercalary cell, also called sacrificial cell or necridium (Vonshak, 1997).

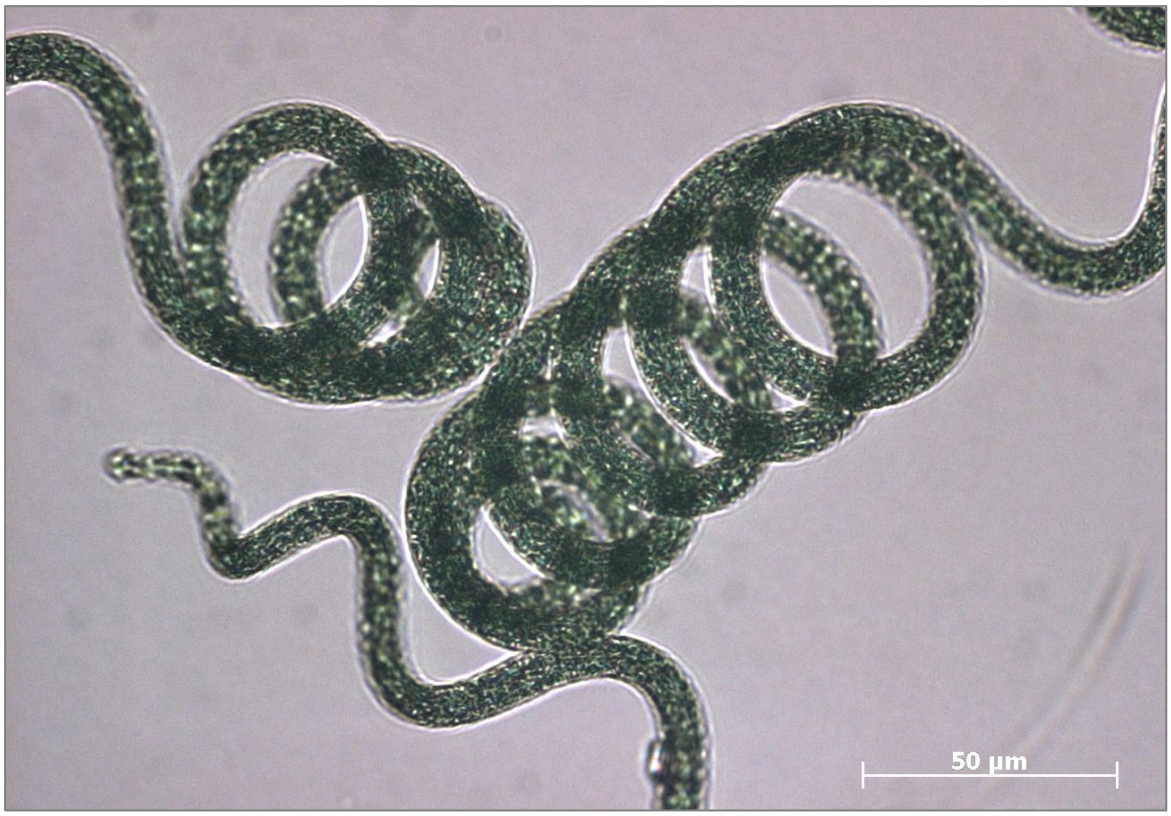

Figure 5 Spirulina under light microscope: multicellular cylindrical trichomes in an open left-hand helix.

Spirulina products are already used in the food industry and their main selling point are their nutraceutical properties because of their very high antioxidant potential. Spirulina is supposed to have anti-inflammatory, anti-cancer, nephroprotective, and hepatoprotective properties (Fernández-Rojas *et al,* 2014). In addition, Spirulina produces high amounts of phycocyanin (PC), the only natural source for blue food colorant. PC is the blue-green pigment responsible for the color of the cyanobacteria. As a phycobiliprotein, PC is part of the peripheral accessory light-harvesting complex called phycobilisome and its main function is to transfer excitation energy to the center. The main benefit for blue-green algae is the ability to harvest energy from light regimes where chlorophyll *a* does not absorb. This highly valuable component can be obtained from red algae (R-PC) or cyanobacteria (C-PC) and is sensitive to light, temperature, pH, and protein concentration. Therefore, extraction and conservation can be quite complex (Akaberi *et al,* 2020).

2.2. Electroporation-based technologies

To explain the biological consequences of PEF treatment in the context of competent cell recovery, it has to be distinguished between the processes happening during and after exposure of a microalgae suspension to an electric field. When broken down to single-cell level, exposure of a single cell to an external electric field leads to electroporation of the cell membrane. The outcome is either reversible permeabilization of the cell membrane or irreversible damage leading to cell death, depending on the strength of PEF treatment as well as the biological consequences of the treated material. To describe the whole process, theoretical considerations, as well as practical experimental data, have to be considered. The following chapter will give a general overview of electroporation.

2.2.1. Theoretical considerations

Resting transmembrane potential difference

For the first theoretical considerations, we will view the cells as consisting of a plasma membrane only and neglect the cell wall as well as extracellular matrices (Kotnik, 2020). The reason for this is that we assume that the cell wall or the extracellular matrix has the same dielectric properties as the surrounding electrolyte, cannot be polarized and therefore, no direct effects are applicable. The biological cell from an electrical point of view consists of an electrolyte inside the cell, the cytoplasm, and an electrolyte outside of the cell with the plasma membrane acting as an electrical insulator. Under physiological conditions without an external field applied, specific ion pumps in the cell membrane lead to the so-called resting transmembrane potential difference (Kotnik, 2020). This is mostly achieved by the work of the Na-K-pumps that actively export 3 Na^+ ions out of the cell while importing 2 K^+ ions into the cell. Together with passive K^+ leak channels leading to efflux of K^+ ions along the concentration diffusion gradient out of the cell, a negative charge is built up inside the cell. After reaching equilibrium, this electrical gradient across the cell membrane determines the continually present resting transmembrane potential difference. It should be mentioned that the unbalanced ions responsible for the resting potential represent only a very small fraction of all ions present in the cytoplasm so osmotic pressure differences from this imbalance are negligible. Additionally, the accumulation of the unbalanced ions takes place close to the membrane surface resulting in electrically neutral cytoplasm and the membrane acting as a charged capacitor (Kotnik, 2020).

Induced transmembrane potential difference

When a cell is exposed to an external electric field, the field will concentrate within the membrane leading to an induced transmembrane potential difference which superimposes onto the resting

transmembrane potential difference. The concentration of the field across the cell membrane is due to the low membrane conductivity and permittivity and results in an induced transmembrane potential difference several orders of magnitudes higher than in the cytoplasm or outside the cell. This induced transmembrane potential difference can result in affecting voltage-gated channels, but most importantly, when sufficiently large, it can lead to membrane electroporation. The electroporated membrane regions are closely correlated with the regions of the highest induced transmembrane voltage difference (Kotnik *et al,* 2010).

For exposure of a cell to a homogenous electric field, the induced transmembrane potential difference $\Delta\Phi_m$ can be determined by solving Laplace's equation. In theoretical considerations, the biological cell will be considered as a perfect sphere and for approximation, the plasma membrane will be treated as a non-conductive thin membrane. With these assumptions, the induced transmembrane potential difference $\Delta\Phi_m$ is calculated by a formula often referred to as the steady-state Schwan's equation (1) (Pauly & Schwan, 1959; Weaver & Chizmadzhev, 1996):

$$\Delta\phi_m = \frac{3}{2} \cdot a \cdot E_{ext} \cdot cos\alpha - \Delta\phi_0 \quad (1)$$

The induced transmembrane potential difference is dependent on the external electric field strength E_{ext}, the cell radius a, and α, the azimuth angle with respect to the direction of the field (see **Figure 6**). The resting potential difference of the cell $\Delta\Phi_0$ superimposes on the induced potential difference and has to be included into the equation as well.

Furthermore, the induced transmembrane potential difference is proportional to the applied electric field and the cell radius. The induced potential difference reaches extremal values at the points where the field is perpendicular to the membrane (the poles of the cell) and in between it varies proportional to the cosine of α (Flickinger *et al,* 2010; Silve *et al,* 2016). The value given by the steady-state Schwan's equation is typically established after a very short time as determined by the time constant of membrane charging τ_c. This value can be calculated with equation (2) using the cell radius a, the membrane capacitance per area C_m and the conductivities σ_i and σ_e of the internal and external of the cell, respectively (Frey *et al,* 2013). τ_c is important for estimation of minimally required pulse duration, so that the applied pulse is not shorter than the period of membrane charging.

$$\tau_c = a \cdot C_m \cdot (\frac{1}{\sigma_i} + \frac{1}{2\sigma_e}) \quad (2)$$

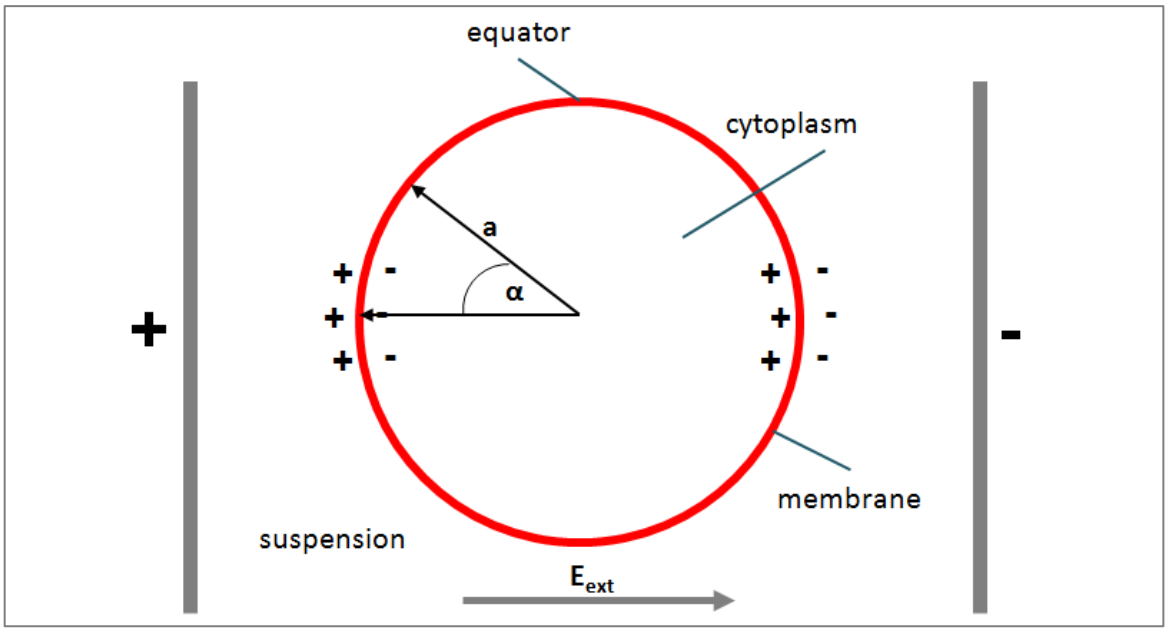

Figure 6 Space charge distribution across the membrane of a spherical cell (author's own, taken from Krust, 2018).

When a cell is exposed to the pulses of an external electric field, the occurring processes can be divided into four stages (Saulis, 2010):

1. Stage: Charging of the cell membrane via the build-up of induced transmembrane potential difference. The time range goes from nanoseconds to milliseconds and is determined by the time constant of membrane charging τ_c.

2. Stage: Creation of small hydrophilic aqueous pores (Weaver & Chizmadzhev, 1996). The time range goes from nanoseconds to milliseconds. Here, water molecules penetrate the lipid bilayer and cause neighboring lipids to reorient their polar head groups towards the water molecules. At this step, pores are formed, and this process can be visualized by molecular dynamics (MD) simulations (Tarek, 2020; Delemotte & Tarek, 2012).

3. Stage: Evolution of pore population with change of number and size of pores. The time range is depending on the length of the electric field treatment. This stage can be influenced by electric field strength, number of pulses, temperature, ionic strength of the medium, and membrane fluidity.

4. Stage: Post-treatment stage. MD simulations have shown that hydrophilic aqueous pores can reseal within nanoseconds when the applied electric field is switched off. Prolonged permeabilization must be attributed to secondary effects (Kotnik *et al,* 2019). The time range goes from milliseconds to hours and even days. Here, intracellular components leak out, extracellular substances can enter the cell and the acquired damage can either be repaired or not.

To describe the processes and consequences occurring during and after exposure of cells to electric fields, certain terminology is necessary. One process that is happening immediately after exposure to an electric field, as an "all-or-nothing event", is called cell electroporation. It is defined as the "electrically induced formation of aqueous pores in the lipid bilayer under the influence of the induced transmembrane voltage" (Kotnik *et al,* 2019). When reaching a certain threshold of electric field strength or pulse duration, the first two stages that are described above, lead to small hydrophilic aqueous pores. At this threshold electroporation (Saulis, 2010) water and small ions are let through, but the membrane is still impermeable to slightly larger molecules. The pores can be small enough to discriminate between K^+, Rb^+ and Na^+ ions and this process is not visible when testing for cell viability (Saulis *et al,* 2007). The term electropermeabilization includes the process of electroporation but can be applied more broadly. It is defined as an "electrically induced increase in the membrane permeability for molecules devoid of physiological mechanisms of transmembrane transport" (Kotnik *et al,* 2019). Here, additional secondary effects with biological and chemical mechanisms are included. Electropermeabilization describes the fraction of cells with their membrane permeable to a certain substance, even after the pulse. Test molecules used for detection of electropermeabilization are usually larger than the ions used for detecting electroporation efficiency (i.e., sucrose with molecular weight (MW) = 342 Da or propidium iodide with MW = 668 Da). Lastly comes the process of inactivation due to strong electric fields. Cell death is also considered an "all-or-nothing event". This can be detected with viability assays either in the short-term by direct staining of live and/or dead cells or long-term by colony formation assays. When cell death is induced by toxic influences it can also be a slow process (Saulis, 2010).

As mentioned, processes and consequences caused by exposure of a cell to an external field are not only due to electroporation but can be also attributed to chemical reactions such as lipid oxidations (Maccarrone *et al,* 1995) or physical activation of voltage-gated membrane channels (Burke *et al,* 2017). Furthermore, there are many biological intracellular effects such as interaction with cytoskeleton components (Berghöfer *et al,* 2009; Kühn *et al,* 2013), modulation of gene expression (Bai *et al,* 2020) or even a growth stimulation in plants and fungi (Eing *et al,* 2009; Frey *et al,* 2011).

Applications

With this knowledge, it becomes clear why numerous electroporation-based biotechnological and biomedical applications have emerged. Applications relying on irreversible electro-permeabilization include tissue ablation, food preservation by inactivation of microorganisms as well as extraction of molecules. Reversible permeabilization is used for the introduction of small or large molecules to the cytoplasm, e.g., in electrochemotherapy or electrotransformation. More

challenging approaches consist of cell fusion or insertion of molecules into the plasma membrane (**Figure 7**).

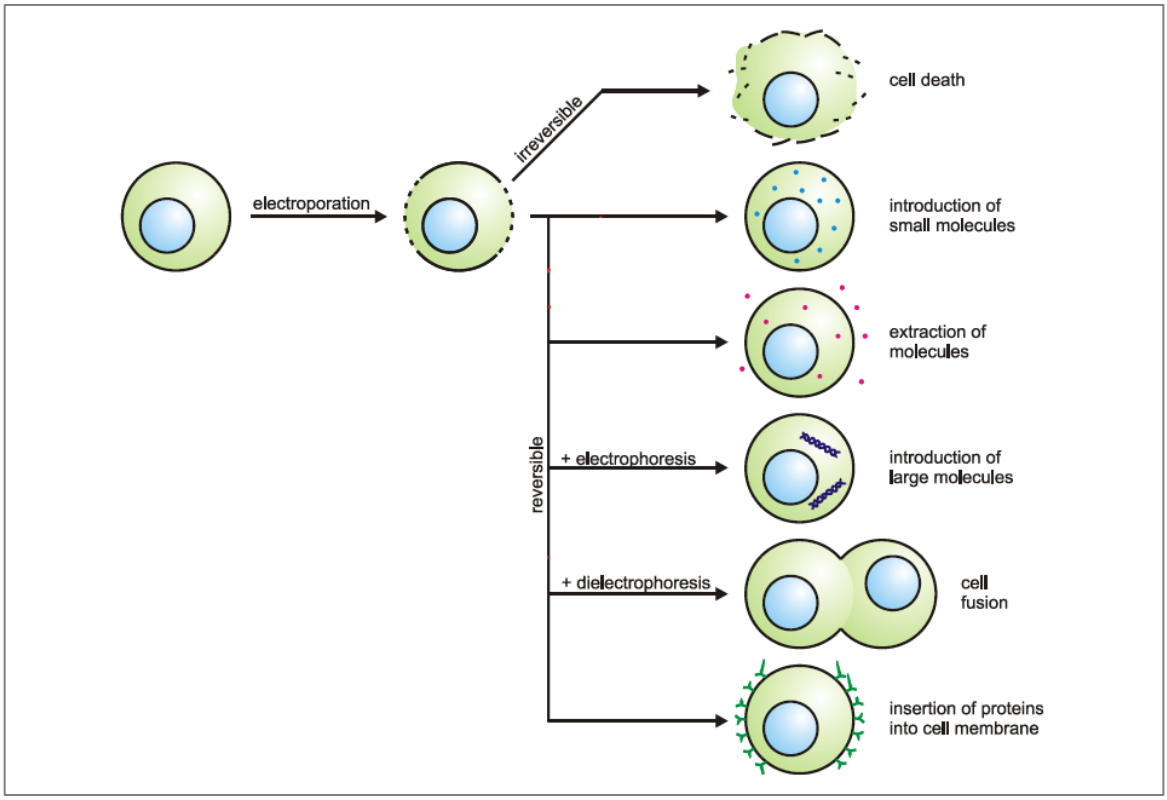

Figure 7 Exposure of a cell to an electric field results either in reversible or irreversible permeabilization of the cell membrane leading to numerous possible applications, modified from Kramar & Miklavčič, 2020, p. 162.

2.2.2. Processing of foods and biomass by PEF treatment

Inactivation of microorganisms

For industrial applications of electroporation, the term PEF treatment is more commonly used. With sufficiently high field parameters PEF treatment is very suitable for inactivation of microorganisms (Frey *et al,* 2013). This can be applied for bacterial decontamination of wastewater, especially important for hospital wastewater containing antibiotic-resistant strains. Since the wastewater temperature remains below 70 °C, DNA degrading nucleases can be preserved, and horizontal gene transfer prevented (Rieder *et al,* 2008). Additionally, sterilization with electroporation does not lead to tolerance or resistance of bacteria and is highly efficient under high mass-flow conditions (Gusbeth *et al,* 2009). Another already established application is the use of PEF treatment for nonthermal food pasteurization (Zhang *et al,* 1995; Toepfl *et al,* 2006; Buckow *et al,* 2013; Saldaña *et al,* 2014). Temperatures need to stay lower than for wastewater sterilization, therefore only yeast and bacteria are susceptible to this treatment and bacterial spores remain resistant (Kotnik *et al,* 2015). This application is used mostly for liquid food (juices, beer, milk, and soups).

Extraction of biomolecules

Electroporation can also be used to produce target biomolecules by transforming microorganisms such as bacteria (Dower *et al,* 1988), yeast (Thompson *et al,* 1998) or microalgae (Shimogawara *et al,* 1998). This electrotransformation is performed via mild and reversible electroporation with the aim of high viability. When the microorganism now contains the potential source of biomolecules for industry, pharmacy or medicine, extraction processes are necessary. Established processes for extraction include mechanical forces (e.g., high-pressure homogenization or ultrasonication) or chemicals, however, those can be detrimental to the structure of the biomolecules. In addition, purification from cellular debris is needed. Here, electroporation comes into play again, now called electroextraction or PEF treatment. The advantages of PEF treatment as an extraction method are vast since it is fast, chemical-free, energy-efficient, and gentle. PEF treatment provides easy upscaling potential and allows processing with high concentrations, up to 100 $g \cdot l^{-1}$ biomass. The microorganism suspension is pumped between two electrodes while applying a pulsed electric field leading to irreversible permeabilization of the cell membrane. Although the main structure of the cell is preserved, soluble intracellular components begin to leak out and accumulate in the supernatant after a certain incubation time. Since this process does not cause cell debris, separation of the supernatant with valuable biomolecules is possible by mild centrifugation or filtration. As already mentioned in chapter 1 (**Figure 1**), this can be followed up by cascade processing (Kotnik *et al,* 2015; Scherer *et al,* 2019; Papachristou *et al,* 2021), allowing entry of hydrolytic enzymes (Akaberi *et al,* 2019) as well as entry of solvents for lipid extraction (Silve *et al,* 2018a; Silve *et al,* 2018b).

This extraction method can not only process unicellular organisms such as bacteria, microalgae, and yeast. Even bigger plant tissues can benefit from PEF electroextraction. One example is the processing of grapes via PEF treatment for wine production, thus enabling fast processing without an adverse influence on taste (Sack *et al,* 2010). Another example is the PEF treatment of sugar beets. On the one hand, this leads to purer juice because less water is required for extraction and on the other hand, electroextraction brings the additional benefit of lower energy consumption during the evaporation stages (Kotnik *et al,* 2015).

2.3. Cell death

When looking at cell death after electroporation in microalgae, except for the fact that cells die and electroextraction can take place, not many details are known so far. It has been shown that PEF treatment of *C. vulgaris* induces leakage of cytoplasmic proteins (Coustets *et al,* 2015). Previous experiments, also with the model organism *C. vulgaris*, have detected proteins of nuclear, chloroplast, and mitochondrial origin in the water-soluble extract after PEF treatment, indicating a breakdown of these cell organelles (Scherer *et al,* 2019). Looking at microscopic pictures after PEF treatment, one can still recognize spherical cells enveloped by the cell wall even though Evans Blue staining shows almost 100 % mortality. DNA analysis of the cellular residue after PEF treatment showed clear DNA laddering from as soon as 1 h after PEF treatment. The cellular residue was separated into two fractions: (1) pellet including the porous cell hulk and (2) supernatant with extracted water-soluble components. Both fractions showed DNA laddering, the pellet already 1 h after PEF treatment and the supernatant 4 h after PEF treatment (Scherer *et al,* 2019). This might be an indication for regulated cell death, even though DNA laddering can be caused either by programmed cell death or necrosis as explained later in this chapter (2.3.1). It has been proposed that facilitated release of valuable contents from *C. vulgaris* under relatively mild PEF treatment conditions might derive from PEF induced programmed cell death. Apoptosis and autolysis after PEF treatment have already been described for yeast (Martínez *et al,* 2018a; Martínez *et al,* 2018b; Simonis *et al,* 2017).

Therefore, is necessary to fundamentally understand inactivation mechanisms leading to cell death and especially cell death in plants and microalgae in particular. There has been substantial research conducted already, however, some questions regarding cell death in plants, phytoplankton, and cell death due to electroporation remain unanswered still and pose open research possibilities. The following chapter will give a general overview of the state of the art to this date.

2.3.1. Programmed cell death

The phrase “destroy to create” (Nick, 2018) poses that disintegration is a requirement for creation and when looking closely, one or another form of regulated cell death with clear functionality can be found all over nature – one example being the destruction of a sacrificial cell in Spirulina trichome breakage for multiplication (Chapter 2.1.2). For analysis of cell death, one must clearly define the terms of regulation or lack thereof and unfortunately, the terminology in this area is quite ambiguous and not smoothly transferrable between plants and animals.

The term **apoptosis**, first coined by Kerr *et al* (1972), describes the controlled and organized destruction of an animal cell with a certain morphology of nuclear and cytoplasmic condensation and breaking up of the cell into apoptotic bodies. In plants, a similarly regulated process can be found and is called **programmed cell death (PCD)**. Both apoptosis in animal cells and PCD in plants cells share a common sequence of biochemical events that leads to regulated cell death. However, the concept of PCD and consequently apoptosis came from plants first, when Allen (1923) conducted research on active and programmed cell death in plant cells while studying fungal infection. In contrast to apoptosis and PCD, the process of **necrosis** is defined as the uncontrolled and chaotic mode of death, resulting from acute cellular injury without specific induction of gene expression. Depending on the level of stress either programmed cell death or necrosis can be induced. However, one must be careful with quick classification since the morphology of dying cells is often confused with the type of cell death. One prime example is the morphology of nuclear fragmentation which can result in DNA laddering (visualized after separation by gel electrophoresis). DNA laddering is described as a hallmark of apoptosis in animal cells caused by caspase activity, cysteine proteases that cut DNA at specified regions. But laddering can also occur during necrosis induced by mitochondrial uncoupling through different proteases targeting serines (Dong *et al,* 1997).

In plant cells, cell death is essential for normal development, most noticeable in fall when the leaves turn color and senescence removes cells for recycling nutrients. In regular plant growth cell death is irreplaceable for sculpting tissues like aerenchyma or tracheary elements. PCD is a part of the immune system in plants as well with a function called hypersensitive response (HR) against pathogens, a self-initiated cell death to prevent the spread of the disease to the whole plant. Abiotic stresses can also lead to perturbation of metabolism and result in PCD (Jones, 2001). Jones (2001) proposes a model for the general mechanism of PCD in plants. At first, different initiating signals from either pathogen signals or plant hormones are integrated to make the decision to die. As the second step, cell death is prepared. This depends on the initiating signal which decides the differential loading of the vacuole with different hydrolases and/or toxins. Thirdly, cell death is triggered by calcium flux leading to vacuole collapse, which is a universal step independent of the initiating signals. At last, the release of vacuole content leads to differential post-mortem events. This can be either cell wall hydrolysis, cytoplasm collapse or autolysis. Other classifications of plant PCD include the differentiation into autolytic and non-autolytic PCD (van Doorn, 2011). Autolytic PCD is defined by tonoplast rupture followed by rapid cytoplasm clearance while non-autolytic PCD is mostly defined by the absence of rapid clearance. Plant PCD requires active protein translation and can be regulated by plant hormones (e.g., cytokinin blocks senescence, ethylene

accelerates senescence). All studies show a common role for calcium, increase of reactive oxygen species (ROS), and caspase-like activities (Jones, 2001; van Doorn, 2011).

In animal cells, caspases initiate and execute PCD. Classic caspases are expressed as proenzymes and their activity is tightly controlled. Functional and structural homologues (but no sequence homologues) of the same C14 cysteine protease family can be found in prokaryotes, yeast, and plants as well. All members of this family harbor a cysteine/histidine catalytic dyad responsible for hydrolyzing peptide bonds (Aravind & Koonin, 2002; McLuskey & Mottram, 2015). The caspase homologue in plants is called **metacaspase**. Metacaspases show a strict preference for substrates containing basic residues and can be classified into three types. Functions of plant metacaspases are apparently not only related to PCD but to the survival of the cell as well (Klemenčič & Funk, 2018). In green chlorophytes constant expression of proteins with caspase epitope could be identified (Zuppini *et al,* 2010; Sirisha *et al,* 2014).

Specific examples in plants show that necrotic cell death can also be part of an adaptive response, for instance when older leaves under salt or drought stress enter cell death after having mobilized energy resources and protective molecules towards the younger leaves that will re-initiate development, once the stress period has finished (Ismail *et al,* 2014). Another example demonstrates salinity-induced PCD at the root tip that allows the formation of lateral roots to explore the neighborhood for regions of reduced salinity (Li *et al,* 2007). Furthermore, the ambiguous signal of DNA laddering in cycling tobacco cells accompanies cell-cycle arrest at the G2/M transition (Kuthanova *et al,* 2008).

2.3.2. Cell death in phytoplankton

On first thought, regulated cell death in unicellular microorganisms is ostensibly counterintuitive since the cell is the organism. Cell death provides no benefit for the individual, even more – it is a first-order fail on organism fate. However, cell death by lysis in field populations of phytoplankton is quite common and it is estimated that over 50 % of growth is lost again in this way (Bidle, 2016). In cyanobacteria, there is morphological evidence of PCD in response to nutrient limitation, high light, or oxidative stress. Additionally, as mentioned in the introduction to this chapter, filamentous cyanobacteria also use PCD as differentiating mechanism for the generation of dispersal cells (hormogonia) that are released from parent colonies after death and during unfavorable conditions. Even in chlorophytes, there is one famous example for PCD. In the colonial alga Volvox, somatic cells die after a set number of divisions in a process of programmed senescence with morphological markers such as cell shrinkage and chlorophyll loss but also involving new protein expression (Franklin *et al,* 2006). But these examples only pertain to multicellular phytoplankton, what about unicellular organisms?

Self-mediated cell death has been observed in other unicellular organisms such as bacteria and yeast. In bacteria, the lysis of mother cells during sporulation involves PCD and in yeast apoptotic markers such as DNA fragmentation and phoshatidylserine inversion can be observed during cell death induced by oxidative stress (Franklin *et al,* 2006). The genetic program of PCD must have some selective advantage to unicellular organisms, otherwise, it would have been deleted from genomes in the evolutionary process. Since the intrinsic and cellular mechanism of unicellular PCD shares core components of death pathways in higher plants and animals, it could even be stated that death represents the default pathway in biology and cells are intrinsically programmed to self-destruct. When continuing this thought, survival would only depend on effective and continued repression of cell death and deficiency in repression would automatically remove less fit cells from population (Bidle, 2016). One strongly plausible evolutionary driver for PCD in unicellular phytoplankton is the argument of individual altruism for the sake of population benefit. The removal of damaged and/or aging cells leads to the provision of surviving cells with nutrients (Bidle & Falkowski, 2004). However, it still remains difficult to understand how nutritional benefits can be restricted to the same species in the planktonic environment (Franklin *et al,* 2006). Another evolutionary key aspect becomes clear when looking at the kin selection model. This model proposes that if a behavior favors the fitness, this behavior can increase in frequency, both in an individual or closely related kin (Hamilton, 1964). Therefore, maintaining genetic fitness via PCD would be an effective strategy for asexually reproducing microorganisms as well. Another evolutionary driver would be co-evolution with other metabolic pathways. PCD-related genes could either be integral components of cellular differentiation and development pathways for specialized phytoplankton, e.g., responsible for nitrogen-fixing or sexual stages. Alternatively, PCD-related genes could even play physiological functions such as participating in housekeeping, stress acclimation, or regulatory functions. Then, retention and expression would be of physiological and therefore evolutionary benefit (Bidle, 2016).

There are numerous examples of PCD in unicellular algae. Salt or cadmium stress induces cell death in unicellular green alga *Micrasterias denticulate* with defined PCD-like morphological changes (Affenzeller *et al,* 2009; Andosch *et al,* 2012). Caspase-dependent PCD can be induced in the green chlorophyte *C. reinhardtii* by menadione or mastoparan (Sirisha *et al,* 2014; Yordanova *et al,* 2013) and acetic acid even leads to PCD with volatile organic compounds (VOCs) putatively acting as infochemicals involved in cell-to-cell communication (Zuo *et al,* 2012). There also have been studies showing PCD in *Chlorella* spp. with typical responses such as an increase in ROS, DNA fragmentation and caspase-like activity (Bai *et al,* 2017b; Zuppini *et al,* 2010).

In short, it can be summarized that phytoplankton PCD is autocatalytic cell death mainly induced by cell age or environmental stresses such as nutrient deprivation, intense light, high salt concentrations or oxidative stress. Analogous to apoptosis and PCD it is recognizable by distinct morphological changes (cell shrinkage, chromatin condensation) and biochemical coordination (metacaspase activity, de novo protein synthesis) and leads ultimately to cellular dissolution (Bidle & Falkowski, 2004). What remains to be thoroughly studied is the role of extracellular signaling between microalgae. It is already known that signaling within bacterial biofilms can lead to PCD via quorum-sensing (Oleskin *et al,* 2000). In that context, it would be interesting to isolate and characterize the exuded biologically active compounds of microalgae and analyze their relationship with the induction of cell death (Franklin *et al,* 2006).

2.3.3. Cell death due to electroporation

In human cell lines, it has been demonstrated early that electric field pulses can induce apoptosis (Hofmann *et al,* 1999). The main morphological features in this study were DNA fragmentation and proven caspase activity. However, it was shown already then, that membrane permeabilization alone is insufficient to activate apoptotic processes. Therefore, it is quite important to take a closer look at cell death due to electroporation and focus on the transition between reversible and irreversible damage, the so-called point of no return. This is dependent on the magnitude of cell injury caused by electroporation. The main mechanisms of cell injury are: (1) membrane damage, (2) DNA and protein damage, (3) increase of ROS, (4) entry of Ca^{2+}, (5) mitochondrial damage, and (6) ATP depletion (**Figure 8**). As thoroughly described in chapter 2.2, exposure to an electric field directly causes membrane damage through structural and dynamic reorganization of the plasma membrane and lipid peroxidation. Additionally, exposure to an electric field can cause direct damage to membrane embedded proteins. Taking this into consideration, cell death following electroporation is a result of multiple cell injuries and often it is very difficult to determine cause and consequence. What can be measured in mammalian cell lines, often almost immediately and therefore most likely directly caused by electroporation, is disruption of intracellular calcium homeostasis. Activation of calcium ATPases and direct ATP leakage results in depletion of intracellular ATP. This results in osmotic imbalance and cell swelling. Additionally, ROS production seems to be a direct effect of exposure to an electric field. For detected damages to mitochondria, DNA, and proteins in general it is not known if it is directly or indirectly caused. After exposure to an electric field, membrane repair may take place. The total energy for closure or expansion of the pore is strongly dependent on the pore size, but in general, only lipid pores of nanometer range may reseal spontaneously. For injuries larger than a few nanometers there are active mechanisms for membrane repair. On the one hand, the removal of

porous patches of membranes can be executed by endocytosis. On the other hand, calcium-induced vesicle exocytosis is used to reduce plasma membrane tension. The actin cortex under the plasma membrane has an important effect on stability and resealing (Batista Napotnik *et al,* 2021). However, most of the mechanisms of cell injury and membrane repair post-electroporation are based on experiments with mammalian cell lines. In consequence, one must be careful when transferring these models to microalgae and cyanobacteria.

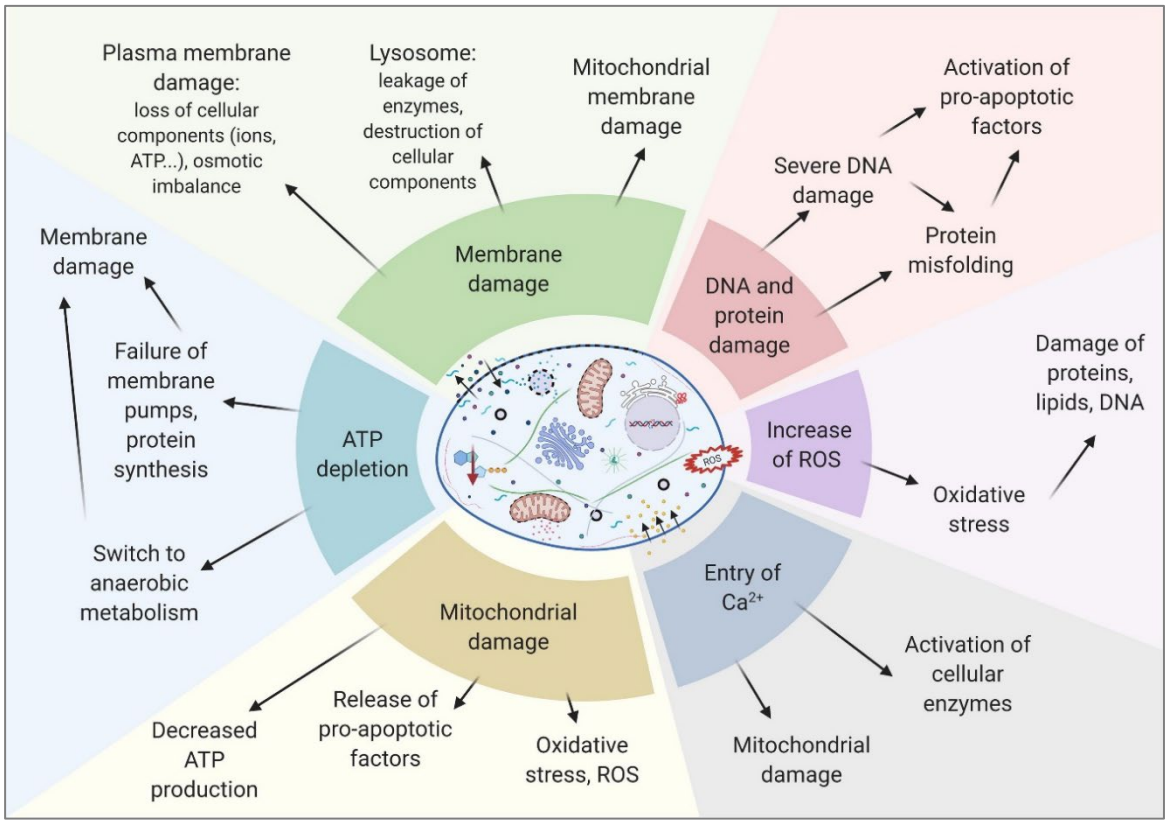

Figure 8 Mechanisms of cell injury in mammalian cells, copied from Batista Napotnik *et al* (2021).

3. Scope of the study

It has already been shown that cell death after PEF treatment for electroextraction of valuable compounds in *C. vulgaris* shows indication of a regulated cell death (Scherer *et al,* 2019). This study aimed to advance understanding of biological aspects of PEF treatment as well as cellular mechanisms of cell death in the unicellular microalgae *C. vulgaris.* For this purpose, methods for analysis of cell death response after PEF treatment on a quantitative base had to be established. The goal of this work was to clarify the subsequent processes related to cell death to understand the extraction and recovery of proteins post PEF treatment in *C. vulgaris.* And, to verify the involvement of enzymatic activity and PCD in protein extraction after PEF treatment of microorganisms in general, the extraction of proteins and pigments from cyanobacterium Spirulina was also investigated in parallel. As a complementary result, the extraction efficiency of the valuable blue pigment C-phycocyanin after PEF treatment could be optimized in further steps.

3.1.1. Optimization of protein and C-PC electroextraction efficiency from Spirulina

To understand and compare the biological aspects of PEF assisted protein extraction for microalgae in general, the other GRAS-certified organism Spirulina was selected. For biotechnological processing, the impact of post-PEF incubation parameters (temperature, pH, homogeneity) on the recovery of proteins, especially C-PC, from Spirulina was investigated. The stability and purity of C-PC during incubation after PEF treatment are important for future industrial application of C-PC electroextraction from Spirulina. Additionally, the consequences of lowering the energy input to half of the original input needed to be analyzed to make the process more energy-efficient. From the extraction efficiencies and kinetics, several conclusions regarding cell death in Spirulina post-PEF treatment can be inferred. The cyanobacterium Spirulina and the chlorophyte *C. vulgaris* can be compared regarding the transferability of cellular mechanisms of cell death and different electroextraction protocols.

3.1.2. Characterization of type of PEF induced cell death in *C. vulgaris*

Since the behavior of cells during and after PEF treatment most likely depends on their developmental state, different ways of cultivation were employed. The first way of cultivation under continuous light resulted in a sigmoidal growth curve with an exponential and a stationary growth phase. Synchronization of cell culture could be achieved by applying a light-dark cycle combined with daily dilution of the cell culture. This second cultivation method resulted in cell division that is limited to a narrow period just before the onset of illumination. Cells taken at a certain time point are predominantly in a defined developmental state and different

developmental states can be compared by analyzing cells harvested at different time points. This way of cultivation allowed to observe whether cell death after PEF treatment depends on the time point within the cell cycle. In a next step, the establishment of a robust method to monitor cell viability after PEF treatment was needed. For this purpose, a viability probe for plant cells called fluorescein diacetate (FDA) was used. Statistically significant quantification could be achieved via flow cytometry. Then the experimental system needed to be adjusted with PEF treatment parameters at an energy threshold where part of the cells stayed viable. This standardizing of response to PEF treatment allowed for quantitative physiology. As introduced in the previous chapter, PCD is a strictly regulated destruction of the cell. Several factors involved in PCD processes (e.g., role of actin, generation of ROS, cytochrome f release) could be analyzed after sublethal PEF treatment in *C. vulgaris* to pinpoint specific molecular players.

3.1.3. PEF treatment extracts a cell-death inducing factor from *C. vulgaris*

Furthermore, one of the most important discoveries of this work was the detection of a water-soluble factor released by PEF treated cells inducing cell death of untreated cells. The term **cell-death inducing factor (CDIF)** was introduced and its phenomenology thoroughly studied. A closer look at the formation of the CDIF in donor cells releasing this factor as well as on the signal perception in recipient cells was taken. The evolutionary context of such a cell-death inducing factor putatively contributing to PCD was discussed. Based on this knowledge a working model of electroporation-induced cell death in *C. vulgaris* has been proposed.

3.1.4. Improvement of protein extraction efficiency in *C. vulgaris*

With the knowledge collected from the bulk of the experiments and putative model, the objective laid in improving the already existing electroextraction protocols established for *C. vulgaris*. For this purpose, protein recovery efficiency in dependence of energy input needed to be tested. With these results, it might be possible to change the biotechnological strategy and administer PEF treatment at lower energy utilizing CDIF related cell death. Furthermore, the processing step using PEF treatment is discussed in the context of the whole value chain of microalgae cultivation and possible industrial applications.

4. Material and methods

Some passages in this chapter have been quoted verbatim or have been reworked and expanded from the following source: Krust *et al,* 2022

4.1. Cultivation of microalgae

4.1.1. Cultivation of *C. vulgaris* under continuous light

Chlorella vulgaris (strain 211-12, SAG, culture collection of algae, Göttingen, Germany) cells were inoculated in 1× Tris-Acetate-Phosphate (TAP) medium (**Supplementary Table 1**) and grown in 1 l Erlenmeyer glass flasks (cultivation volume 400 ml). After inoculation to an initial optical density at 750 nm (OD_{750}) of 0.1, the suspension culture was cultivated at 23 °C for 7 days post inoculation (dpi) under constant exposure to light (photosynthetically active radiation (PAR) 90 $\mu mol \cdot m^{-2} \cdot s^{-1}$) and shaking at 150 rpm. For routine laboratory cultivation, OD_{750} is widely used to monitor microalgal growth since it is inexpensive and reliable. Measurement at this wavelength avoids the absorbance of light by cellular pigments (chlorophyll and carotenoids) and is treated as a pure light scattering measurement (Chioccioli *et al,* 2014). When recording a growth curve, OD_{750} was used to monitor cell density, additionally, pH and conductivity of the medium were used to monitor consumption of nutrients (**Figure 9**). The growth curve of cultivation under continuous light shows a characteristic sigmoidal form with an exponential growth phase from 0-4 dpi and reaching a stationary growth phase (>5 dpi) mostly due to limiting nutrient supply and mutual shading of the cells. The TAP medium contains acetic acid as an organic carbon source and in combination with exposure to light this leads to mixotrophic growth of the algae. The rising pH during cultivation shows the consumption of acetic acid resulting in the alkalinization of the culture. Decreasing conductivity is caused by nutrient consumption. During the stationary phase, the population is composed of cells in different stages of the cell cycle.

The average cycling time can be calculated by plotting the natural logarithms of the optical density measurements against time in the exponential growth phase (0-4 dpi). In this plot, the slope (calculated via linear regression) constitutes the time constant *k*. From the value of *k*, the doubling time τ (= duration of the cell cycle) can be derived as follows: $\tau = \ln(2)/k$. For *C. vulgaris* with cultivation under continuous light, the duration of the cell cycle is around 20 h.

Cells were counted using a cell counter (CASY Model TT System, Roche Diagnostics GmbH, Germany) and a representative size distribution of *C. vulgaris* in the stationary phase 7 dpi is shown in **Figure 10A**. The average cell size was around 3 µm. The shoulder at the right flank of the

distribution is due to the formation of some aggregates as confirmed by bright-field microscopy (Axio Imager.M2 with 63× objective LD Plan-NEOFLUAR, Zeiss, Jena, Germany) (**Figure 10B**).

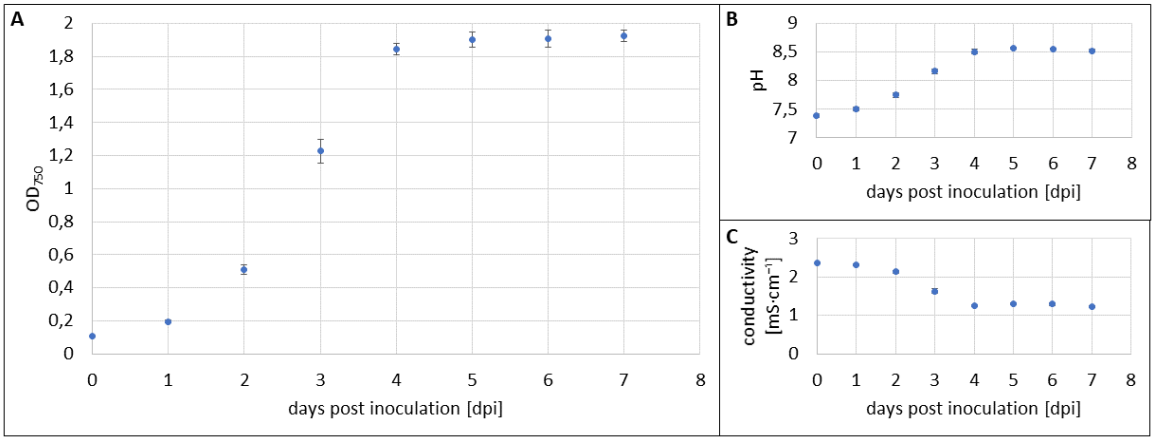

Figure 9 Growth curve of *C. vulgaris* for cultivation under continuous light over the period of one week. **A)** Optical density at 750 nm (OD_{750}), **B)** pH shift during cultivation time and **C)** conductivity shift during cultivation time. Data represent averages and standard errors from at least three biological replicates.

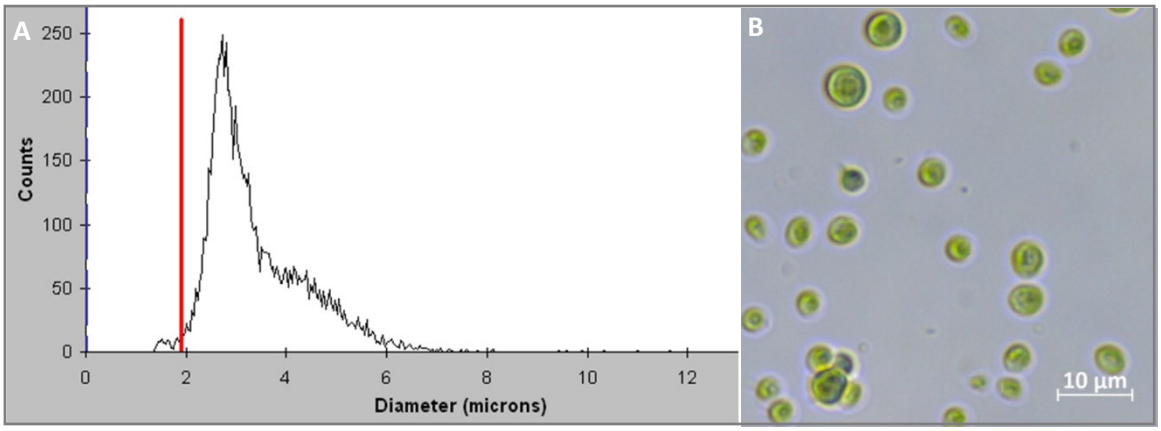

Figure 10 Monitoring of cultivation with cell counting and microscopic imaging. **A)** Size distribution of *C. vulgaris* in the stationary phase 7 days post inoculation measured with CASY cell counter, micron = µm **B)** Microscopic imaging of *C. vulgaris* cells, pictures were acquired using Axio Imager.M2 (bright-field). Data represents a representative from three biological replicates.

4.1.2. Cultivation of *C. vulgaris* in a synchronized culture

For synchronization, *C. vulgaris* was inoculated in TAP medium (**Supplementary Table 1**) to a cell count of $2 \cdot 10^6$ cells·ml^{-1} (≈ OD_{750} 0.05) in 500 ml glass flasks (cultivation volume 200 ml) and then cultivated under a light-dark cycle (12 h : 12 h). For this purpose, a manually constructed dark chamber with constant ventilation for cooling during the light period was used (**Figure 11B** and **C**). Hereby, cells grew under a lower PAR (65 µmol·m^{-2}·s^{-1}), again under shaking at 150 rpm and with temperatures ranging from 23 to maximal 25 °C. The culture was diluted to the initial density ($2 \cdot 10^6$ cells·ml^{-1}) prior to the onset of each light period. After 2 weeks of these cycles, the culture

was considered synchronous as verified by flow cytometry and microscopy. In a synchronized culture, cell division is restricted to a short period just before the onset of light (**Figure 11A**). By this procedure, the culture is always kept in the exponential growth phase, such that samples collected at different time points during the synchronization cycle are in a defined developmental state that proceeds with the time of sampling (Carroll *et al,* 1970; Senger *et al,* 1972; Lorenzen & Hesse, 1974; Chioccioli *et al,* 2014).

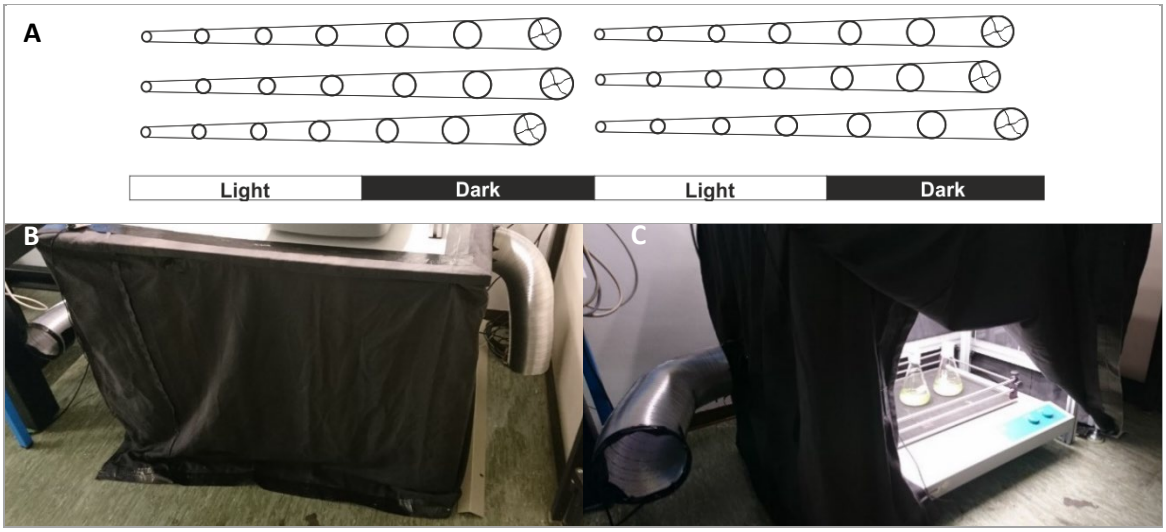

Figure 11 Establishment of a synchronized cell culture. **A)** Diagram showing the experimental design, redrawn from Senger *et al* (1972), p. 304. **B)** and **C)** Custom-made dark chamber with constant ventilation to achieve synchronized cultivation.

4.1.3. Cultivation of *A. platensis*

The cyanobacterium *Arthrospira platensis* (SAG strain 21.99) was inoculated in Full Zarouk medium (**Supplementary Table 2**) and grown in 1 l Erlenmeyer glass flasks with a cultivation volume of 400 ml. The culture was inoculated to an initial OD_{750} of 0.1 and the medium provided elevated pH and salinity with an initial pH of 9.2 and initial conductivity of 21 $mS \cdot cm^{-1}$ at the start of cultivation. The suspension culture was cultivated at 23 °C for 7 dpi under constant exposure to light (PAR 90 $\mu mol \cdot m^{-2} \cdot s^{-1}$) and shaking at 150 rpm. After 7 dpi the cells were in the stationary phase and harvested with OD_{750} increased to 1.5, pH elevated to 11.5 and conductivity slightly risen to 22.5 $mS \cdot cm^{-1}$. From the following, *A. platensis* will be only called Spirulina.

4.1.4. Cultivation of *S. almeriensis* and *A. protothecoides*

The green microalgae *Scenedesmus almeriensis* (strain CCAP 276/24, Culture Collection of Algae and Protozoa of the Centre for Hydrology and Ecology, Ambleside, U.K.) cells were inoculated in 1× Arnon medium (Arnon *et al,* 1974) and grown in round glass flasks. The medium provided an elevated pH of 9-10 at 25 °C and the suspension culture was bubbled with air at the rate of 5000 $cm^3 \cdot min^{-1}$ to prevent cell sedimentation. After 7 dpi under constant exposure to light (PAR

50–80 µmol·m^{-2}·s^{-1}) at 23 °C, the cells were harvested while still in exponential growth phase (Akaberi *et al,* 2019).

Auxenochlorella protothecoides (SAG strain 211-7a) were grown mixotrophically in a modified Wu medium (170 mM glucose, 5 mM KH_2PO_4, 1.7 mM K_2HPO_4, 1.2 mM $MgSO_4$, 10 µM $FeSO_4$, 1 mM glycin and 4 g·l^{-1} of yeast extract) with a pH of 6.8 ± 0.1. After inoculation to an initial OD_{750} of 0.1 in 1 l conical polycarbonate cultivation flasks, the suspension culture was cultivated at 23 °C for 10 dpi under constant exposure to light (60 µmol·m^{-2}·s^{-1}) and shaking at 100 rpm. The cells were harvested at the beginning of the stationary phase after the glucose in the medium was exhausted (Silve *et al,* 2018b; Papachristou *et al,* 2020).

4.1.5. Harvest and determination of cell dry weight

Eukaryotic microalgae cells (*C. vulgaris*, *S. almeriensis* and *A. protothecoides*) were harvested by centrifugation at 10,000 g for 2 min at 23 °C (Heraeus Primo Centrifuge, fixed-angle rotor, Thermo Scientific), and the suspension adjusted to the desired concentration. Harvest of Spirulina was conducted slightly varied by centrifugation at 10,000 g for 12 min at 10 °C. The pelleted Spirulina cells were washed using phosphate buffer saline (PBS) at pH 7.2 containing 0.39 µM NaH_2PO_4 and 0.55 µM Na_2HPO_4 (conductivity 0.1 mS·cm^{-1}). Washing was repeated once or twice until reaching the desired conductivity of 1.7 mS·cm^{-1}, this modified PBS buffer containing Spirulina is called initial buffer (IB). The filamentous structure of Spirulina leads to easy aggregation, especially after centrifugation. Homogenization was achieved either by carefully pipetting up and down with a 50 ml pipette or by addition of magnetic fish and stirring for at least 5 min. The suspensions were then adjusted to the desired concentration.

The cell dry weight (CDW) was determined by weighing 3 ml of wet concentrated algae suspension and 3 ml of medium from the supernatant in aluminum plates. The wet suspensions were dried at 85 °C using a circulation air oven (ULP 500, Memmert, Germany) After weighing the dry algae suspension and dry medium, the dried biomass can be calculated with equation (3):

$$\mathrm{CDW}\left[\frac{\mathrm{mg}}{\mathrm{g}_{sus}}\right] = \frac{m(algae,\ dry)}{m(algae, wet)} \cdot 1000 - \frac{m(medium,\ dry)}{m(medium, wet)} \cdot 1000 \qquad (3)$$

The samples were weighed before and after drying with a fine balance (AE163, Mettler-Toledo, Switzerland). Taking the density of water and thereof derived the algae suspension (ρ = 1 g·ml^{-1}) into account, CDW can be expressed in mg·g_{sus}^{-1} ≙ mg·ml^{-1} – the second unit will be used throughout this thesis.

Since CDW is proportional to cell density and therefore to measurements of OD_{750}, a calibration curve can be drawn with sufficient data input and then be used for quick estimation of *C. vulgaris* CDW via simple measurement of OD_{750}. (**Figure 12**).

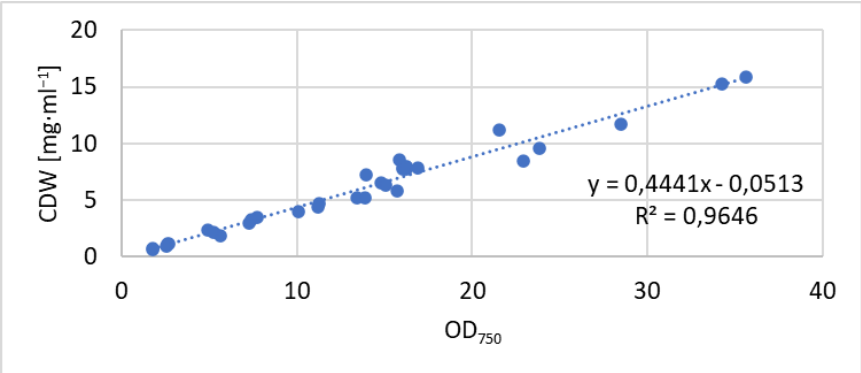

Figure 12 Calibration curve for quick estimation of *C. vulgaris* CDW via optical density measurement at 750 nm (OD_{750}).

4.2. Cell disruption methods

For mechanical cell disruption, high-pressure homogenization (HPH) was employed. The cell suspension was passed through a high-pressure homogenizer (EmulsiFlex-C3 homogenizer, Avestin, Canada) at 2000 bar with 5 cycles under constant cooling on ice. Afterward cell debris was removed by centrifugation (10,000 g, 10 min, 4 °C, Heraeus Megafuge 8R, fixed-angle rotor, Thermo Scientific). This method had been demonstrated to allow complete diagnostic access to the entire protein content of the sample (Scherer *et al,* 2019).

To disrupt the cells by PEF treatment, there were two setups. Depending on the sample volume and the desired electroporation parameters, PEF treatment was performed in continuous flow or in batch treatment with commercial cuvettes. For calculation of the specific energy ΔW_{spec} delivered to the sample, the parameters of initial conductivity of the suspension σ, pulse duration Δt, electric field strength E_{ext} and number of impulses N are required. Since densely packed cells behave differently than practically isolated cells, the concentration of cells (volume fraction p) has to be considered and the following equation (4) applies only if $p < 0.20$.

$$\Delta W_{spec} = \sigma \cdot \Delta t \cdot E_{ext}^2 \cdot N \tag{4}$$

Table 1 shows exemplary parameters for each setup. In either setup, the algal suspensions had an initial temperature of 21 °C, while during pulse treatment with a maximum specific energy of 36.8 $J \cdot ml^{-1}$, the output temperature never exceeded 30 °C. For large volumes, the PEF treatment was conducted in continuous flow in a uniform-field flow chamber with a volume of 525 µl, enclosed by two planar stainless steel electrodes with a gap of 2 mm in-between (Goettel *et al,* 2013). The conductivity of *C. vulgaris* suspension (at stationary phase around 1.2 $mS \cdot cm^{-1}$, see

Figure 9C) was adjusted to 1.5 mS·cm^{-1} by adding the necessary amount of NaCl (end concentration 2.7 mM). For treatment, the suspension was pumped through silicon tubing by means of a peristaltic pump (MS-4/12-100 ISMATEC, Cole-Parmer GmbH, Wertheim, Germany). The flow rate was set to 3 ml·min^{-1} resulting in a retention time of 10.5 s in the flow treatment chamber. A transmission-line pulse generator delivered square pulses of 1 µs length. From a preparatory study adjusting treatment energies for *C. vulgaris* suspension, the parameters were set to a field strength of 20 kV·cm^{-1} and frequency of 1.5 Hz resulting in a specific treatment energy of 9.4 J·ml^{-1}. This specific energy was sufficient to induce subsequent cell death in *C. vulgaris*. For continuous flow treatment of Spirulina biomass, the field strength was set to 40 kV·cm^{-1}, leading to specific energies of 56 J·ml^{-1} (frequency 2 Hz) and 114 J·ml^{-1} (frequency 4 Hz). When pulsing volumes that were bigger than 50 ml, homogenization of the sample was achieved with a magnetic stirrer.

For batch treatment of *C. vulgaris*, commercially available electroporation cuvettes (Electroporation Cuvettes Plus, BTX Harvard Apparatus, Holliston MA, USA) with a treatment volume of 420 µl and a gap of 2 mm between the aluminum electrodes were used. In this setup, for both untreated and PEF treated samples the conductivity of the concentrated algal suspension was adjusted to 2 mS·cm^{-1}, using the necessary amount of NaCl (end concentration max. 7.3 mM). The field strengths were set to either 20 kV·cm^{-1} or 40 kV·cm^{-1}. Again, the electric field distribution in the treatment cuvette was uniform. Here, the specific energy was adjusted through the number of pulses, whereby each pulse was 1 µs long, delivered by a transmission-line pulse generator. Using a field strength of 20 kV·cm^{-1}, the specific energies ranged from 0.8 J·ml^{-1} with 1 pulse up to 36.8 J·ml^{-1} with 46 pulses, while at 40 kV·cm^{-1}, the specific energies ranged from 3.2 J·ml^{-1} (1 pulse) up to 150.4 J·ml^{-1} (47 pulses). For one experiment, part of the *C. vulgaris* suspension was diluted with sterile supernatant directly after PEF treatment and then both sets were incubated in parallel at 23 °C.

Table 1 Exemplary parameters of PEF treatment of *C. vulgaris* in continuous flow and batch treatment.

	Gap	Field strength	Pulse duration	Conductivity	Flow rate	Frequency	Number of pulses	Specific energy
Continuous flow	2 mm	20 kV·cm^{-1}	1 µs	1.5 mS·cm^{-1}	3 ml·min^{-1}	1.5 Hz	16	9.4 J·ml^{-1}
Batch treatment	2 mm	20 kV·cm^{-1}	1 µs	2.0 mS·cm^{-1}	-	-	2	1.6 J·ml^{-1}

4.3. Fluorescence microscopy

Invitrogen™ **Hoechst 33342**, Trihydrochloride, Trihydrate (Fisher Scientific GmbH) is a dye staining double-stranded DNA of the nucleus, plastids, and mitochondria. Cells from cultivation under continuous light as well as cells sampled at different time points from a synchronized culture were incubated with Hoechst in a working concentration of 8.1 µM in PBS buffer with 33 % dimethylsulphoxide (DMSO). After 10 min of incubation in the dark, cells were centrifuged (10,000 g, 2 min, 23 °C, Micro Star 17R, fixed-angle rotor, VWR), the supernatant discarded, and the cell pellet washed twice with PBS buffer. Microscopic imaging was performed using a fluorescence microscope (Axio Imager.M2, Zeiss with Compact Light Source HXP, LEJ, Jena, Germany) with 63× objective (LD Plan-NEOFLUAR, Zeiss, Jena, Germany). Chlorophyll autofluorescence was recorded after excitation in the range of 625-655 nm (exposition time: 600 ms) by collecting an emission wavelength of 665-715 nm. For detection of Hoechst, excitation was at 335-383 nm (exposition time: 150 ms) and emission in the range of 420-470 nm.

FDA is a non-fluorescent, cell permeating esterase substrate for the intracellular esterases of living cells that cleave FDA to fluorescein, which yields a fluorescent readout for viability and cell membrane integrity by retention of the fluorescent product. This assay has allowed measuring algal esterase activity in several microalgae including *C. vulgaris* (Regel *et al,* 2002; Hadjoudja *et al,* 2009). For microscopic imaging of *C. vulgaris,* a stock solution of 10 mM FDA in 100 % DMSO was used and staining of cells (cultivated under continuous light) was achieved using a working concentration of 100 µM FDA in 1 % DMSO. The cells were incubated in the dark for 5 min and afterward, without washing, directly analyzed under the fluorescence microscope (ApoTome Axioplan 2 imaging, Zeiss, Jena, Germany) with 63× objective (LD Plan-NEOFLUAR, Zeiss, Jena, Germany). Chlorophyll autofluorescence was recorded after excitation in the range of 625-655 nm (exposition time: 300 ms) by collecting an emission wavelength of 665-715 nm. Fluorescein fluorescence was recorded after excitation in the range of 450-510 nm (exposition time: 10 ms) by measuring at emission wavelength spanning from 500-550 nm. As a control sample for negative signal (100 % dead cells), one part of the cells was incubated at 100 °C for 10 min and after cooling down again stained accordingly with FDA.

4.4. Viability assays

4.4.1. FDA staining

To quantify the viability of *C. vulgaris* by flow cytometry, the following FDA staining method was established. A stock solution of 1 mM FDA (Thermo Fisher Scientific) was prepared in 100 % DMSO and kept at 4 °C until use. Using sterile supernatant, the algae suspension was diluted to an OD_{750}

of 0.1-0.2. FDA staining was achieved using a working concentration of 50 µM FDA in 5 % DMSO. The stained sample was incubated for 5 min in the dark and after incubation, the sample was diluted by factor 10 with Attune™ Focusing Fluid 1× (Thermo Fisher Scientific). Then, the fluorescein signal was quantified using a flow cytometer (Attune™ Nxt, Thermo Fisher Scientific) equipped with a blue argon ion laser (excitation at 488 nm). Cell debris particles were excluded from analysis by gating the homogenous population visible in the forward scatter (FSC) versus side scatter (SSC) histogram, one way to visualize the size and complexity of the measured particles (**Figure 13A**). Furthermore, cell aggregates were excluded by plotting a histogram of the forward scatter area signal (FSC-A) versus the forward scatter height signal (FSC-H) to use area scaling to gate only individual particles for analysis (**Figure 13B**). Chlorophyll autofluorescence is also excited by the blue laser and can be detected using a far-red bandpass filter of 695±40 nm (BL3-H). A positive chlorophyll *a* fluorescence allowed to select microalgae cells for analysis (**Figure 13C**). Summing up, only single cells of the correct size with a positive chlorophyll signal were used for further analysis of the fluorescein signal. Green fluorescence from fluorescein was recorded through a bandpass filter of 530±30 nm (BL1-H).

The sample volume yielded more than 100,000 events for analysis with a flow rate of 1000-2000 events per second. After data collection, the data was displayed as histograms showing BL1-H (height of fluorescein fluorescence signal in logarithmic mode) versus count (linear mode, **Figure 13D**). Cells with a signal higher than 10,000 (BL1-H) were defined as viable and the percentage of viable cells over the total analyzed cell number was calculated as readout for viability (in %). The mortality rate (in %) can be calculated by subtracting the value for viability from 100 and is used partially in the thesis.

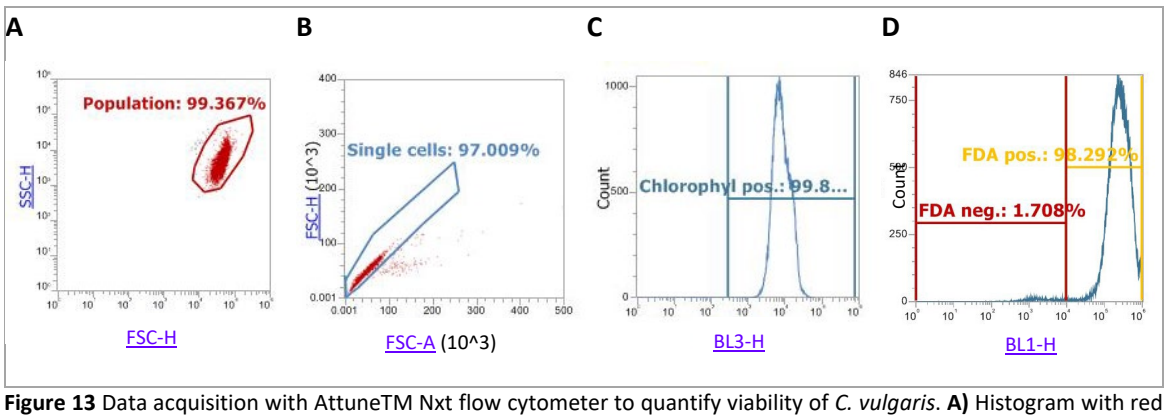

Figure 13 Data acquisition with AttuneTM Nxt flow cytometer to quantify viability of *C. vulgaris*. **A)** Histogram with red polygonal gate showing population visible in forward scatter (FSC-H) versus side scatter (SSC-H). **B)** Histogram of forward scatter area signal (FSC-A) versus forward scatter height signal (FSC-H) with blue polygonal gate selecting single cells for analysis. **C)** Histogram showing BL3-H (chlorophyll autofluorescence signal) versus count. **D)** Histogram showing BL1-H (height of fluorescein fluorescence) versus count with gate cutting at a signal higher than 10,000 (10^4) for determination of percentage of viable cells (FDA pos. = FDA positive; FDA neg = FDA negative).

4.4.2. YO-PRO staining

Green-fluorescent dye YO-PRO®-1 iodide (Fisher Scientific GmbH) stains DNA and can only enter permeabilized cells that are in the process of dying or already dead. A stock solution of 100 µM YO-PRO was stored at -20 °C. Prior to use the stock solution was thawed and diluted with KCl solution (2 $mS \cdot cm^{-1}$) to a concentration of 10 µM. The algae suspension was diluted to a biomass concentration of 0.1 $mg \cdot ml^{-1}$ using KCl-buffer. YO-PRO staining was achieved using a working concentration of 1 µM YO-PRO in algae suspension. The stained sample was incubated for 10 min in the dark and after incubation, the sample was diluted by factor 20 with Attune™ Focusing Fluid 1×. Then, the fluorescence signal was quantified using a flow cytometer, green fluorescence from YO-PRO was recorded through a bandpass filter of 530 ± 30 nm (BL1).

4.4.3. Evans Blue staining

Evans Blue is a non-permeable azo dye and staining can be used to analyze membrane integrity, showing damaged or non-viable cells with Evans Blue uptake. After different treatments (live: control, dead: 100 °C 10 min, PEF treatment in a cuvette at 1.6 $J \cdot ml^{-1}$ with 2 h incubation) an equal volume of 5 % Evans Blue solution (MW: 961 Da) was added to the cell suspension and vortexed. After 10 min incubation the cells were centrifuged (10,000 g, 2 min, 23 °C, Micro Star 17R, fixed-angle rotor, VWR), the supernatant discarded, and the cell pellet washed twice with cultivation medium. Microscopic imaging was performed using a microscope (Axio Imager.M2, Zeiss, Jena, Germany) with 63× objective (LD Plan-NEOFLUAR, Zeiss, Jena, Germany). Cells were counted and the permeabilization efficiency was calculated by dividing the number of stained cells by the number of total cells multiplied by 100.

4.5. Incubation conditions after PEF treatment

4.5.1. Spirulina

After treatment, Spirulina samples were incubated at different conditions while protected from light by covering them in aluminum foil. To study the effect of temperature on protein and C-PC release, the CDW of fresh Spirulina biomass was adjusted to 7.96 ± 0.43 $mg \cdot ml^{-1}$. PEF-treated samples were incubated in initial buffer under agitation at 4 and 23 °C in dark. As benchmark for total protein and C-PC content, HPH extract was similarly incubated in initial buffer under agitation at 23 °C in dark. Samples were taken 1, 2, 3, 4, 6 and 24 h post-treatment. The supernatant was then analyzed for protein and C-PC content.

For incubation in pH-buffers, samples were centrifuged immediately after PEF treatment (10,000 g, 12 min, 10 °C, Heraeus Primo Centrifuge, fixed-angle rotor, Thermo Scientific). The

supernatant was exchanged with the desired pH-buffer (100 mM sodium phosphate buffer at pH 6 or pH 8), the cells were resuspended and kept under agitation at 23 °C in dark. For comparison, resuspension and incubation in the initial buffer were executed as well. Not only did the buffers change the pH of the external medium, but they had an increased conductivity of 7 $mS \cdot cm^{-1}$ (pH 6) and 11.9 $mS \cdot cm^{-1}$ (pH 8) respectively and therefore the ionic strength of the medium was increased compared to the initial buffer with 1.7 $mS \cdot cm^{-1}$. Samples were taken every hour till 5 h post-treatment and after 24 h. The supernatant was then analyzed for protein and C-PC content.

4.5.2. Factors influencing the viability of *C. vulgaris*

Energy variations

To thoroughly study the factors influencing the viability of *C. vulgaris* after PEF treatment, PEF treatment parameters needed to be adjusted in a way that a set ratio of cells undergo cell death after treatment, while the other part stays viable. The high energy input (150 $J \cdot ml^{-1}$) of previous studies was used because based on empirical data, these parameters ensure that all cells are irreversibly permeabilized (Eing *et al,* 2013; Goettel *et al,* 2013; Frey *et al,* 2013) and thus were also applied for other works from this group (Silve *et al,* 2018b; Scherer *et al,* 2019). To find the threshold energy input at which *C. vulgaris* cells partially survive, the specific energy subjected to the cell suspension was varied by reducing the number of pulses. At first, the energy input was reduced up to factor 15 with a range from 150 $J \cdot ml^{-1}$ to 10 $J \cdot ml^{-1}$ and the viability of the cells was monitored over a period of 24 h (**Figure 14A**). This first energy variation already shows that even with the lowest energy input of 10 $J \cdot ml^{-1}$ no difference in long-term viability can be seen compared to the highest energy input. The lowest energies show slightly increased survival in the first hour due to recovery, but not later than 2 h after PEF treatment, almost 100 % of cells are inactivated. From this experiment, it was concluded that determination of post-PEF viability is sufficient after 2 h incubation. When reducing the energy further to a range of 3.2 $J \cdot ml^{-1}$ to 0.5 $J \cdot ml^{-1}$ (**Figure 14B**), partial survival is visible starting at the specific energy of 1.6 $J \cdot ml^{-1}$. The energy input of 1.0 $J \cdot ml^{-1}$ and lower resulted in survival of 80 % and higher. Since standardizing of the response to PEF treatment is necessary for quantitative physiology, the specific energy of 1.6 $J \cdot ml^{-1}$ was selected for the majority of the following experiments. This low energy input led to a viability rate of around 40-60 % of cells and for further dissection of the response of *C. vulgaris*, a time course of FDA and YO-PRO staining was performed covering a period of 6 h (**Figure 14CD**). FDA staining shows a slight lag phase in the first 30 min most likely due to still active enzymes in already permeabilized cells (**Figure 14C**). YO-PRO staining shows the counterpart to viability with around 60 % mortality, converted into viability for direct comparison in **Figure 14D**. Here, staining of cells is possible immediately after PEF treatment since the entrance of this dye is dependent on cell

permeabilization which is a direct result of electroporation. In conclusion, it can be said that PEF treatment with energy input at survival threshold (1.6 J·ml^{-1}) leads to a stable ratio of cells that undergo cell death after treatment, while the other part stays viable.

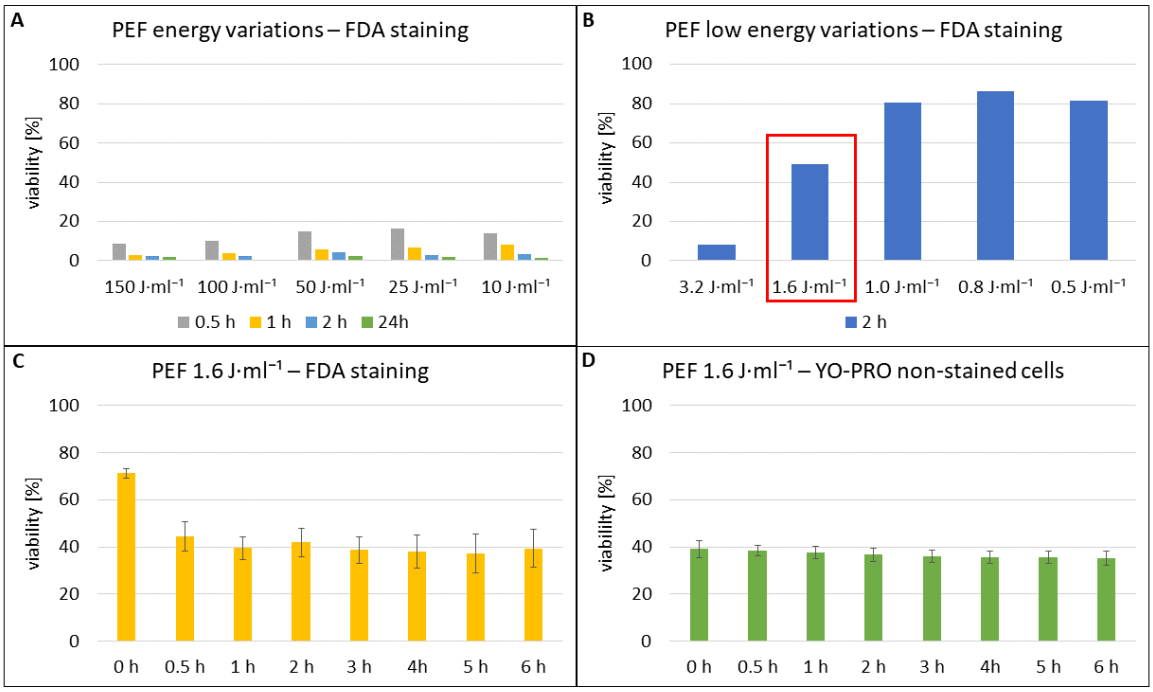

Figure 14 Determination of energy input at survival threshold using *C. vulgaris* cultivated under continuous light and in the stationary phase (7 dpi). **A)** PEF treatment with different specific energies ranging from 150 J·ml^{-1} to 10 J·ml^{-1} followed by incubation over 24 h at 23 °C while measuring viability at 0.5, 1, 2 and 24 h via FDA staining (500 µM) **B)** PEF treatment with different specific energies ranging from 3.2 J·ml^{-1} to 0.5 J·ml^{-1} followed by 2 h incubation at 23 °C and viability assay via FDA staining (500 µM) **C)** PEF treatment (1.6 J·ml^{-1}) followed by incubation over 6 h at 23 °C while measuring viability via FDA staining (500 µM). The experiment was performed in quadruplicate. Error bars represent standard errors. **D)** PEF treatment (1.6 J·ml^{-1}) followed by incubation over 6 h at 23 °C while measuring mortality via YO-PRO®-1 iodide staining (1 µM), data shown of non-stained cells. The experiment was performed in duplicate. Error bars represent standard errors.

Inhibitor experiments

To test the effect of Gadolinium (III) chloride ($GdCl_3$) as calcium channel inhibitor, *C. vulgaris* from a synchronized culture (time point 0 h, biomass around 0.2 mg·ml^{-1}) were incubated with $GdCl_3$ (50 µM, Sigma-Aldrich, Germany) and immediately pulsed with two specific energies at the survival threshold (0.8 J·ml^{-1} and 1.6 J·ml^{-1}). Viability was measured via FDA assay 3 h after PEF treatment. The compound diphenyleneiodonium chloride (DPI) inhibits oxidative burst by plasma membrane bound NADPH oxidases (O'Donnell *et al,* 1993). The stress signal phosphatidic acid (PA), generated by phospholipase D (PLD), can be inhibited by n-butanol (Testerink & Munnik, 2005). PLD uses n-butanol as an acceptor of the transphophatidylation reaction instead of water and consequently, inactive phosphatidyl alcohols are generated. For assessing the role of actin filaments,

latrunculin B (LatB) was used to inhibit actin polymerization (Morton *et al,* 2000). To modulate plasma membrane fluidity (Sangwan *et al,* 2002; Wang & Nick, 2017; Guan *et al,* 2021), membrane rigidifier DMSO, a polar aprotic solvent, can be used (Notman *et al,* 2006). In contrast, membrane fluidizer benzyl alcohol (BA), an amphiphilic molecule, affects bilayer structures in the opposite direction (Ebihara *et al,* 1979). To test the effect of these inhibitors and membrane modulators, *C. vulgaris* from cultures grown under continuous light (7 dpi), as well as from a synchronized culture (time points -6, 0 and 6 h), were used with normalized biomass around 0.2 mg·ml^{-1}. Samples were incubated with either DPI (20 µM, Sigma-Aldrich, Germany), n-butanol (0.5 %, Merck, Germany), tert-butanol (0.5 %, Merck, Germany), LatB (2 µM, Sigma-Aldrich, Germany), DMSO (2 %, Roth, Germany) or BA (25 mM, Roth, Germany). After 30 min incubation with inhibitor or membrane modulator, the cell suspensions were pulsed with the energy input at the survival threshold (1.6 J·ml^{-1}). Viability was measured via FDA assay 0.5, 1.5, 6 and 24 h after PEF treatment.

4.6. Protein and phycocyanin quantification

After PEF treatment, the algae suspension remained at 23 °C (if not indicated otherwise) to allow for the release of proteins up to 24 h for a time response experiment. In contrast, protein content in HPH samples was measured directly after treatment. Prior to the determination of protein concentration, *C. vulgaris* cells were centrifuged at 10,000 g for 10 min at 23 °C and Spirulina cells were centrifuged at 12,300 g for 20 min at 10 °C, (Heraeus Primo Centrifuge, fixed-angle rotor, Thermo Scientific). Protein quantification in the supernatant was executed with a modified protocol of the Lowry Assay (Detergent Comatible, DC™, BioRad, Munich) according to the manufacturer's protocol. Using this assay, color development is primarily due to several reduced species which have a characteristic blue color. The protein concentration could be determined by measuring the absorbance at 750 nm photometrically by either using cuvettes (UV-spectrophotometer, Genesys 10S UV-VIS, Thermo Scientific) or using a microplate reader (Varioskan™ Lux multimode microplate reader, Thermo Scientific). The readout was calibrated using a standard curve with a serial dilution of BSA (bovine serum albumin) and was normalized to CDW. C-phycocyanin concentration in Spirulina supernatant could be determined by measuring absorbances at 652 and 620 nm and by use of following equations (5) and (6) (Bennett & Bogorad, 1973; Yoshikawa & Belay, 2008):

$$C-PC\ [\mathrm{mg}\cdot\mathrm{ml}^{-1}] = \frac{A_{620}\ - 0.474\cdot\ A_{652}}{5.34} \tag{5}$$

$$C-PC\ [\%\ \mathrm{CDW}] = \frac{C-PC\ [\mathrm{mg}\cdot\mathrm{ml}^{-1}]}{CDW\ [\mathrm{mg}\cdot\mathrm{ml}^{-1}]}\cdot 100 \tag{6}$$

Additionally, the absorbance spectra from 250 to 750 nm can be evaluated and the purity of the crude extract can be monitored by measuring the purity ratio of A_{620}/A_{280} according to Patel *et al,* 2005.

4.7. SDS-PAGE and western blot

Qualitative analysis of proteins can be achieved by conducting sodium dodecyl sulfate polyacrylamide gel electrophoresis (SDS-PAGE). First, the protein sample was mixed in 4:1 ratio with 4× Lämmli buffer (200 mM Tris-HCl, 8 % (w/v) SDS, 40 % (v/v) glycerol, 4 % (v/v) ß-mercaptoethanol, 0.8 % (w/v) bromphenol blue). The mixture was heated at 95 °C for 15 min (Laemmli, 1970). 25 µl of the sample was loaded onto the SDS-PAGE gel (12 % or 15 %) submerged in running buffer (25 mM glycine, 192 mM tris, 0.1 % SDS). The gel was run for 2 h at 100 V (BioRad). Afterward, the gel was stained with Coomassie blue colloidal (Candiano *et al,* 2004) overnight and on the next day washed with dH_2O.

As alternative to Coomassie blue staining, the size-separated proteins in the gel can be blotted onto a nitrocellulose membrane (Roth, Roti®-NC 0.45). After submerging the closed blotting chamber into ice-cooled transfer buffer (20 mM tris, 150 mM glycine, 20 % (v/v) methanol, 0.02 % (w/v) SDS), the protein was transferred from the gel to the membrane at 100 V for 1 h (BioRad). The complete transfer was verified by staining the membrane with Ponceau S (2 % (w/v) ponceau S, 30 % (w/v) trichloroacetic acid, 30 % (w/v) sulfosalicylic acid) for 1 min and subsequent washing with water. Unspecific binding was blocked by incubating the membrane in 10 ml of Baileys® Original Irish Cream for 30 min. The membrane was washed (3x 5 min) with 1× TBS-T (tris buffered saline, 50 mM tris-HCl pH 7.4, 150 mM NaCl, 0.1 % (v/v) tween-20) and incubated with 10 ml of primary antibody (1:2000 in 1× TBS-T, 5 % BSA, 0.01 % Thimerosal) overnight at 4 °C under constant agitation. The antibodies used were raised against (1) cytochrome c (cyt c), Agrisera AS08 343A and (2) cytochrome f (cyt f), Agrisera AS06 119.

On the next day, the washing steps (3x 5 min with TBS-T) were repeated, and the membrane was incubated with the secondary antibody Goat anti-Rabbit IgG H&L (1:5000 in 1× TBS-T, 5 % BSA, 0.01 % Thimerosal; abcam ab6721) for 1 h at room temperature under constant agitation. The antibody was washed off (3x 5 min with TBS-T) and signal detection was conducted with 1-Step™ TMB-Blotting (Thermo Scientific). TMB solution (1 ml) was added onto the membrane and incubated for 5 min until a blue color appeared.

4.8. Measurement of reactive oxygen species

Samples were generated using synchronized cultures of *C. vulgaris* that were 50× concentrated, prior to PEF treatment in cuvettes. The specific energies used were 0.8 $J \cdot ml^{-1}$, 1.6 $J \cdot ml^{-1}$ and 8.0 $J \cdot ml^{-1}$. Directly after PEF treatment, the algal samples were re-diluted by the factor 50 to ensure a stable survival ratio over time. After 3 h of incubation, viability was determined via the FDA assay. Afterward, the algal suspension was centrifuged (10,000 g, 10 min, 23 °C, Micro Star 17R, fixed-angle rotor, VWR), and after discarding the supernatant and determining the fresh weight (fw), the algal sediment was frozen in liquid nitrogen. For processing, the algal precipitates were ground (TissueLyser; Retsch) with a 4 mm steel bead in 2 ml of 3 % trichloroacetic acid (TCA) in the reaction tube (twice for 30 s at 2 Hz). After removing the bead, the suspension was centrifuged at 10,000 g for 1 min and ROS levels were measured in the supernatant.

Lipid peroxidation: Malondialdehyde (MDA) is generated by lipid peroxidation of polyunsaturated fatty acids during oxidative stress. MDA reacts with thiobarbituric acid (TBA) to a product that serves as a photometrical readout (Heath & Packer, 1968). MDA content was determined by mixing 750 µl of the supernatant with 750 µl of TBA (0.5 % in 20 % TCA) and 75 µl of butylated hydroxytoluen (BHT, 4 % in absolute ethanol). This mixture was heated at 95 °C for 30 min, quickly cooled on ice, and then centrifuged (10,000 g, 30 s, 23 °C) before measuring the absorbances at 532 and 600 nm. MDA concentration was determined by dividing the difference in absorbance (A(532 nm) – A(600 nm)) by the molar extinction coefficient (155 $mM \cdot cm^{-1}$). The results were normalized to 1 g of fresh weight.

Hydrogen peroxide (H_2O_2): Superoxide is generated as the first stress signal after disruption of photosynthetic electron flow, but the molecule is very unstable. H_2O_2 is a breakdown product from superoxide dissipation. Steady-state levels of the more stable H_2O_2 report, therefore, the oxidative homeostasis of the chloroplast. H_2O_2 reacts with potassium iodide (KI), giving rise to a colored educt that can be determined photometrically (Velikova *et al,* 2000). H_2O_2 content was determined by mixing 750 µl of the supernatant with 750 µl of 1 M potassium phosphate buffer (pH 7.0) and 1.5 ml KI. After incubation in the dark for 3 h, absorbance at 390 nm was measured. For calibration, a serial dilution of H_2O_2 was measured and the results were normalized to 1 g of fresh weight.

4.9. PEF and HPH extract experiments (*C. vulgaris*)

The phenomenology of the CDIF was thoroughly studied by implementing the following experimental design. Differential generation in donor cells releasing this factor as well as influences like heat, cold, protease inhibition, or dilution were analyzed. Additionally, a closer look at signal perception in recipient cells was taken.

Experimental setup

The experimental setup is depicted in **Figure 15**. PEF extract was generated using *C. vulgaris* as donor cells grown either under continuous light or from a synchronized culture. The cell suspension was concentrated to high cell density (CDW of 7-10 mg·ml^{-1}) and PEF treatment was administered in cuvettes or continuous flow **(1)**. After 24 h of incubation at 23 °C, the PEF-treated and control sample were centrifuged at 10,000 g for 10 min at 23 °C (Heraeus Primo Centrifuge, fixed-angle rotor, Thermo Scientific) and the sediment discarded **(2)**. In the following, these extracts will be called PEF supernatant (PEF SN) and control supernatant (CTRL SN), respectively. HPH extract (HPH SN) was used as a positive control since it contained the entire content of the cell. To test the effect of these donor extracts, viable cells were used as recipients. Without further concentration, synchronized *C. vulgaris* provided biomass of around 0.2 mg·ml^{-1} at the beginning of the light cycle after dilution (time point 0 h, just after light induction; see **Figure 11A**). For comparison, viable cells from cultures under continuous light (undiluted or with normalized biomass concentration) were used. 900 µl of live recipient cells were centrifuged (14,000 g, 30 sec, 10 °C, Micro Star 17R, fixed-angle rotor, VWR) and the supernatant was discarded. Subsequently, different donor extracts were added to the remaining sediment of viable cells **(3)**. As a negative control, one recipient sample of viable cells remained with the original supernatant after centrifugation (called medium). Next, the sediments were resuspended using a vortex mixer and the suspensions incubated for up to 24 h while following the viability with the FDA assay **(4)**.

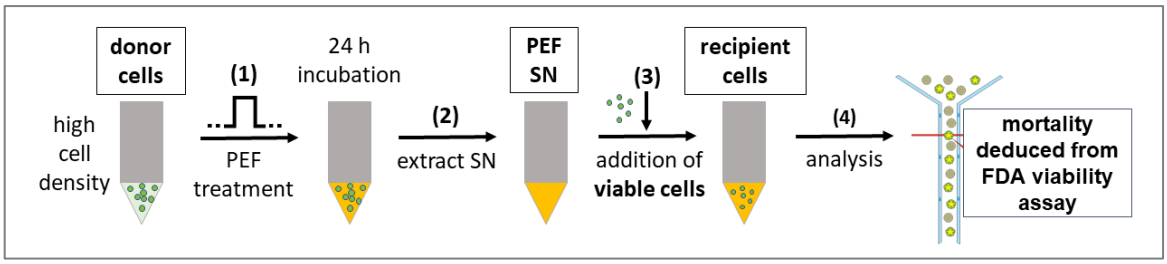

Figure 15 Schematic figure showing experimental setup. SN: supernatant, FDA: fluorescein diacetate. Modified from Krust *et al,* 2022.

PEF extract subjected to different treatments

First, PEF SN was generated as described above with donor cells from cultures grown under continuous light (7 dpi). Between steps 2 and 3, the generated extract was split into different reaction tubes (2 ml) for heating in water baths at 23, 40 and 50 °C for 2 h. In parallel, one batch of PEF SN was treated with a 1× cOmplete™ protease inhibitor cocktail (PI, Roche) for 2 h (23 °C). As a negative control, 2 ml TAP medium was mixed with 40 µl 50× PI to attain a control sample containing 1× PI (23 °C). After 2 h of respective incubation, the different extracts were added to viable recipient cells and the cells were resuspended using a vortex mixer. Viability was monitored at 4 h and 24 h via FDA assay. Secondly, extracts were generated with donor cells from cultures grown under continuous light (7 dpi) and added to viable cells as described above. Between steps 3 and 4, the suspension of viable cells in CTRL, PEF and HPH SN was incubated at 4 °C (fridge) for 24 h while following the viability via FDA assay. Thirdly, extracts were generated with donor cells from cultures grown under continuous light (7 dpi) as described above. Between steps 2 and 3, PEF and HPH SN were diluted using sterile TAP medium generating a dilution series with 1 : 2, 1 : 5, 1 : 10, 1 : 50 and 1 : 100 dilutions. The diluted extracts were added to viable recipient cells and viability was monitored at 4 h and 24 h via FDA assay.

Donor cell: analysis of the generation of the CDIF

Donor cells were either taken from *C. vulgaris* cultures grown under continuous light at different time points of the growth curve (2, 3, 4, 5 and 7 dpi), or from a synchronized culture (time point 0 h, just after light induction and time point 6 h after light induction; see **Figure 11A**), all with normalized CDW. Steps 1 to 4 was conducted as described above and viability was monitored at 4 h and 24 h via FDA assay.

Recipient cell: analysis of cell response to the CDIF

PEF SN was generated as described from steps 1 to 3 with donor cells from cultures grown under continuous light (7 dpi). At step 3, viable recipient cells were taken from synchronized cultures at different times of the cell cycle, the time points were set in the dark (- 6 h), at the onset of light (0 h) and 6 h into the light period (**Figure 11A**). Undiluted PEF SN and HPH SN diluted by factor 2 were added to viable recipient cells and viability was monitored at 4 h and 24 h via FDA assay.

Recipient cells from different species

An extract containing CDIF was tested on viable recipient cells from related species *S. almeriensis* and *A. protothecoides*. PEF SN and HPH SN was generated as described from steps 1 to 3 with *C. vulgaris* donor cells from cultures grown under continuous light (7 dpi). The biomass of both recipient algal species was diluted to 0.2 $mg \cdot ml^{-1}$ with cultivation medium to be able to compare

the different recipient cell types. *S. almeriensis* and *A. protothecoides* were incubated in their own cultivation medium, CTRL SN (TAP medium), PEF and HPH SN. Viability was monitored for 4 and 24 h via YO-PRO assay since the FDA assay is not established for those species and YO-PRO staining had been validated in previous studies of this lab (data not published).

Fractionation of protein content and mass spectroscopy analysis

PEF extract was fractionated using activity-guided size-exclusion chromatography (SEC). As the first step, fresh PEF extract from cultures grown under continuous light (7 dpi) was concentrated by ultrafiltration (Amicon Ultra-15, Merck, Germany) at 5,000 g for 20 min at 20 °C (Heraeus Primo Centrifuge, fixed-angle rotor, Thermo Scientific) resulting in first fractionation (protein concentration 12 $g \cdot l^{-1}$). In a next step, the cultivation medium was changed to SEC buffer (12.5 mM Tris, 1.25 mM EDTA, 75 mM NaCl, pH 7.8) using a NAP column (illustra NAP™-10, Cytiva, US) resulting in dilution of the sample (protein concentration 7 $g \cdot l^{-1}$ in SEC buffer). The size-exclusion chromatography was conducted using a Sephacryl S 300 column (GE Healthcare, Germany) at 4 °C and a protein elution profile was generated by measuring absorbance at 280 nm. After testing the separated protein fractions on viable recipient cells from a synchronized culture (*C. vulgaris*), the fractions containing the most potent activity were pooled and concentrated again by ultrafiltration cutting off smaller than 3 kDa (5,000 g, 100 min, 4 °C, protein concentration 1.5 $g \cdot l^{-1}$). This sample was sent to collaboration partners at Laboratoire de Spectrométrie de Masse Bio-Organique, Institut Pluridisciplinaire Hubert Curien (LSMBO-IPHC) at the University of Strasbourg, France to perform MALDI-TOF mass spectroscopy (Matrix Assisted Laser Desorption/Ionization, Time-Of-Flight) analysis.

5. Results and discussion

5.1. Optimization of electroextraction efficiency from Spirulina

Since PEF induced protein extraction efficiency for *C. vulgaris* was demonstrated to be driven by enzymatic autolysis (Scherer *et al,* 2019), the follow-up question pertained to whether this is transferable to other microorganisms in general. For this purpose, the extraction of proteins from the GRAS-certified cyanobacterium Spirulina was investigated. Since this organism also contains the highly valuable blue pigment C-phycocyanin, the extraction efficiency of C-PC after PEF treatment was analyzed.

5.1.1. Effect of incubation temperature

As the first step, the influence of varied incubation temperatures was investigated since the extraction kinetics are strongly dependent on this parameter. PEF treated Spirulina biomass (7.96 ± 0.43 mg·ml^{-1}) was incubated at 4 and 23 °C and the kinetics of protein and C-phycocyanin release into the external medium were determined as represented in **Figure 16**. The biomass incubated at 4 °C showed lower protein and C-PC recovery that cannot be compensated by an additional incubation step of 24 h after PEF treatment. Moreover, for both temperatures at least 24 h of incubation after PEF treatment is required to obtain comparable amounts of protein and C-PC as has been accomplished via HPH treatment. Therefore, for the following experiments, the temperature of 23 °C and timeframe of 24 h was chosen for post-PEF incubation.

HPH represents the benchmark for determination of the total protein and C-PC content in the sample and these values were similarly measured over time to compare the stability of proteins and C-PC in the HPH sample. The total protein and C-PC content in the HPH sample is highest just after cell disintegration, however, especially C-PC starts degrading as soon as 1 h after treatment. Based on this data, a mechanism for C-PC release is proposed. In general, two reaction kinetics are happening simultaneously: (1) C-PC is released over time, (2) released molecules undergo degradation due to unfavorable surrounding conditions (e.g., temperature, pH, ionic strength). Therefore, the reported value shown in the graphs can be inferred from equation (7) as the absolute C-phycocyanin concentration over time *t* (Akaberi *et al,* 2020):

$$[\mathrm{C-PC}](t)_{\mathrm{absolute}} = [\mathrm{C-PC}](t)_{\mathrm{released}} - [\mathrm{C-PC}](t)_{\mathrm{degraded}} \quad (7)$$

For the following experiments, the total protein and C-PC content was always measured immediately after HPH treatment, and this value was used as a benchmark.

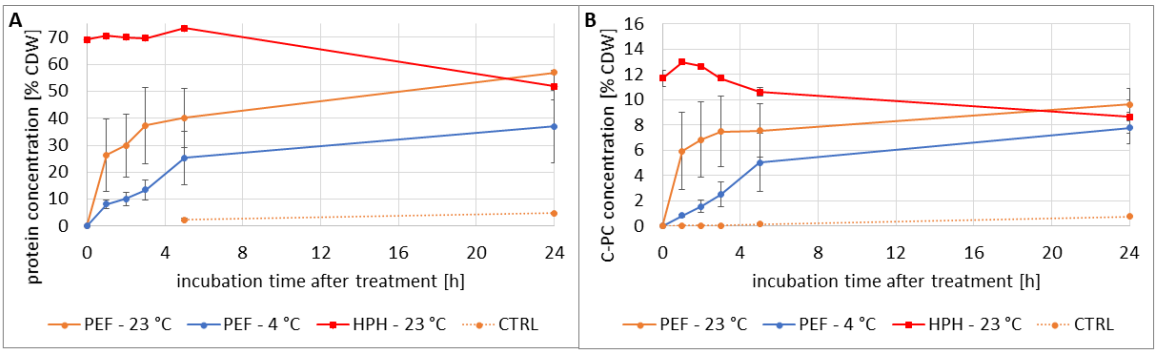

Figure 16 Effect of temperature on **A)** protein and **B)** C-phycocyanin release of Spirulina following PEF and HPH treatment. The biomass concentration was set to 7.96 ± 0.43 mg·ml^{-1} and PEF treatment was executed at 114 J·ml^{-1} followed by incubation of samples on a shaker (80 rpm) at specified temperatures (4 and 23 °C). High-pressure homogenization (HPH) represents benchmark for total protein and C-PC content in sample. CTRL: control without PEF treatment incubated at 23 °C. The experiment was performed in duplicate. Error bars represent standard errors.

5.1.2. Effect of the post-PEF incubation buffer

To gain insight into the influence of pH of the external medium, the effect of incubation in different pH-buffers (pH 6 and pH 8) on protein and C-PC liberation and the stability of the products during post-PEF incubation compared to incubation in the initial buffer were investigated. Incubating untreated biomass (CTRL) in pH 8 buffer resulted in partial protein and C-PC release during incubation. This can be attributed to mechanical influences of the magnetic stirring that effect the cells' integrity during the incubation period. Post-PEF incubation of Spirulina cells in pH 6- and pH 8-buffers at both low (3.62 ± 0.84 g·l^{-1}) and high (9.68 ± 0.58 g·l^{-1}) biomass concentrations enhanced the protein extraction efficiency (**Figure 17AC**). Both exchanged external mediums (pH 6 and pH 8) ultimately resulted in a higher protein content in the sample after 24 h incubation independent of the biomass concentration of the Spirulina suspension. In contrast, post-PEF incubation in the initial buffer showed a comparable increase of protein release at the beginning. However, the protein amount in the initial buffer diminished gradually over time and reached the lowest yield after 24 h of incubation caused by a partial decrease in protein concentration due to degradation. For low biomass concentrations (**Figure 17A)**, it could be observed that the pH of the PEF treated sample incubated in the initial buffer is considerably falling over time (initially: pH 10.5, after 24 h: pH 7.6). In contrast, the incubation-buffers had enough capacity to maintain the desired pH. This drastic shift of pH in the initial buffer can explain the visible degradation of protein. It has been shown that PEF-treated biomass incubated at pH 8.5 achieved a higher protein extraction yields than the PEF-treated biomass incubated in basic medium at pH 11.0 (Parniakov *et al,* 2015), which is in agreement with the high protein yield obtained in the current study when using pH 8-buffer. For high biomass concentrations (**Figure 17C)**, the amount of released protein

increases slower over incubation time and reaches the saturation phase later than observed for lower biomass concentrations.

When looking at C-PC extraction yield (**Figure 17BD**), relatively high amounts within 4 h post-PEF incubation could be obtained by incubation in pH 8-buffer. C-PC concentration of PEF-treated biomass incubated in pH 6-buffer increased more slowly, but steadily over time and ultimately yielded even higher C-PC concentrations. Although C-PC concentration of PEF treated biomass incubated in pH 8-buffer showed an initial fast increase, a decrease was also revealed for longer incubation periods. In contrast, incubation in pH 6-buffer showed no visible decrease, but a steady, slow increase of C-PC concentration over incubation time. Same observations could be made both for low and high Spirulina biomass concentrations regarding C-PC liberation and stability in pH-buffers. When looking at the incubation in the initial buffer, a strong decrease of C-PC content can be seen at low biomass concentrations starting at 3 h post-PEF (**Figure 17B**). The decrease in the initial buffer continued drastically and the lowest concentration was determined 24 h post-PEF treatment. Simultaneously, the blue color of C-PC visibly faded. This reduction of C-PC concentration incubated in the initial buffer caused by degradation could be attributed to the significant pH shift mentioned above. The integrity of C-phycocyanin can be altered by a medium exhibiting a pH far from the isoelectric point of C-PC of about 4.5 to 5.0 (Safaei *et al,* 2019). This would consequently affect C-PC stability, in accordance with the suggested mechanism of simultaneous release and degradation (equation (7)). The impact of the pH distance from the isoelectric point also explains the higher stability of C-PC in pH 6-buffer compared to pH 8-buffer that could be observed at both low and high biomass concentrations.

At high biomass concentrations, the drastic C-PC reduction in initial buffer as observed at low biomass concentration could not be seen, only a mild reduction in C-PC yield was observed (**Figure 17D**). In general, the kinetics of protein and C-PC release at high biomass concentration is significantly slower in comparison to the kinetics obtained at low biomass concentration. One possible reason can be a slower diffusion rate in concentrated biomass. A slower diffusion rate affects the number of liberated ions and charged molecules reducing the pH-shift. Another possible reason for the general improvement in C-PC stability at high biomass concentration can be attributed to the amount of released proteins. Since the data is normalized to biomass content, the absolute protein concentration is roughly three times higher in the samples with high biomass concentrations. It has been indicated that at high protein concentrations, C-PC is found in the stable structures of trimers or hexamers, whereas at low protein concentrations they dissociate to form unstable monomers (Houghton, 1996). When considering ionic strength during incubation, the initial buffer has a significantly lower ionic strength than the pH-buffers used in

this study. It is known that increased ionic strength positively influences C-PC aggregation state (Berns & MacColl, 1989). Therefore, it can be concluded that in the current study the relatively low ionic strength in the initial buffer also impairs C-PC stability. In contrast, incubation in pH-buffers with considerably higher ionic strength do not only impede the pH shift but also compensate for the low ionic strength. In conclusion, post-PEF incubation in pH-buffers enhanced the overall stability of C-PC.

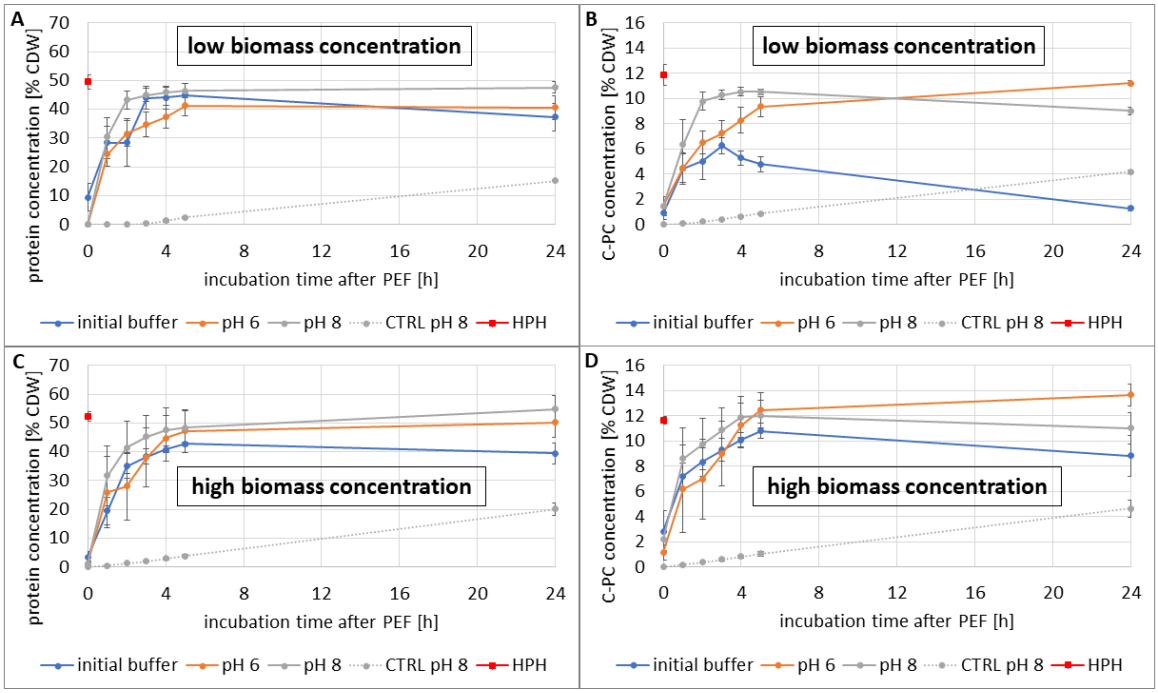

Figure 17 Effect of pH of the external medium at different biomass concentrations on protein and C-phycocyanin release of Spirulina following PEF treatment. **A)** Protein concentration and **B)** C-phycocyanin concentration at biomass concentration of 3.62 ± 0.84 g·l^{-1}. **C)** Protein concentration and **D)** C-phycocyanin concentration at biomass concentration of 9.68 ± 0.58 g·l^{-1}. PEF treatment at 114 J·ml^{-1} and incubation of samples with magnetic stirrer (150 rpm). High-pressure homogenization (HPH) represents benchmark for total protein and C-PC content in sample. CTRL pH 8: control without PEF treatment incubated at pH 8. The experiment was performed in triplicate. Error bars represent standard errors. Modified from Akaberi *et al,* 2020.

5.1.3. PEF treatment at lower energy input of 56 J·ml^{-1}

PEF energy demand was reduced by applying the lower energy input of 56 J·ml^{-1} to Spirulina with high biomass concentration (9.12 ± 0.16 mg·ml^{-1}). Protein and C-PC concentrations during the incubation period are shown in **Figure 18**. The kinetics of protein and C-PC release at this reduced treatment energy significantly differed from that obtained with PEF treatment at 114 J·ml^{-1}. No initial fast increase could be observed. The kinetics can be described as almost linear, especially compared to the exponential saturation curves shown in **Figure 17**. A longer incubation is mandatory for recovering the maximal protein and C-PC yield at lower energy input. Hardly any

advantage regarding incubation in pH-buffers could be observed at this high biomass concentration with reduced energy input. Regardless of the extraction kinetics, the maximum yields were obtained for all post-PEF incubation conditions. To obtain the maximum protein and C-PC yield at a low energy input of 56 J·ml^{-1}, a longer post-PEF incubation is necessary.

At reduced energy input, the slow increase towards the saturation value reached only after 24 h of incubation can be explained by ineffective membrane permeabilization resulting in reduced release of intracellular valuables. Higher energy input enables efficient permeabilization with a faster release of intracellular valuables into the medium, which results in a higher protein/C-PC extraction yield over a shorter post-PEF incubation period. In contrast, the lower energy input of 56 J·ml^{-1} provided comparable extraction rates only after longer post-PEF incubation, corresponding to inefficient permeabilization. PEF-treated Spirulina trichomes at both treatment energies were observed under the light microscope after 6 h. This observation revealed higher rate of cell rupture after PEF treatment at 114 J·ml^{-1} than after PEF treatment at 56 J·ml^{-1} (**Figure 19**). Though fragmented trichomes were visible at either treatment energy, the morphological alteration of the trichomes was more frequent for PEF treatment at 114 J·ml^{-1}. At either energy input, PEF treatment led to cell disruption and the release of intracellular valuables and cell debris.

It has been demonstrated that when reducing PEF treatment energy, post-PEF incubation is indispensable to enhance the diffusion process and obtain satisfactory release of intracellular valuables (Goettel *et al,* 2013; Coustets *et al,* 2015) or for achieving high lipid extraction yields (Silve *et al,* 2018a). The literature proposes that during post-PEF incubation enzyme-dependent autolysis-like processes take place, which subsequently improves lipid-extraction yield in *A. protothecoides* even at lowest treatment energy (Silve *et al,* 2018a) or protein recovery of *C. vulgaris* (Scherer *et al,* 2019). When taking the findings of this work into account, the necessary incubation time after PEF treatment at lower specific energy can also be attributed to autolytic processes in the cell. Looking at the physical damage visible under a light microscope after PEF treatment, fragmentation of trichomes seems to be partially proportional to the energy input. The fact that less fragmentation leads to a similar maximum yield after 24 h must be attributed to biological processes occurring after the pulse. In particular, low extraction efficiency in Spirulina could point towards a low mortality at the beginning of the externalization process. The increase in extraction efficiency over 24 h would then be explainable by autolytic processes as well as triggering of cell death in neighboring cells.

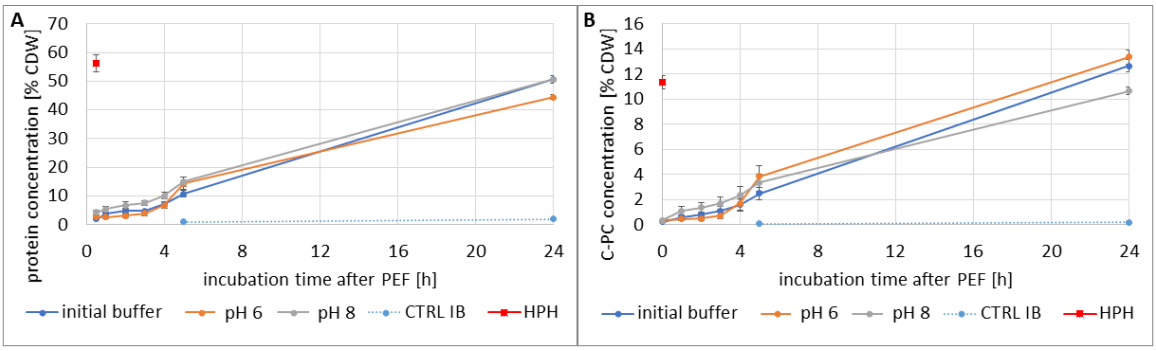

Figure 18 Effect of PEF treatment at 56 J·ml^{-1} and pH of the external medium on **A)** protein and **B)** C-phycocyanin release of Spirulina following PEF treatment. The biomass concentration was set to 9.12 ± 0.16 mg·ml^{-1} and PEF treatment was executed at 56 J·ml^{-1} followed by incubation of samples on shaker (80 rpm) at 23 °C. CTRL IB: control without PEF treatment in initial buffer (IB). High-pressure homogenization (HPH) represents benchmark for total protein and C-PC content in sample. The experiment was performed in triplicate. Error bars represent standard errors. Modified from Akaberi *et al,* 2020.

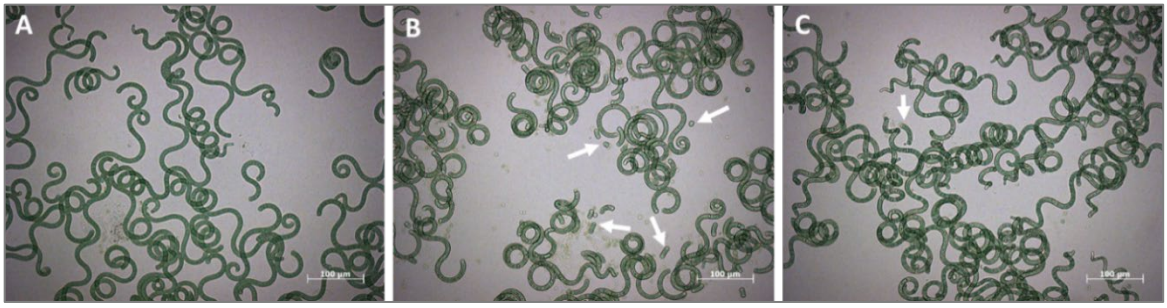

Figure 19 Effect of PEF-treatment on morphology of Spirulina. Light microscopic images of Spirulina showing fragmentation of trichomes by PEF treatment. **A)** Control untreated, **B)** PEF-treatment at 114 J·ml^{-1}, **C)** PEF-treatment at 56 J·ml^{-1} of Spirulina fresh biomass after 6 h post-PEF treatment and incubated in pH 8 buffer. Fragmented trichomes are shown with white arrows.

5.1.4. Influence of cell aggregation on PEF extraction efficiency

Due to its long filamentous structure, Spirulina easily clumps and forms large aggregates during harvest. These aggregates possibly affect electroporation efficiency during PEF treatment and thus influence subsequent extraction efficiency. Therefore, an experiment was designed to study the influence of cell aggregation prior to PEF treatment on the amount of protein and C-PC release. For this purpose, a heterogeneous cell suspension with clustered and aggregated trichomes in comparison to a homogeneous cell suspension were prepared prior to PEF treatment. The protein and C-PC release kinetics were significantly influenced by the homogeneity of suspension prior to PEF treatment (**Figure 20**). PEF treatment of an aggregated, heterogeneous suspension showed slow kinetics of protein and C-PC release, whereas PEF treatment of a suspension with homogenous distribution of cells exhibited fast kinetics. Mutual shielding of cells causes a decrease in the amplitude of induced transmembrane potential difference (Guittet *et al,* 2017).

Additionally, a similar decrease is known for spherical cells when they are arranged in closer vicinity (Pavlin *et al,* 2002), showing an influence of both volume fraction and cell arrangement. It has been shown that higher pulse amplitudes were required to achieve the same fraction of cell permeabilization in dense cell suspensions (Pucihar *et al,* 2007). In addition, heterogeneous clusters with irregularities at the boundaries due to their long spirals lead to further reduction of induced transmembrane potential difference in these areas. The slower release kinetics of the heterogenous suspension containing visible cell aggregates compared to homogenous suspensions are consistent with those findings stated in literature. Furthermore, the component release kinetics of suspensions treated at high energy input and containing visible aggregates is similar to that obtained with lower energy input in homogenous cell suspensions (56 J·ml^{-1}, **Figure 18**). This additionally supports the explanation of mutual electric shielding of cells packed in dense clusters. In conclusion, to dissolve cell aggregation, a gentle homogenization is necessary to maintain high extraction efficiency.

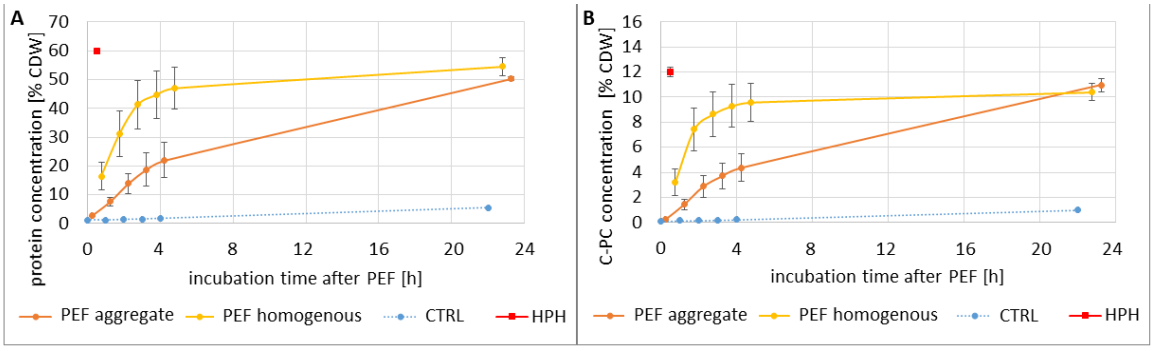

Figure 20 Influence of cell aggregation on PEF extraction efficiency of **A)** protein and **B)** C-phycocyanin. The biomass concentration was set to 11.86 ± 0.80 mg·ml^{-1} and the suspension was either left aggregated (PEF aggregate) or homogenized via magnetic stirrer for at least 5 min prior to treatment (PEF homogenous). PEF treatment was executed at 114 J·ml^{-1} followed by incubation of samples on shaker (80 rpm) at 23 °C. CTRL: control without PEF treatment. High-pressure homogenization (HPH) represents benchmark for total protein and C-PC content in sample. The experiment was performed in triplicate. Error bars represent standard errors. Modified from Akaberi *et al,* 2020.

5.1.5. Purity of crude extract: PEF- vs. HPH-treatment

To further characterize the electroextraction efficiency of C-PC, the influence of the treatment method on the purity of C-PC extract was investigated. **Figure 21** depicts the absorbance spectra of crude extracts of PEF-treated samples after 24 h of incubation either in initial buffer or in pH 8 buffer, as well as for HPH treated samples. The crude extract after HPH-treatment showed high chlorophyll contamination (peaks at 440 and 675 nm), whereas the crude extract of PEF-treated samples barely showed chlorophyll contamination. Incubation in initial buffer and HPH crude extract showed comparable C-PC content in relation to the peak at 620 nm, whereas incubation in pH 8-buffer obtained the highest signal at 620 nm.

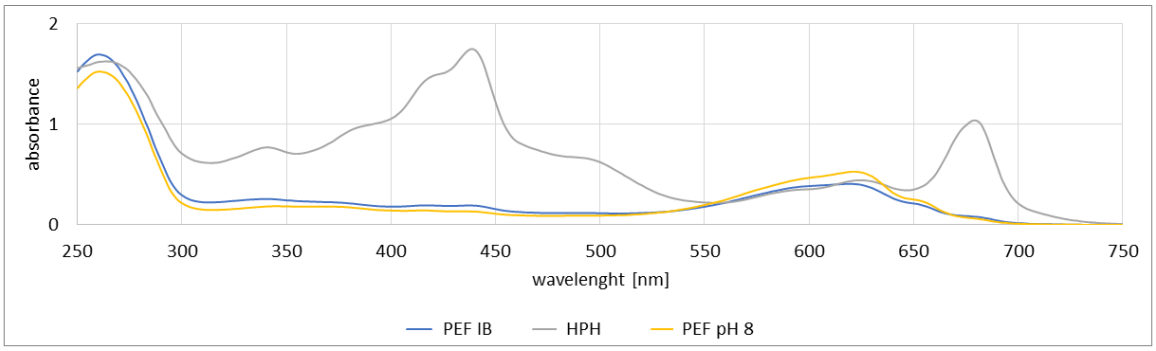

Figure 21 Absorbance spectra of crude C-phycocyanin extract obtained from Spirulina 24 h post-PEF-treatment (114 J·ml^{-1}) incubated either in initial buffer (IB) or in extraction buffer at pH 8. Benchmark with crude extract obtained after HPH treatment. Corresponding experiment and results in Figure 16.

The purity of crude extract was analyzed by measuring the purity ratio of A_{620}/A_{280} (**Table 2**). Crude extract obtained 24 h post-PEF treatment at 56 J·ml^{-1} incubated in pH 8-buffer has a purity ratio of 0.51. In contrast, crude extract collected after HPH treatment has a purity ratio of 0.32. This result clearly indicates the enhancement of C-PC purity using PEF-treatment assisted by incubation in pH 8-buffer. PEF treatment can therefore be employed for C-PC electroextraction with the advantages of avoiding chlorophyll contaminations and a large amount of cell debris. Compared to mechanical methods, less treatment energy is required.

Table 2 Comparison of PEF treatment at 56 J·ml^{-1} incubated in pH 8-buffer for 24 h and HPH treatment on protein and C- phycocyanin extraction yield, purity ratio of crude C-phycocyanin extract and energy input of Spirulina fresh biomass at 9.12 mg·ml^{-1}. Corresponding experiment and results in Figure 18. Data points represent mean values ± standard error (n=3). Modified from Akaberi *et al,* 2020.

Cell disruption method	**Protein [% CDW]**	**C-PC [% CDW]**	**Purity ratio**	**Energy input**
PEF (56 J·ml^{-1}, pH 8, 24 h)	50.7 ± 1.6	12.65 ± 0.6	0.51	less energy
HPH treatment	56.2 ± 3.8	11.35 ± 0.7	0.32	energy intensive

5.1.6. Conclusion

It can be concluded that with higher biomass concentration and lower treatment energy, post-PEF incubation at controlled conditions is crucial for autolytic processes resulting in C-PC liberation. However, investigation of electroextraction efficiency in Spirulina shows that cell death due to PEF treatment is a very complex mechanism and cannot easily be transferred from one microalgae species another. The next chapters will therefore concentrate on the characterization of PEF induced cell death in the eukaryote *C. vulgaris*.

5.2. Validation of methods for *C. vulgaris*

To be able to generate reliable data, newly established methods need to be validated. For this purpose, to prove the successful synchronization of *C. vulgaris* cultures, tools such as DNA staining followed by microscopy or flow cytometry were used. For validation of the viability assay using FDA, a standard curve in addition to counterstaining with two different dyes were the selected methods. This thorough work ensures that the following experiments are based on reliable methods and reproducible.

5.2.1. Synchronization of algal cells

DNA replication starts approximately 4 -5 h after the onset of the light phase (**Figure 22A,** Lorenzen & Hesse, 1974). YO-PRO®-1 iodide stains nuclear DNA and can only enter permeabilized cells, therefore, this stain can be used to visualize the permeabilization of cells by PEF treatment (ΔW = 32 $kJ \cdot kg_{sus}^{-1}$, 30 min prior to staining). By comparing two different time points during the light cycle, the YO-PRO intensity is supposed to show the start of doubling of nuclear DNA with the hypothesis assuming one peak just after the onset of light (9 am) and two peaks 6 hours later (3 pm). The intracellular fluorescence signal was quantified using a flow cytometer. Control staining was performed with a population of cells that had been cultivated under continuous light (*C.v. cont*), where the frequency distribution shows two peaks independently of the time point (**Figure 22B**). At the first time point just after the onset of light (9 am), when comparing a synchronized culture (*C.v. syn*) with *C.v. cont*, the synchronized cells show one main peak overlapping with the lefthand peak of *C.v. cont* (**Figure 22C**). This shows that, as predicted, the synchronized cells are still in the G1 phase of the cell cycle and contain only one-stranded DNA. When comparing the two cultivation types at the second time points 6 h after light induction (3 pm), the staining shows a shifted peak for the synchronized culture (**Figure 22D**). DNA replication apparently is in process already and the peak from *C.v. syn* is now starting to overlap with the right-hand peak of *C.v. cont* (representing double-stranded DNA), indicating partial DNA replication.

As further validation of synchronization, Hoechst staining of DNA followed by microscopy was conducted. Cells from cultivation under continuous light and during the early stationary phase (7 dpi) show a population composed of cells in different stages of the cell cycle and in all sizes (**Figure 23**). In general, chlorophyll autofluorescence is stronger in larger cells, such that the merged signal from the two channels appears in red. However, during cell division, the Hoechst signal is stronger since multiple nuclei are present in the cells, such that the overlay of the two channels appears in blue (**Figure 23B**, yellow circle). Very small cells that are just released from

the mother cell show mostly equal fluorescence signals for chlorophyll autofluorescence and Hoechst staining of the nucleus, such that the merged signal appears in magenta. When staining cells from synchronized cultivation at one time point just after completed division (**Figure 24AB**), and another time point 6 h after light induction during the non-cycling phase (**Figure 24CD**), the increase in cell volume is quite visible. The first time point contains daughter cells that were just released from the mother cell with similar magenta fluorescence signals for chlorophyll autofluorescence and Hoechst staining of the nucleus (**Figure 24B**). The second time point shows photosynthetically very active cells with strong red chlorophyll autofluorescence. The cells produce the necessary energy needed for metabolic activity in order to prepare for the next division. Even though the cells are already comparable in size to cells cultivated under continuous light, cells with multiple nuclei cannot be detected (**Figure 24D**), indicating that these cells have not entered M-phase yet. When taking both experiments into consideration, synchronization of *C. vulgaris* cultures can be declared as successful.

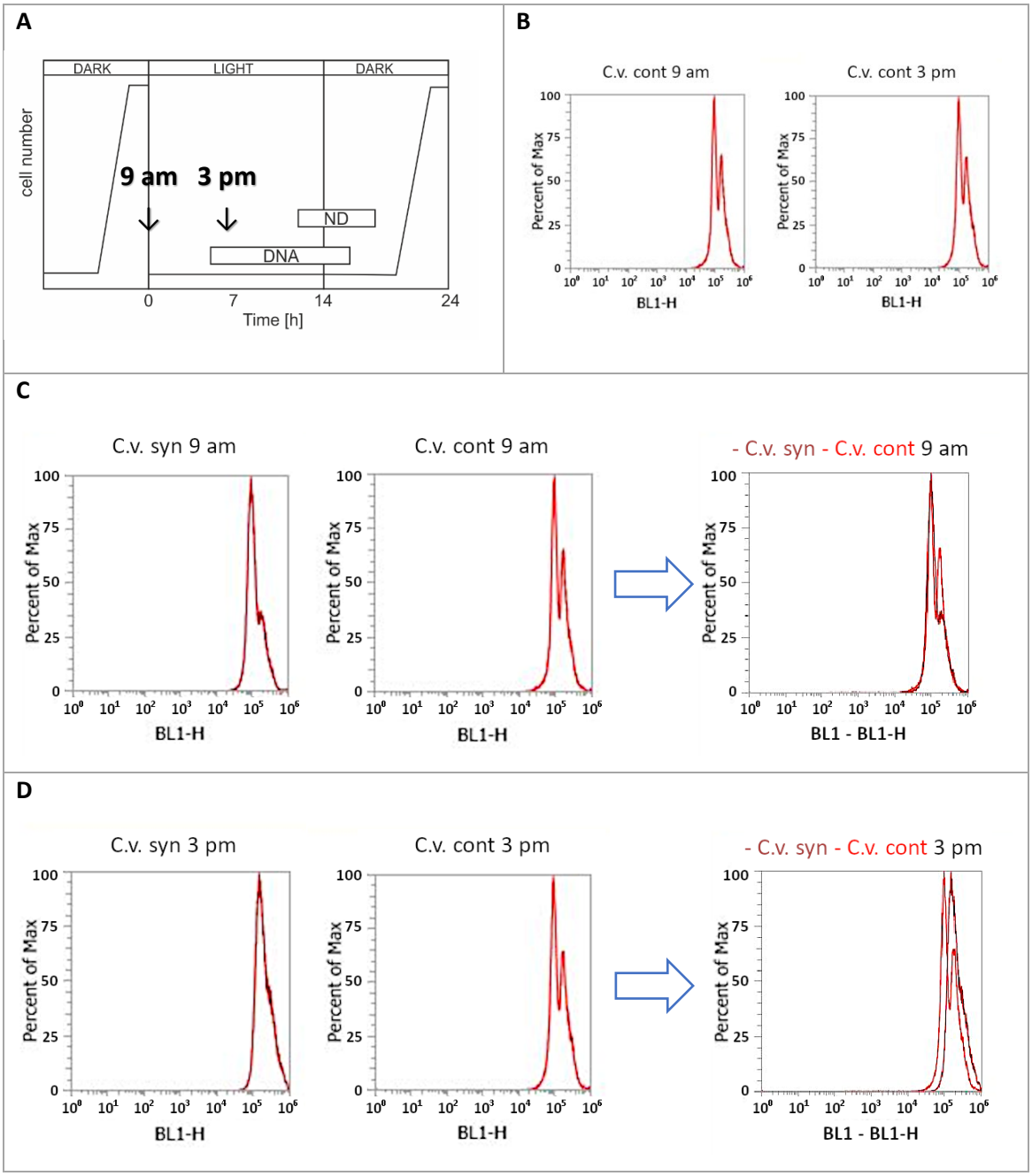

Figure 22 Validation of synchronization via YO-PRO staining. **A)** Theoretical time course of variation in cell number during light-dark cycle, DNA represents the time of DNA synthesis, ND represents the time of four nuclear divisions, redrawn from Lorenzen & Hesse (1974), p. 898. **B)** Control staining with YO-PRO®-1 iodide (1 µM) with cells from cultivation under continuous light (*C.v. cont*) at two different time points (9 am and 3 pm) **C)** Staining of synchronized cells (*C.v. syn*) with YO-PRO®-1 iodide (1 µM) at early time point (9 am) and comparison with *C.v. cont*, overlay of both graphs in right-side image. **D)** Staining of *C.v. syn* with YO-PRO®-1 iodide (1 µM) at late time point (3 pm) and comparison with *C.v. cont*, overlay of both graphs in right-side image. Quantification of signal via flow cytometer (Attune™ Nxt, Thermo Fisher Scientific), green fluorescence from YO-PRO was recorded through a bandpass filter of 530 ± 30 nm (BL1).

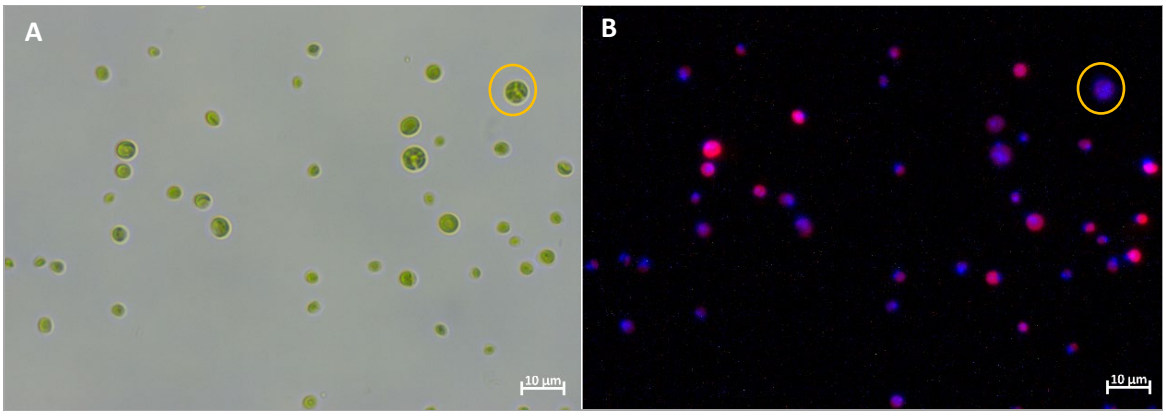

Figure 23 Hoechst staining of DNA of *C. vulgaris* cultivated under continuous light and in the stationary phase (7 dpi). **A)** Brightfield **B)** Overlay of channels showing chlorophyll autofluorescence (red) and Hoechst staining (blue). Yellow circle indicates cell undergoing division. Pictures were acquired using fluorescence microscope Axio Imager.M2. Data represents a representative from three biological replicates.

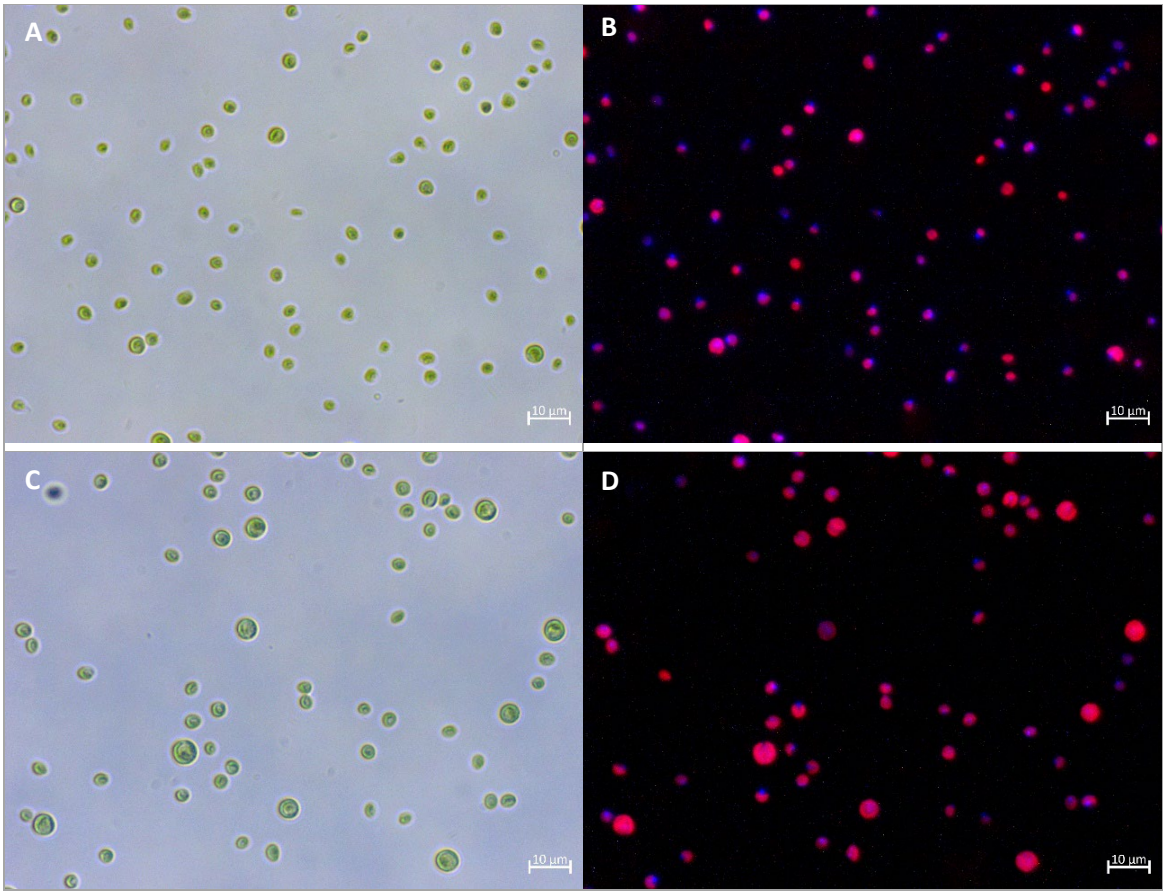

Figure 24 Hoechst staining of DNA of *C. vulgaris* from synchronized cultivation at two different time points. **A)** Brightfield just after induction of light phase (shortly after autosporulation) **B)** Overlay of channels showing chlorophyll autofluorescence (red) and Hoechst staining (blue). **C)** Brightfield 6 h after induction of light phase (during non-cycling phase, when cells increased in volume) **D)** Overlay of channels showing chlorophyll autofluorescence (red) and Hoechst staining (blue). Pictures were acquired using fluorescence microscope Axio Imager.M2. Data represents a representative from three biological replicates.

5.2.2. Viability assay by FDA staining

In a first step, FDA staining efficiency was monitored qualitatively via fluorescence microscopy. The signal of FDA can easily be located in the cytoplasm of living cells (**Figure 25A**), however, heat inactivation of algae cells (100 °C for 10 min) leads to complete loss of FDA signal (**Figure 25B**) showing that intracellular esterases are not functional, even if the chloroplast is still mostly intact. The slightly auto fluorescent background already shows some chlorophyll leakage, especially in comparison with live cells without FDA staining (**Figure 25C**).

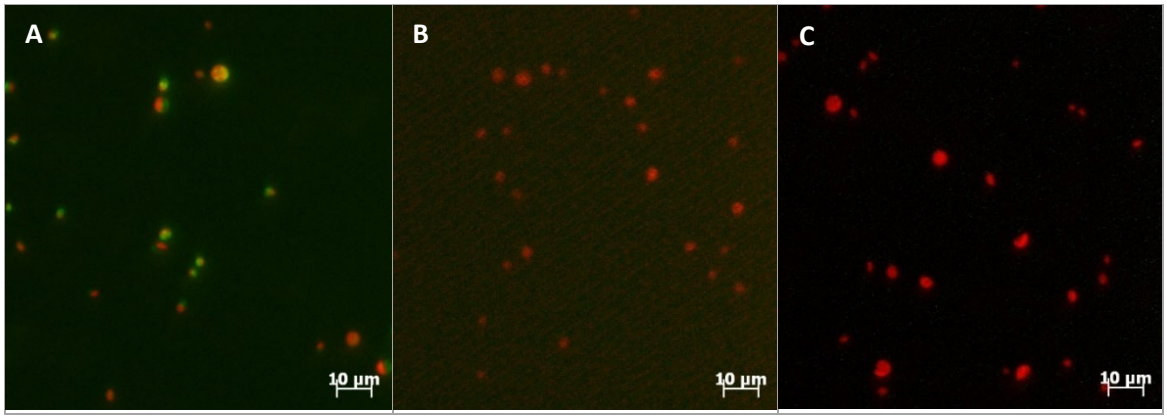

Figure 25 FDA staining (100 µM) of *C. vulgaris* in the stationary phase cultivated under continuous light. Overlay of channels showing chlorophyll autofluorescence (red) and FDA staining (green) **A)** FDA staining of live cells. **B)** FDA staining of dead cells (100 °C for 10 min) **C)** Live cells without FDA staining showing only chlorophyll autofluorescence. Pictures were acquired using fluorescence microscope ApoTome Axioplan 2 imaging.

For the first validation of FDA staining followed by flow cytometer quantification, a sample set with different ratios of live-dead cells was prepared. Dead cells were generated via heat inactivation (100 °C, 10 min) and after cooling down mixed again with live cells in six different ratios to quantify via FDA staining. This experiment reproduced the ratios of live and dead cells perfectly and clearly showed the high reliability for FDA staining followed by flow cytometer analysis (**Figure 26A**).

In addition, parallel staining with YO-PRO was performed to quantify the mortality of cells. For that purpose, cells were pulsed with one specific low energy (1.6 $J \cdot ml^{-1}$) resulting in partial inactivation of cells with roughly 40 % mortality 2 h post-PEF treatment. When measuring viability via FDA and mortality via YO-PRO in the same samples (**Figure 26B**), it can be seen clearly that live cells can only be stained by FDA dye and dead cells are stained only by YO-PRO dye. When a ratio of live and dead cells is present, these can be stained respectively with both dyes adding up to 100 % of total cells.

Lastly, microscopic imaging of Evans Blue staining shows that heat inactivation leads to complete loss of cell integrity (**Figure 26C**, left) while PEF treatment with very low energy input (1.6 $J \cdot ml^{-1}$)

results in partial inactivation of cells (**Figure 26C**, right). Evaluation of permeabilization efficiency shows a mortality of around 30 % (**Figure 26D**). This value is around 10 % lower than could be seen with YO-PRO staining, however, Evans Blue staining with microscopic imaging leads to time-consuming analysis of around 300 cells per replicate while flow cytometry generates 100,000 events for analysis in no time. Therefore, the statistics of FDA and YO-PRO analysis are more trustworthy since they are based on larger data sets.

In conclusion, it can be said that the FDA viability assay followed by flow cytometer quantification and using *C. vulgaris* as the model organism can be used as a validated method. This could be shown using a standard curve representing different viabilities and counterstaining with two different dyes, one validating the flow cytometer itself and one validating the viability measurement independently of flow cytometer analysis.

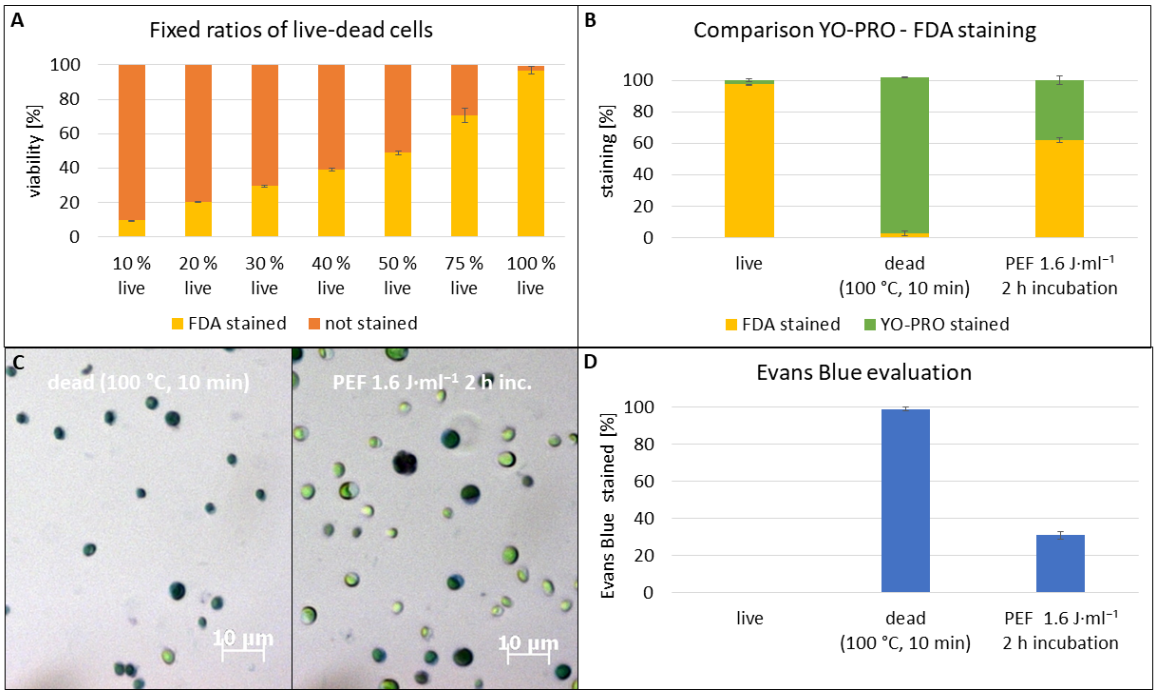

Figure 26 Validation of FDA viability assay via flow cytometry using *C. vulgaris* cultivated under continuous light and in the stationary phase (7 dpi). **A)** FDA staining (500 µM) of samples with fixed ratios of live and dead cells (heat inactivation: 100 °C, 10 min) **B)** YO-PRO (working concentration 1 µM) and FDA staining (working concentration 500 µM) in parallel of sample with PEF treatment (1.6 J·ml^{-1}) 2 h prior to staining. **C)** Brightfield of Evans Blue staining, left: dead cells, right: PEF-treated cells. Pictures were acquired using light microscope Axio Imager.M2. **D)** Evaluation of microscopic images. The experiment was performed in duplicate. Error bars represent standard errors.

5.3. Characterization of PEF induced cell death in *C. vulgaris*

To understand the biological aspects of PEF treatment, as well as cellular mechanisms of cell death in the unicellular microalgae *C. vulgaris*, many puzzle pieces are needed to form a complete picture. The following chapter gives a detailed description of the studies undertaken. In a first step, the influence of the cell cycle stage, as well as changes in redox homeostasis of the cell in response to PEF treatment, helps to determine the kind of stress PEF treatment can provoke. In a broad inhibitor study, the involvement of many factors involved in PCD processes (e.g., role of calcium, membrane fluidity and cytochrome release) were analyzed after sublethal PEF treatment. To make the connection to biotechnological application, lastly, the influence of increasing biomass, manifested in higher cell density suspensions, was investigated to be able to achieve high mortality combined with maximum extraction efficiency at minimum energy input.

5.3.1. Dependency of PEF induced mortality on the cell cycle

Synchronized cultures are in different stages of the cell cycle depending on the time point of sampling (**Figure 27A**). To test whether the cellular response to PEF treatment depends on the cell cycle, *C. vulgaris* from synchronized cultures sampled at different time points of the cell cycle were pulsed with the determined energy input at survival threshold (1.6 $J \cdot ml^{-1}$). The time points were set in the dark (- 6 h, before division), at the onset of light (0 h, just after completed division) and in the light period (6 h, non-cycling phase, cells increased in volume). Control samples without PEF treatment were taken at the same time points. Mortality was measured at 2 h incubation after PEF treatment (**Figure 27B**) for the rapid response. As has been demonstrated in the methods part, the viability does not change in the first 6 h after PEF treatment at the survival threshold (**Figure 14**). Additionally, the slow response 24 h after PEF treatment was analyzed (**Figure 27C**). When comparing the mortality of cells after PEF treatment at the survival threshold, the response is strongly dependent on the time point of sampling during the cell cycle. The cells at time point 6 h, during the non-cycling phase, show a substantially increased PEF induced mortality of more than a factor of 2, compared to cells at the time points before and shortly after division. This pronounced difference is especially visible when looking at the rapid response 2 h after pulsing, even though the difference is still significant 24 h after pulsing. When comparing the time points -6 h and 0 h, PEF induced mortality is at comparable levels for both the rapid response (2 h) as well as the slow response (24 h) after PEF treatment.

The induced transmembrane potential difference and therefore electroporation efficiency is directly proportional to the cell radius. Therefore, higher field strengths are required for electroporation of smaller organisms such as bacteria when compared to bigger organisms like

microalgae or yeast (Saulis, 2010; Kotnik *et al,* 2015). This could provide a possible explanation for reduced mortality at time point 0 h, since the cell radius of synchronized *C. vulgaris* increases around 10 % from 0 h to 6 h. However, this increase is not sufficient to cause higher mortality of more than factor 2. Furthermore, from 6 h to -6 h, cell radius increase is even greater, but mortality does not increase. On the contrary, mortality from time point 6 h to -6 h drops to a lower value again, refuting this explanation completely. More likely, PEF induced mortality is dependent on progression through the cell cycle. Differences in sensitivity during the cell cycle could already be indicated in experiments investigating radiation resistance in *Chlorella pyrenoidosa*. Cells immediately before DNA synthesis were found to be most sensitive to radiation treatment (Hampl *et al,* 1971). Here, cells at time point 6 h are caught during DNA synthesis as well, as demonstrated in the validation experiments (**Figure 22**). In summary, this result can be considered as the first sign, that PEF treatment at lower energy input acts as an abiotic stress signal combined with physically inflicting damage due to electroporation.

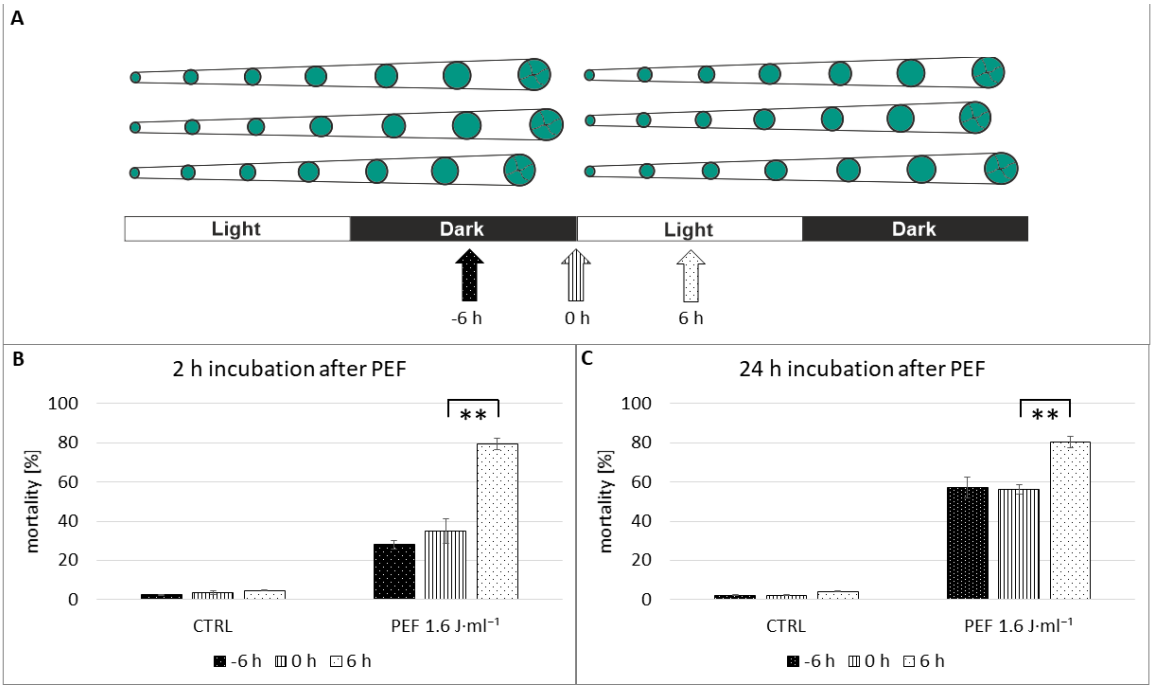

Figure 27 Mortality in response to PEF treatment depends on cell cycle. **A)** Diagram showing experimental design with different time points for sampling at -6 h (in the dark; black), 0 h (at the onset of light; striped) and + 6 h (in the light period; white), redrawn from Senger *et al* (1972), p. 304 **B)** and **C)** Cell mortality after PEF treatment at different cell cycle stages. *C. vulgaris* from synchronized cultures at different times of the cell cycle were pulsed with a specific energy of 1.6 J·ml^{-1}. Viability was monitored at 2 and 24 h via FDA assay (50 µM). CTRL: control without PEF treatment. Data represent averages and standard errors from three biological replicates. Brackets indicate differences that are significant at $P \leq 0.01$ (**), using two-sample *t*-test assuming equal variances. Modified from Krust *et al,* 2022.

5.3.2. The effect of PEF on the redox homeostasis of *C. vulgaris*

PEF induced cell death can be further analyzed by assessing potential oxidative stress. For this purpose, oxidative membrane damage was quantified by detecting MDA content (**Figure 28A**). Photosynthesis-related oxidative stress was quantified by measuring steady-state levels of hydrogen peroxide (**Figure 28B**). Synchronized cells at time point 0 h, just after division, were pulsed with different specific energies to establish a range of viabilities from high survival (90 %), survival threshold (50 %) to low survival (2 %). After 3 h of incubation, MDA and H_2O_2 content were measured and normalized to the fresh weight of the sample. When looking at PEF samples at the lowest specific energy (0.8 J·ml^{-1}), resulting in high survival, neither MDA nor H_2O_2 content were increased compared to the untreated control sample. When pulsing the cells at the survival threshold (1.6 J·ml^{-1}), both MDA and H_2O_2 content were increased 3 h after treatment. The highest specific energy of this experiment (8.0 J·ml^{-1}), which results in low survival of cells, causes an increase in MDA readout. However, H_2O_2 content is not increased when compared to the control sample.

The redox homeostasis of the cell is measured in two ways to paint the picture: MDA as final product represents the integral of oxidative stress and H_2O_2 as an unstable molecule represents a snapshot of oxidative stress. Hydrogen peroxide accumulation is only visible after PEF treatment at the survival threshold since this is an active process requiring that a part of the cells is alive. H_2O_2 measurements show steady-state levels of ROS, where generation by oxidative burst and dissipation by catalases is happening in parallel, continuously. At higher specific energies (8.0 J·ml^{-1}), PEF generated ROS molecules are dissipated after a 3 h incubation period. Since for that energy input PEF induced mortality is high, active H_2O_2 generation is not possible after 3 h incubation. At lower specific energies, cells are still viable, but PEF treatment did not cause significant perturbances of redox homeostasis 3 h after treatment. In contrast, MDA accumulation reports whether the cells had experienced considerable oxidative stress before death, which can especially be seen at higher specific energy accompanied by a high mortality of cells.

The generation of ROS constitutes one of the key signaling components of PCD (Petrov *et al,* 2015), with lower doses of ROS acting as a signal to activate stress responses and high concentration of ROS resulting in PCD. One of the enzymes responsible for signal-related production of ROS in plants is the NADPH oxidase, also called respiratory burst oxidase homologue (RboH) (reviewed in Marino *et al,* 2012). NADPH oxidases are located in the plasma membrane and catalyze the reaction of oxygen to superoxide radicals, which react later or are converted to the signal molecule H_2O_2 by superoxide dismutases. ROS molecules then can lead to lipoxygenation resulting in the generation of MDA. Lipoxygenation can occur in a direct, non-enzymatic way or can be

accomplished enzymatically by lipoxygenases. Besides lipid hydroperoxides, lipoxygenases also generate oxylipins including jasmonates, the central stress hormones in land plants, as well as superoxides (Roy *et al,* 1994) which contributes additionally to oxidative bursts. It is under dispute whether green algae utilize jasmonate signaling, but lipoxygenases generating precursors of jasmonates have been purified from *C. pyrenoidosa* (Nuñez *et al,* 2002). Homologues for all relevant steps of the pathway and most relevant members of the signaling complex could be found in *C. reinhardtii* (Han, 2017), however, the JAZ proteins seem to be absent.

From these findings, two alternative scenarios emerge: (1) PEF treatment leads to disruption of thylakoid membrane integrity in the chloroplast, resulting in perturbed electron transport. The transfer of excess electrons onto oxygen would give rise to superoxide which could be dissipated to H_2O_2 by plastidic superoxide dismutase, while non-enzymatic lipid peroxidation would lead to MDA accumulation. (2) PEF treatment acts as stress signal activating enzymes such as RboH and plastidic lipoxygenase, giving rise to increased H_2O_2 content and accumulation of MDA. The second scenario would trigger perturbed redox homeostasis as a consequence of PEF treatment, while the first scenario causes perturbed redox homeostasis directly. When examining previous experiments (Scherer *et al,* 2019), plastid protein release was monitored after PEF treatment with a much higher energy input (150 J·ml^{-1}) and even then, the release of the stroma located ribulose bisphosphate carboxylase (RuBisCO) required 4 hours to become relevant. This shows that thylakoid integrity in response to a 100-fold stronger treatment was well retained and in conclusion, the first non-enzymatic "damage scenario" seems unlikely. Therefore, the second "stress-signaling scenario" was tested by subsequent experiments.

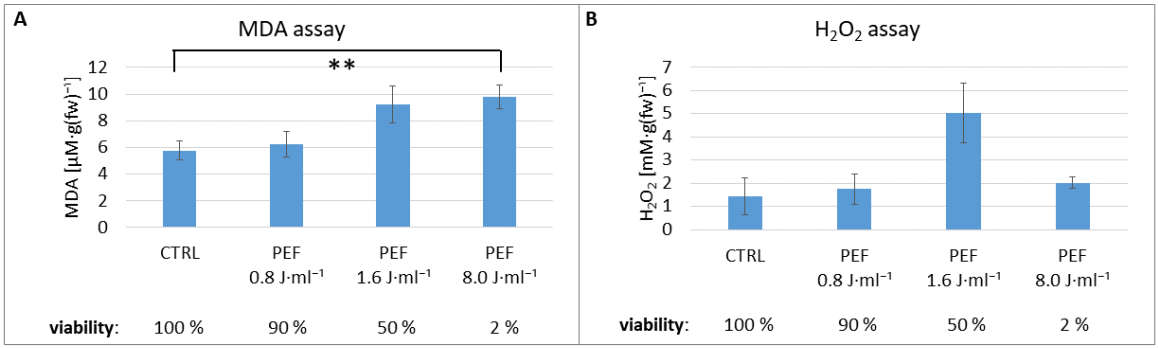

Figure 28 Generation of ROS in response to PEF treatment. *C. vulgaris* from synchronized cultures (time point 0) were pulsed with three specific energies establishing viabilities of around 90 % (0.8 J·ml^{-1}), 50 % (1.6 J·ml^{-1}) or 2 % (8.0 J·ml^{-1}), respectively, as determined via FDA assay (50 µM) 3 h after PEF treatment. The generated algae sediments were analyzed for **A)** MDA and **B)** H_2O_2 levels, normalized to fresh weight (fw) accordingly. CTRL: control without PEF treatment. Data represent averages and standard errors from six biological replicates. Brackets indicate differences that are significant at P ≤ 0.01 (**), using two-sample *t*-test assuming equal variances. Modified from Krust *et al,* 2022.

5.3.3. The effect of PEF on specific molecular players connected to PCD

To further dissect the cell death response after sublethal PEF treatment in *C. vulgaris* and pinpoint specific molecular players, several factors involved in ROS generation and connected to PCD processes, in general, were blocked or interfered with using a set of inhibitor experiments. The schematic model shown in **Figure 29** is showing the crosstalk of different compartments, enzymes, and processes. First, calcium influx from the external medium as well as from internal stores is interconnected with the generation of ROS and constitutes one of the early stress signals (Swarbreck *et al,* 2013). As mentioned in the previous chapter, direct generation of ROS signaling is executed by NADPH oxidase, which is converting oxygen (O_2) to superoxide radical ($\bullet O_2^-$). This unstable radical is quickly converted to more stable ROS molecules that are imported back into the cytoplasm (Marino *et al,* 2012). One of the signal molecules subsequently triggering NADPH oxidase is PA, a multifunctional stress signaling lipid in plants (Testerink & Munnik, 2005). PA is generated from structural phospholipids in the membrane by the enzyme PLD. Furthermore, signaling in PCD involves many cellular processes including reorganization of the cytoskeleton (Smertenko & Franklin-Tong, 2011). The important role of actin in plant cell death has been shown before (Chang *et al,* 2015) and requires further study for PEF induced cell death in microalgae. Next, the fluidity of the membrane plays a big role in maintaining the regular homeostasis of the cell, especially when faced with electroporation. A more rigid or fluid membrane influences the stage of pore evolution during the pulse and can play a role in the processes of membrane repair (Kanduser *et al,* 2006). Lastly, cyt c release from mitochondria is considered one of the hallmarks of PCD in animals as well as plants (Reape *et al,* 2008). Additionally, cyt f release from chloroplast is involved in PCD processes in *Chlorella sp*. (Zuppini *et al,* 2009) and release of both cytochrome c and f can trigger signal cascades resulting in the generation of ROS followed by PCD.

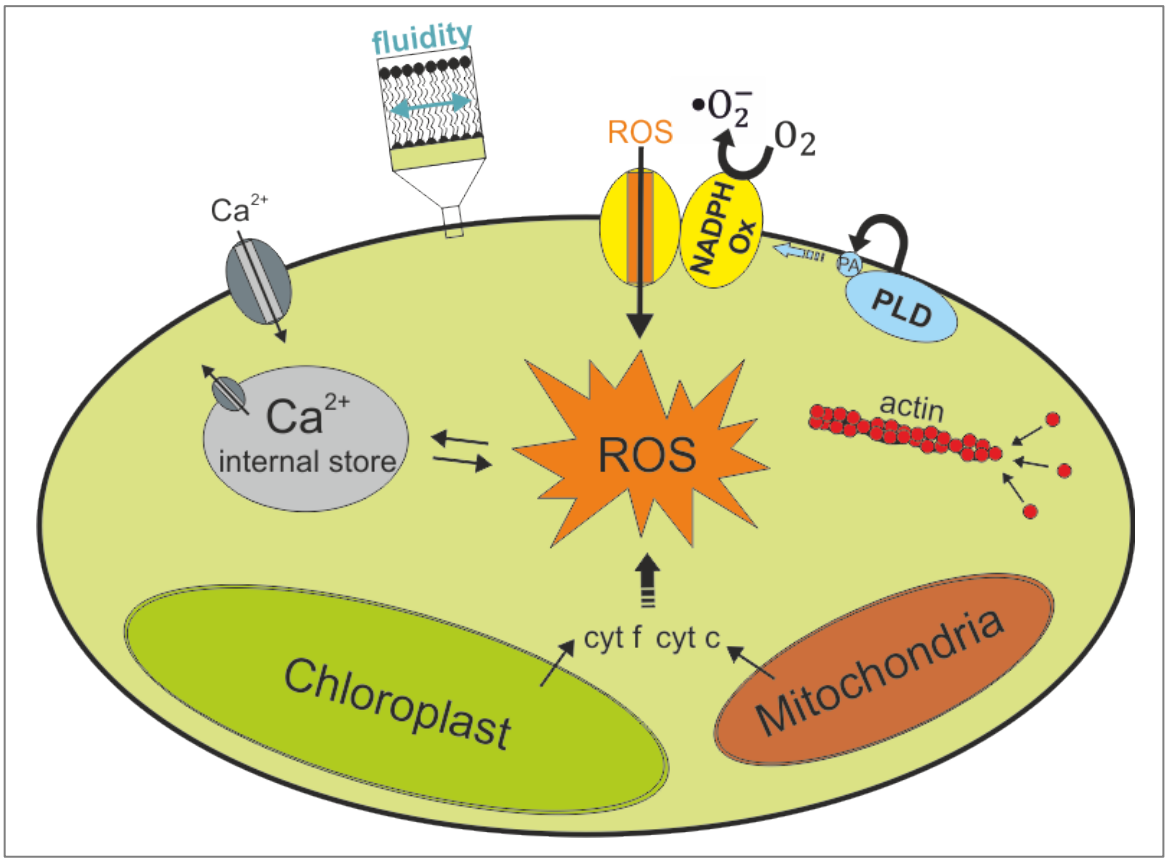

Figure 29 Schematic model of *C. vulgaris* showing different pathways leading to generation of reactive oxygen species (ROS). Grey: vacuole containing calcium (Ca^{2+}) internal store, yellow: NADPH Oxidase converting oxygen (O_2) to superoxide radical ($\bullet O_2^-$), blue: phospholipase D (PLD) generating phosphatidic acid (PA), red: polymerization of actin filament, green: chloroplast releasing cytochrome f (cyt f), brown: mitochondria releasing cytochrome c (cyt c).

Inhibition of calcium channels

Gadolinium (III) chloride ($GdCl_3$) dissociates into 3 Cl^- and Gd^{3+}, the second being a trivalent ion with very high charge density and similar ionic radius to calcium (Ca^{2+}). Therefore, it is well-suited to block calcium channels in the cell (Bai *et al,* 2020). For this experiment, *C. vulgaris* cells were taken from a synchronized culture at time point 0 h, just after division. The cell suspension was treated with $GdCl_3$ and pulsed immediately, resulting in viabilities between 50 % and 90 %. Viability was monitored at 1 h (**Figure 30B**) and 3 h (**Figure 30C**) after PEF treatment. The inhibition of calcium channels showed no significant effect – neither in control samples without PEF treatment nor in pulsed samples.

Since $GdCl_3$ was administered immediately before PEF treatment, the inhibitor might only affect calcium channels in the plasma membrane during the pulse and not the internal stores. After PEF treatment and during the incubation period, inhibition should affect all calcium channels. The slight, but not significant increase of mortality for the rapid response (1 h) would suggest that calcium channels are more likely involved in triggering activation of rescue pathways rather than processes resulting in PCD. Activation of PCD through calcium channels would more likely manifest in higher survival and lower mortality after blockage of channels. The proposed stress response due to PEF treatment can also be connected to calcium channels when including the voltage-gated calcium channels, one kind of voltage-gated channel found in green algae (Wheeler & Brownlee, 2008). Since the opening of voltage-gated calcium channels in the plasma membrane stands as a central component of early stress signaling in plants (reviewed in Swarbreck *et al,* 2013), this could constitute the first step of inducing PCD. Since neither significant reduction nor increase of mortality is visible in this experiment, the conclusion can be drawn that neither direct calcium signaling nor voltage-gated calcium channels play a dominant role in PEF induced cell death. In this context, another effect is known for $GdCl_3$ treatment: direct blocking of membrane permeabilization during the pulse (André *et al,* 2010; Gianulis & Pakhomov, 2015). The trivalent ion is apparently able to obstruct electropores during the pulse, which can lead to the reduction of cell death, albeit with nanosecond pulses. From these considerations, another interesting hypothesis can be drawn. When combining the two effects of $GdCl_3$, it might be involved in first blocking membrane permeabilization (mortality goes down) while in parallel blocking calcium signaling (mortality increases). This would result in the two working modes canceling each other out and what is visible would be a steady-state level rather than no effect. To test this hypothesis, an experiment using artificial calcium influx (i.e., by adding calcium ionophores) would be able to dissect the real response of cells.

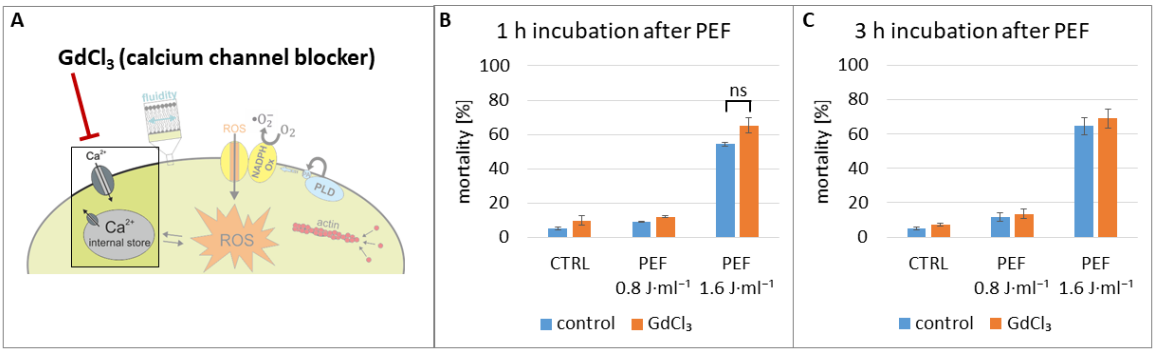

Figure 30 Influence of calcium channel blocker on PEF induced mortality. **A**) Schematic figure showing the effect of $GdCl_3$. *C. vulgaris* cells from a synchronized culture (time point 0) were treated with $GdCl_3$ (50 µM) and immediately pulsed establishing viabilities of around 90 % (0.8 J·ml^{-1}) and 50 % (1.6 J·ml^{-1}), respectively. Viability was measured via FDA assay (50 µM) 1 h (**B**) and 3 h (**C**) after PEF treatment. CTRL: control without PEF treatment. Data represent averages and standard errors from two biological replicates. Brackets indicate non-significant (ns) differences ($P > 0.05$), using two-sample *t*-test assuming equal variances.

Inhibition of NADPH oxidase, PA generation, actin polymerization and membrane modulation

In general (**Figure 31**, **Figure 32**, **Figure 33 and Figure 34**), *C. vulgaris* cells from the stationary phase (7 dpi) and from a synchronized culture at two time points (-6 h and 0 h) were compared. Cell suspensions were treated with inhibitor and pulsed at survival threshold after 30 min of incubation with the compound. The red line always represents control samples without inhibitor (CTRL + PEF) and will be used as a reference. The dotted lines represent control samples without PEF treatment (CTRL) to exclude general detrimental effects of the compound. In general, cells from cultivation under continuous light in the stationary phase (**B**) show a stable PEF induced mortality from the rapid response to 24 h incubation. However, cells from a synchronized culture at time point - 6 h (**C**) show different kinetics for PEF induced mortality over time. In the rapid response, the mortality still increases in all samples independent of PEF treatment (but in CTRL decreases again). PEF induced mortality in the control sample reaches over 40 % after 1.5 h incubation and rises to 60 % after 24 h. Similarly, cells from a synchronized culture at time point 0 h (**D**) show slightly increasing PEF induced mortality over time. The PEF induced mortality in the control sample starts at 20 % after 30 min incubation and reaches 40 % after 24 h.

When looking closely, a difference between the control PEF samples (without inhibitor) can be seen when comparing the time points -6 h and 0 h in contrast to **Figure 27**. The previous experiment showed no difference in mortality when comparing those two time points, while the following experiment shows higher PEF induced mortality for time point -6 h when compared to 0 h. However, the experiment in **Figure 27** was conducted using synchronized cell suspensions on the same day (-6 h and 0 h), but with sampling and pulsing at the different time points. These

inhibitor experiments were conducted one month apart for -6 h (**C**) and 0 h (**D**), with freshly synchronized cell cultures respectively. It definitely should be noted that PEF induced mortality is fluctuating depending on the culture, however, for the following experiments CTRL+ PEF samples are used only as reference to compare inhibitor-treated samples.

DPI inhibits **NADPH oxidase** and consequently interferes with oxidative burst and ROS signaling from this source. Cells from cultivation under continuous light in the stationary phase, as well as cells from a synchronized culture at time point -6 h (**Figure 31BC**), show no altered PEF induced mortality after treatment with DPI. In contrast, when looking at cells from a synchronized culture at time point 0 h (**Figure 31D**), treatment with DPI leads to higher PEF induced mortality over time. This higher mortality caused by treatment with DPI is not visible in the control sample without PEF treatment. Since increased H_2O_2 concentration has been shown in the synchronized culture at time point 0 h (**Figure 28**), the enzyme responsible for the generation of ROS was inhibited and visible alteration in mortality would assign a signaling role to ROS. A visible, but no significant effect of increased mortality in the synchronized culture at time point 0 h implicates that possible rescue pathways cannot be activated in young cells. Therefore, the inability to generate ROS signaling for stress response would lead to higher mortality. In older cells (-6 h) or cells in the stationary phase, no higher or lower mortality caused by activation of ROS signaling could be measured. In conclusion, PEF induced cell death affects redox homeostasis on the enzyme level (activation of NADPH oxidase) dependent on the cell cycle. ROS signaling plays an important role in adaptive stress responses (Mittler *et al,* 2011). In other microalgae such as *C. reinhardtii,* nsPEFs induce first (immediate) and second (several days later) waves of oxidative burst leading to the formation of immobile palmella stage, which can also be inhibited by DPI (Bai *et al,* 2017a). In cold adaption of grapevine, the role of ROS for cold-induced signaling has been demonstrated (Wang & Nick, 2017). Here, inhibition by DPI could effectively stop depolymerization of central and cortical microtubules, emphasizing the role of ROS signaling for the stress response in plants. When considering this experiment combined with the results of measuring direct generation of ROS (**Figure 28**), the previously proposed “stress-signaling scenario” would still apply to young cells in dependence of the cell cycle. For cells in the stationary phase, the “damage scenario” seems more likely when looking at these results.

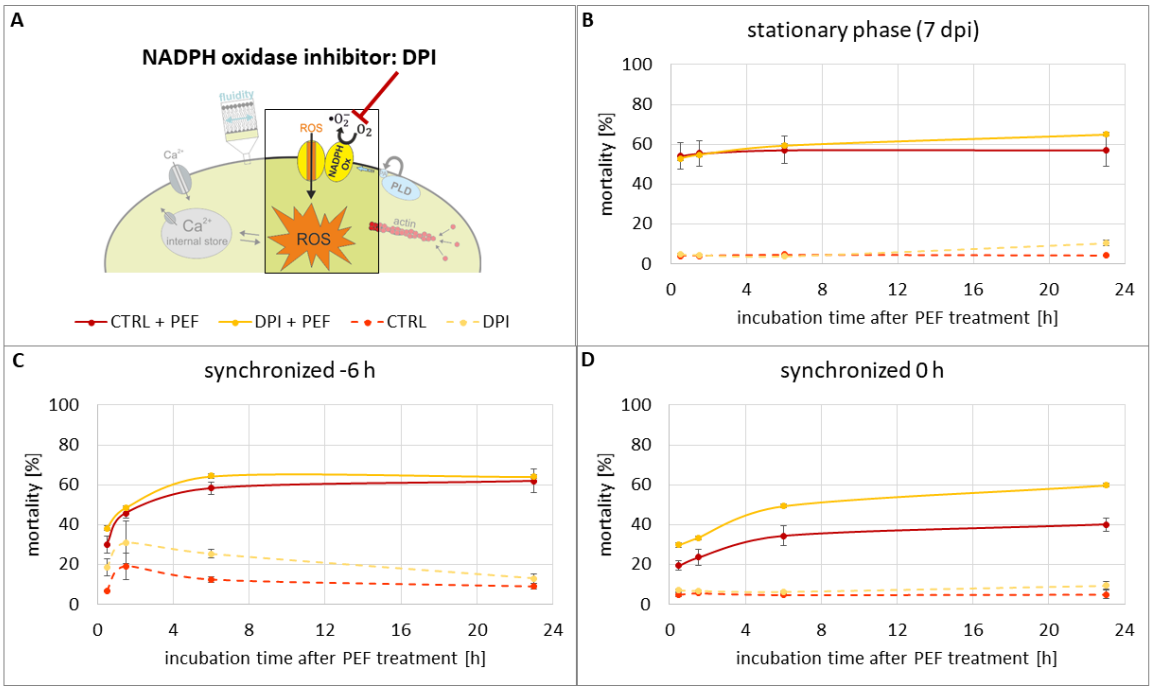

Figure 31 Influence of NADPH oxidase inhibitor on PEF induced mortality. **A**) Schematic figure showing the effect of diphenyleneiodonium chloride (DPI). *C. vulgaris* cells (normalized density 0.2 mg·ml^{-1}) **A)** cultivated under continuous light and in the stationary phase (7 dpi), **B)** from a synchronized culture at time point -6 h or **C)** from a synchronized culture at time point 0 h were treated with DPI (20 µM). After 30 min of incubation, the cell suspensions were pulsed with a specific energy of 1.6 J·ml^{-1} (viability around 50 %). Viability was measured via FDA assay (50 µM) 0.5, 1.5, 6 and 24 h after PEF treatment. CTRL: control without inhibitor and PEF treatment; CTRL + PEF: control without inhibitor, but with PEF treatment. Data represent averages and standard errors from two biological replicates.

The **generation of the stress signal PA** can be inhibited by n-butanol, with n-butanol acting as the acceptor of the transphophatidylation reaction instead of water. Consequently, inactive phosphatidyl alcohols are generated, however, the PA-independent pathways of PLD activation are not affected by n-butanol. Cell suspensions were treated with n-butanol or the inactive compound *tert*-butanol as a negative control. When looking at the cells from the cultivation under continuous light in the stationary phase (**Figure 32B**), treatment with n-butanol leads to slightly higher PEF induced mortality over time while treatment with *tert*-butanol leads to slightly lower PEF induced mortality over time. However, the control sample treated with n-butanol but without PEF treatment (blue dotted line) shows slightly higher mortality over time mirroring the slightly higher PEF induced mortality. Cells from a synchronized culture at time point -6 h (**Figure 32C**) show higher PEF induced mortality for the rapid response when treated with n-butanol and *tert*-butanol. After 6 h the values level off and there are no significant differences between samples treated with inhibitor and control samples after 24 h. When looking at cells from a synchronized culture at time point 0 h (**Figure 32D**), treatment with both n-butanol and *tert*-butanol lead to higher PEF induced mortality over time. Treatment with inhibitor results in a mortality of 60 %

after 24 h incubation, compared to a PEF induced mortality of 40 % in the control sample. The higher mortality caused by treatment with inhibitor is not visible in the control samples without PEF treatment. When comparing the two applied compounds, n-butanol activates PLD, but inhibits the formation of PA, while *tert*-butanol neither activates PLD nor acts as a substrate and therefore can be applied as a control for any non-specific butanol effects. PEF induced increase in mortality is only visible, albeit not significant, in the synchronized culture at time point 0 h. However, this increase can be seen for both n- and *tert*-butanol and therefore must be attributed to non-specific butanol effects. In *Arabidopsis thaliana,* PA has been shown to regulate NADPH oxidase activity through a binding motif (Zhang *et al,* 2009). This connection to ROS signaling shows one way of influencing adaptive stress responses, another way is that PLD as membrane associated protein acts in concert with a G-protein as a central regulator for the interaction of cytoskeleton and membrane (Nick, 2013; Testerink & Munnik, 2011). Since the increase in PEF induced mortality seems to be unspecific, both the role of PA signaling in connection with ROS generation as well as PA-independent stress pathways activated by PLD appear to be not necessary for survival after PEF treatment.

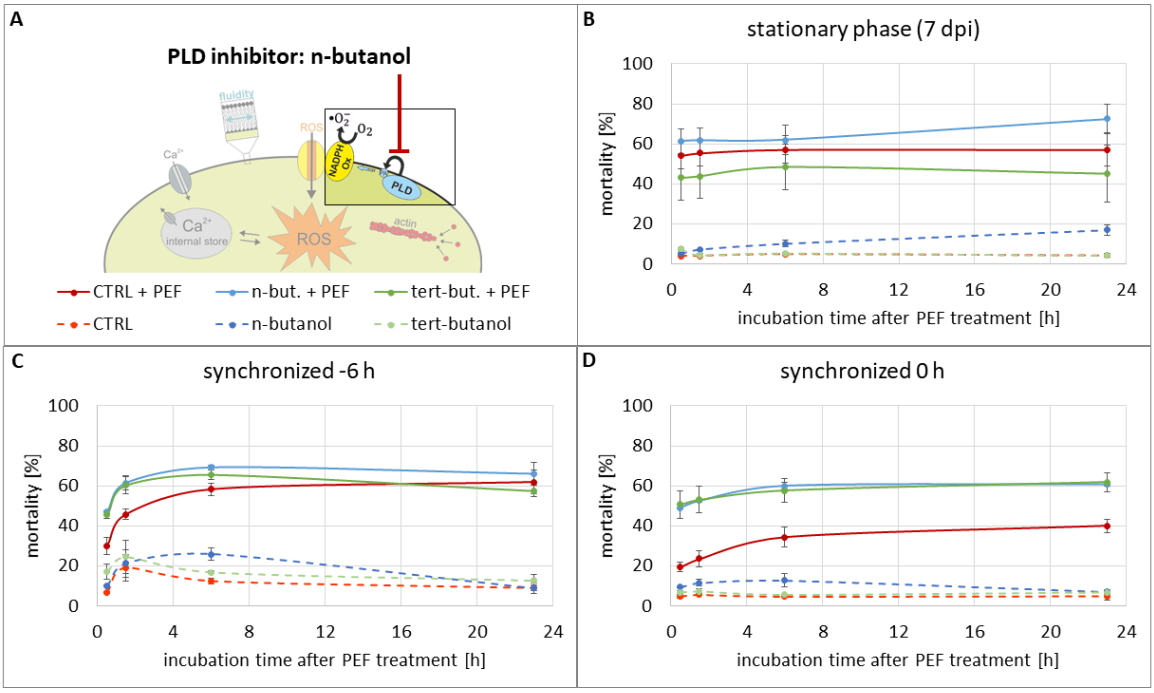

Figure 32 Influence of PLD inhibitor on PEF induced mortality. **A**) Schematic figure showing the effect of n-butanol. *C. vulgaris* cells (normalized density 0.2 mg·ml^{-1}) **A)** cultivated under continuous light and in the stationary phase (7 dpi), **B)** from a synchronized culture at time point -6 h or **C)** from a synchronized culture at time point 0 h were treated with n-butanol (0.5 %) or *tert*-butanol (0.5 %). After 30 min of incubation, the cell suspensions were pulsed with a specific energy of 1.6 J·ml^{-1} (viability around 50 %). Viability was measured via FDA assay (50 µM) 0.5, 1.5, 6 and 24 h after PEF treatment. CTRL: control without inhibitor and PEF treatment; CTRL + PEF: control without inhibitor, but with PEF treatment. Data represent averages and standard errors from two biological replicates.

LatB was used to inhibit **actin polymerization** for assessing the role of actin filaments. Cells from cultivation under continuous light in the stationary phase, as well as cells from the synchronized culture at time point -6 h (**Figure 33BC**), show no altered PEF induced mortality after treatment with LatB. When looking at cells from a synchronized culture at time point 0 h (**Figure 33D**), inhibition of actin polymerization leads to higher, but not significant, PEF induced mortality over time which is not visible in the control sample without PEF treatment. It has been demonstrated that change of actin dynamics can trigger PCD in animal, yeast and plant cells (Franklin-Tong & Gourlay, 2008). Specifically, actin remodeling (via treatment with aluminum) activates defense signaling in grapevine (Wang *et al,* 2022). These results again suggest that the "stress-signaling scenario" only applies to young cells at the beginning of the cell cycle, while older cells do not show any signs of signaling in response to PEF treatment.

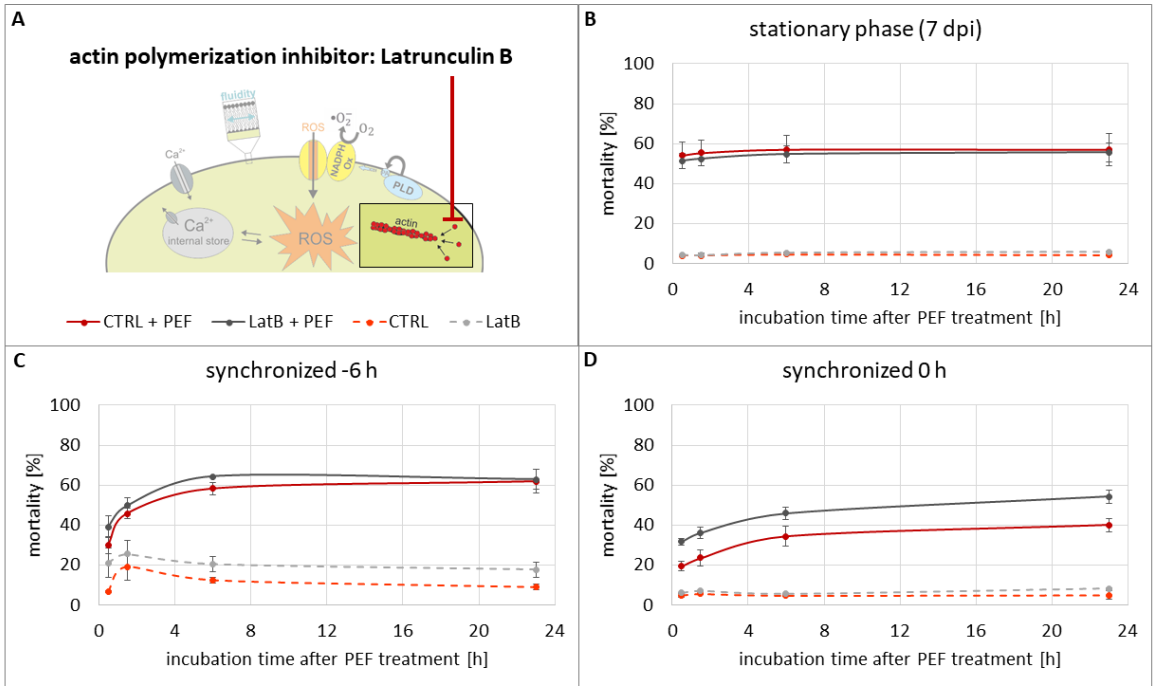

Figure 33 Influence of actin polymerization inhibitor on PEF induced mortality. **A**) Schematic figure showing the effect of latrunculin B (LatB). *C. vulgaris* cells (normalized density 0.2 mg·ml^{-1}) **A)** cultivated under continuous light and in the stationary phase (7 dpi), **B)** from a synchronized culture at time point -6 h or **C)** from a synchronized culture at time point 0 h were treated with LatB (2 µM). After 30 min of incubation, the cell suspensions were pulsed with a specific energy of 1.6 J·ml^{-1} (viability around 50 %). Viability was measured via FDA assay (50 µM) 0.5, 1.5, 6 and 24 h after PEF treatment. CTRL: control without inhibitor and PEF treatment; CTRL + PEF: control without inhibitor, but with PEF treatment. Data represent averages and standard errors from two biological replicates.

Membrane rigidifier DMSO and **membrane fluidizer** BA were used to modulate membrane fluidity. Treatment with BA already leads to very high mortality in control samples without PEF treatment, so PEF induced mortality of BA treated samples is almost 100 % in all three cultivation types. For treatment with membrane rigidifier DMSO, cells from cultivation under continuous light in the stationary phase, as well as cells from a synchronized culture at time point -6 h (**Figure 34BC**), show no altered PEF induced mortality. When looking at cells from a synchronized culture at time point 0 h (**Figure 34D**), rigidified membranes lead to higher PEF induced mortality over time. This higher mortality caused by treatment with DMSO is not visible in the control sample without PEF treatment. In retrospect, the applied BA concentration was too high with 25 mM and should have been in the range of 4-10 mM, as has been used for grapevine (Wang & Nick, 2017; Guan *et al,* 2021). The very high membrane fluidity leads to cell death independently of PEF treatment and additional PEF treatment is the final straw resulting in cell death for all cells. Interestingly, the synchronized culture at time point 0 h (**Figure 34D**) is the most sensitive to BA. A possible explanation for this observation could be that the cell wall is still very thin and not providing much additional protection (Yamamoto *et al,* 2004). DMSO as rigidifier only shows slightly, but not significantly, increased mortality in a synchronized culture at time point 0 h. Decreased cell membrane fluidity means slower resealing of the electropores, increased cell membrane fluidity faster resealing (Kanduser *et al,* 2006). Similar to the reasoning why synchronized cultures at time point 0 h are the most sensitive to BA, the slightly higher PEF induced mortality after treatment with DMSO could be owing to the cell wall composition. Less additional protection by a rigid cell wall combined with slower resealing of electropores seems to affect the mortality of young daughter cells.

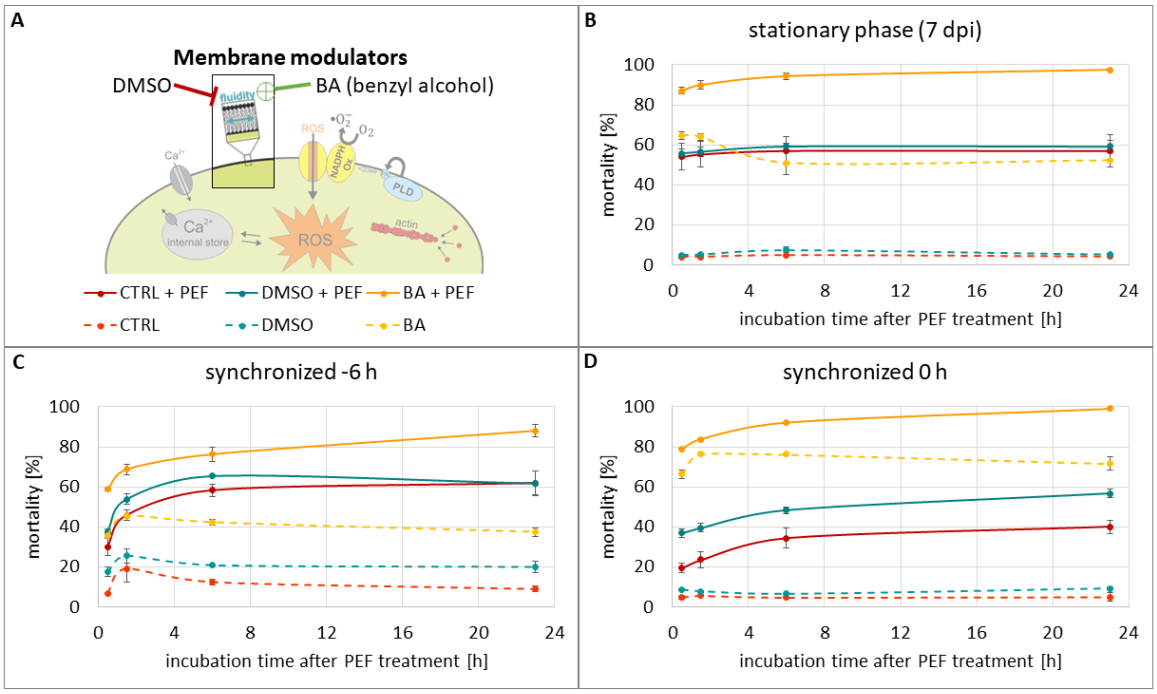

Figure 34 Influence of membrane modulators on PEF induced mortality. **A**) Schematic figure showing the effect of membrane rigidifier DMSO and membrane fluidizer benzyl alcohol (BA). *C. vulgaris* cells (normalized density 0.2 mg·ml^{-1}) **A)** cultivated under continuous light and in the stationary phase (7 dpi), **B)** from a synchronized culture at time point - 6 h or **C)** from a synchronized culture at time point 0 h were treated with DMSO (2 %) and BA (25 mM). After 30 min of incubation, the cell suspensions were pulsed with a specific energy of 1.6 J·ml^{-1} (viability around 50 %). Viability was measured via FDA assay (50 µM) 0.5, 1.5, 6 and 24 h after PEF treatment. CTRL: control without modulator and PEF treatment; CTRL + PEF: control without modulator, but with PEF treatment. Data represent averages and standard errors from two biological replicates.

Cytochrome release after PEF treatment

To investigate the effect of PEF treatment on the release of cyt c from mitochondria and cyt f from chloroplast (see **Figure 29**), a western blot assay was performed to screen the extracted supernatant for these proteins. As a positive control, supernatant after HPH treatment containing the total protein content of *C. vulgaris* was screened. The protein content of both PEF (40 J·ml^{-1}) and HPH samples was normalized. Cyt c is a protein with an apparent size of 14 kDa on western blots. One band around this size could be very faintly detected after HPH treatment (**Figure 35A**), however, PEF treatment with different specific energies of 0.8, 1.6 and 40 J·ml^{-1} establishing a range of viabilities (2 %, 50 % and 100 %, respectively) did not release detectable quantities of cyt c even after 24 h post PEF incubation. The antibody against cyt f has confirmed reactivity with the related species *C. reinhardtii* and can be detected on western blots with an apparent size of 31-32 kDa. The western blot incubated with cyt f antibody showed a corresponding band around 30 kDa in the sample containing HPH supernatant (**Figure 35B**). A second faint band smaller than 10 kDa could be detected in the same sample. PEF treatment followed by 24 h incubation did not

generate any bands, independent of the specific energy. Even though cyt c release in connection with PCD is reported for plants (Reape *et al,* 2008), it has not been reported for microalgae. Cell death in the related species *Micrasterias denticulate* in response to salt stress led to the degradation of organelles and DNA laddering, however, cyctochrome c release (also tested by western blotting) could not be measured (Affenzeller *et al,* 2009). Similarly, oxidative stress induced PCD in *C. reinhardtii* but did not result in cyt c release (Vavilala *et al,* 2015). This would coincide with the results shown in this experiment, where even the faint band after HPH treatment (**Figure 35A**) can be questioned since it also appears unspecifically on the western blot detecting cyt f. In contrast, cyt f release has been demonstrated to be involved in PCD like processes in *Chlorella* sp. (Zuppini *et al,* 2009). At least cyt f can specifically be detected in western blots after HPH treatment, even if not after PEF treatment at various specific energies. In conclusion, it can be said that cyt f seems to be abundant in cells as confirmed by total cell extract, however, PEF treatment does not lead to the release of this compound independent of the specific energy. Compared to PEF induced release of the stroma located RuBisCO (Scherer *et al,* 2019), cyt f seems to be contained in the chloroplast after PEF. Cyt c remains mysteriously absent in both total cell extract as well after PEF treatment.

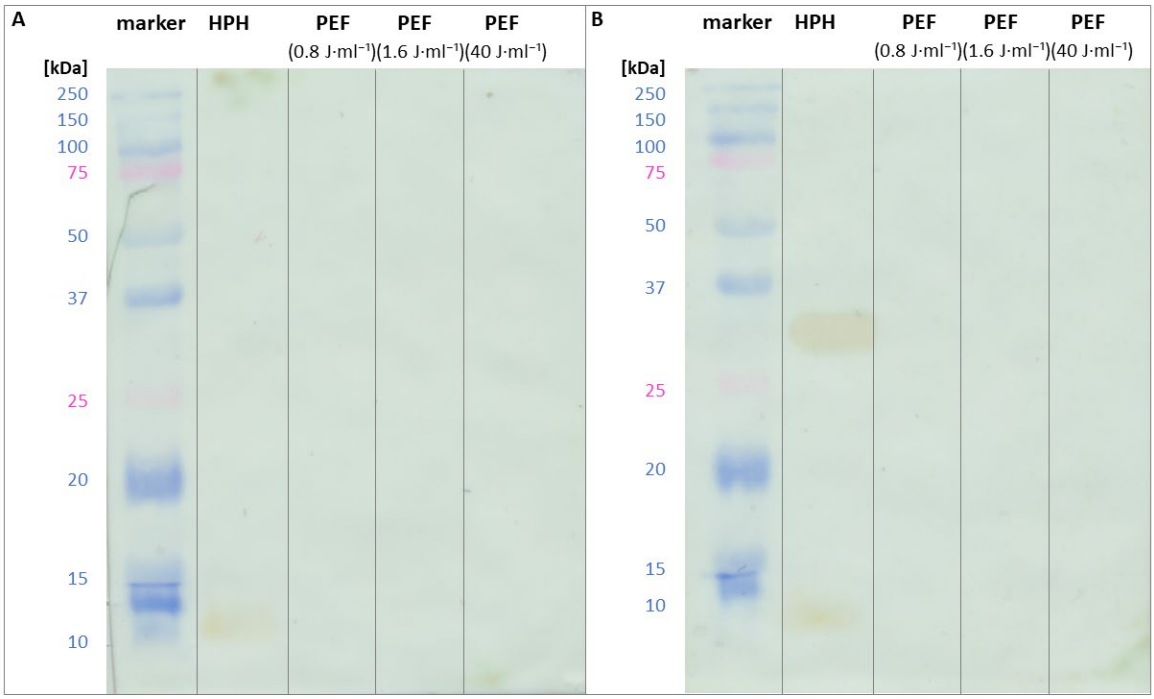

Figure 35 Detection of cytochrome c and f. *C. vulgaris* cultivated under continuous light and in the stationary phase (7 dpi) were concentrated to a high cell density (10 mg·ml^{-1}), one part pulsed with three specific energies of 0.8, 1.6 and 40 J·ml^{-1}, and the other part treated with HPH. After 24 h incubation, the generated supernatants were further size separated on a 15 % polyacrylamide gel and then assayed on western blots in order to detect cyt c (**A**) and cyt f (**B**). Input was analyzed by detecting the signal of horseradish peroxidase (HRP) coupled secondary antibodies (colorimetric assay). Blot is representative for n = 2 independent repetitions of the experiment.

5.3.4. Dependency of PEF induced mortality on cell density

PEF treatment as a cell disruption method requires high biomass concentrations to render the technology cost-effective. The following experiment investigated the influence factor of cell density on PEF induced mortality (**Figure 36**). Directly after PEF treatment with different specific energies of 0.8, 1.6 and 37 J·ml^{-1}, respectively, one part of the high cell density algal suspensions was diluted with sterile supernatant to low cell density suspensions. The other part of the algal suspensions was incubated at high cell density. Control samples without PEF treatment were incubated in parallel and showed no increased mortality. When observing the cell suspension at lower cell density, the initial mortality measured 2 h after PEF treatment does not change over the incubation period of 24 h independently from the energy input. When treated with a high specific energy of 37 J·ml^{-1}, the mortality was close to 100 % at the earliest time point – this could be observed both at low and high cell density. However, for lower specific energies the PEF induced mortality of high cell density suspensions differs considerably. PEF induced mortality increased drastically from 30 % to almost 90 % (0.8 J·ml^{-1}) and from 70 % to around 95 % (1.6 J·ml^{-1}) when the pulsed cells remained at high cell density.

At the rapid response (2h and 4 h) mortality is not significantly different at both cell densities, but after 24 h the mortality at high cell density is significantly increased in a slow response. Since the cells were only separated after pulsing, the difference cannot come from physical parameters during the PEF treatment and can only result from biological processes after the pulse. This has been followed up in subsequent experiments.

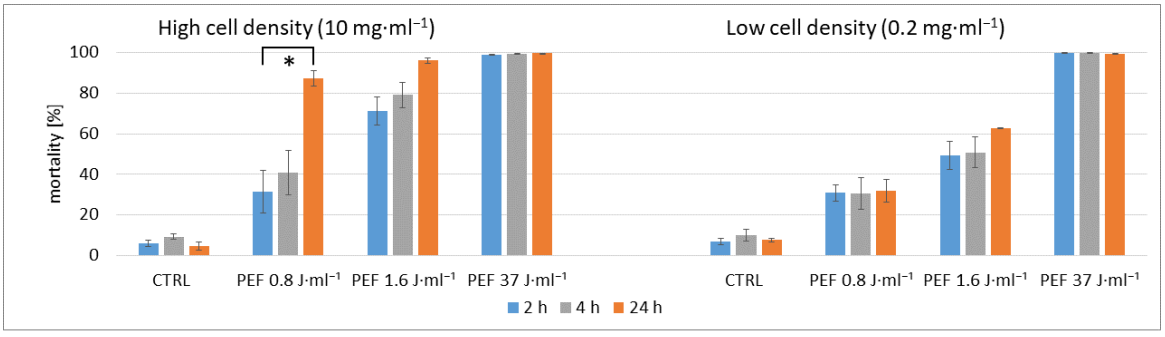

Figure 36 Influence of cell density on the mortality induced by PEF treatment with different energies. *C. vulgaris* from cultures grown under continuous light (7 dpi) were concentrated to a high cell density of 10 mg·ml^{-1} and pulsed with three specific energies chosen to establish around 70 % (0.8 J·ml^{-1}), 50 % (1.6 J·ml^{-1}), or 0 % viability (37 J·ml^{-1}), respectively. Immediately after PEF treatment, the sample was divided. One set remained at high-density, while the other set was diluted by a factor of 50 by adding sterile medium. Then, in both samples, viability was monitored over 24 h via FDA assay (50 µM). CTRL: control without PEF treatment. Data represent averages and standard errors from three biological replicates. Brackets indicate differences that are significant at P ≤ 0.05 (*), using two-sample t-test assuming equal variances. Modified from Krust *et al,* 2022.

5.4. PEF extracts a cell-death inducing factor from *C. vulgaris*

Higher cell death in high cell density suspensions surely provides advantages for biotechnological applications. Apart from that, the biology behind this phenomenon is very exciting to investigate. Why do cells die if they seem to have survived the first blow handed out by PEF treatment itself? And why is this effect only visible in high cell density suspensions? One possible explanation for PEF induced, time-dependently increasing mortality of high cell density suspensions (**Figure 36**) could be the release of a water-soluble factor that induces cell death in the neighboring cells. But is this putative cell-death inducing factor specific or merely a heightened concentration of some unspecific toxic compound? The following chapter will provide answers to some of these questions.

5.4.1. *C. vulgaris* releases the CDIF in response to PEF

To test the hypothesis regarding such a factor, an experiment was designed (**Figure 15**) where high cell density suspensions (donor cells) were incubated for 24 h after PEF treatment and the generated supernatant was defined as PEF SN. This extract was added to viable recipient cells and viability, converted into mortality, was measured after different incubation times. As negative controls, one part of viable recipient cells was incubated in their original medium and another part incubated in supernatant generated from non-pulsed donor cells, defined as CTRL SN. Viable recipient cells were taken from a synchronized culture (**Figure 37A**) as well as from the stationary phase (**Figure 37B**). In response to treatment with PEF SN, recipient cells from a synchronized culture showed a strong and rapid mortality of around 70 % after 3 h incubation followed by over 80 % after 24 h incubation. Recipient cells from the stationary phase showed rising mortality to a much lower extent with values reaching just over 40 % mortality after 24 h incubation in PEF SN. This cell-death inducing effect could be seen in both types of recipient cells independently of the specific energy. Neither in the negative control containing medium nor in the CTRL SN sample, any significant mortality could be observed. For subsequent experiments, the specific energies of 8.0 or 9.4 $J \cdot ml^{-1}$ were chosen for generating PEF SN since the PEF SN induced mortality did not change in the range of 0.8 to 37 $J \cdot ml^{-1}$.

The increased mortality in recipient cells can be explained by the hypothesis that *C. vulgaris* releases a cell-death inducing factor in response to PEF treatment. Such a compound generated by *C. vulgaris* can be dated back to the 1940s, where high-density cells in the stationary phase were found to generate a compound called Chlorellin that inhibited multiplication of cells (Pratt *et al,* 1944). Later this was identified as a mixture of fatty acids responsible for inhibiting growth (DellaGreca *et al,* 2010). However, other groups refuted Chlorellin, attributing the effect to high

bicarbonate concentrations in the medium of high-density cultures (Mandalam & Palsson, 1995). When looking at cell death in response to PEF treatment, it has been demonstrated to be an enzyme-driven process resulting in autolysis facilitating protein liberation (Scherer *et al,* 2019). Autolytic processes associated with cell death have already been described for yeast cells (Martínez *et al,* 2018a; Martínez *et al,* 2018b). Whether PEF treatment followed by autolysis is also responsible for the release of the CDIF is not clear. What can already be shown in this experiment is the fact, that the CDIF is released in consequence of perturbed membrane integrity since it also is released after applying the lowest tested specific energy which does not result in 100 % mortality of donor cells. Further studies are needed to identify the CDIF. As educated guesses, the CDIF could be classified as a protein or lipid-derived compound.

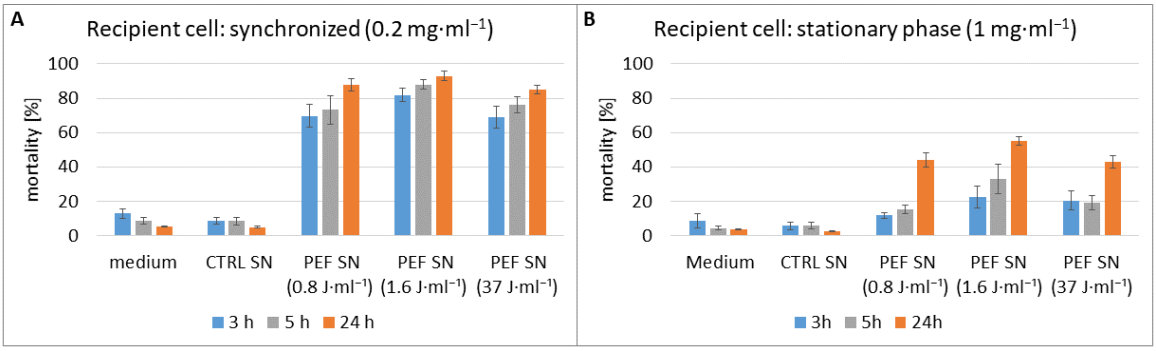

Figure 37 Cell mortality in response to supernatant of PEF treated cells. *C. vulgaris* cells from cultures grown under continuous light (7 dpi) were concentrated to a high cell density of 10 mg·ml^{-1}, as donor cells pulsed with three specific energies (0.8, 1.6 and 37 J·ml^{-1}) and incubated for 24 h. After centrifugation, the water-soluble extract in the supernatant (SN) of the PEF treated donor cells was added to viable recipient cells **A)** from a synchronized culture (time point 0) or **B)** grown under continuous light in the stationary phase (7 dpi). Viability of recipient cells was monitored over an additional 24 h via the FDA assay (50 µM). Medium: recipient cells without exchanging supernatant. CTRL SN: recipient cells treated with supernatant from untreated donor cells. PEF SN (specific energy): recipient cells treated with supernatant from PEF treated donor cells at given specific energies. Data represent averages and standard errors from three biological replicates. Modified from Krust *et al,* 2022.

5.4.2. The CDIF is heat-labile and dose-dependent

To further analyze the nature of the CDIF found in the extract after PEF treatment, the effects of preheating, protease inhibition (**Figure 39AB**) and cooling during the incubation period (**Figure 39CD**) were investigated. Incubation of PEF SN for 2 h at 40 °C and 50 °C completely disables the cell-death inducing effect when compared to incubation of extract for 2 h at 23 °C. This is visible for both recipient cells from a synchronized culture as well as recipient cells from the stationary phase. Visualization of the PEF extract incubated at different temperatures (**Figure 38**) shows clear separate bands for 23 °C, however, the intensity of the bands fades with higher temperatures. But contrary to expectation, there is not one prominent band that disappears completely that would

be able to account for containing the CDIF. The fact that the CDIF is prone to heat inactivation shows that either denaturing of protein content results in denaturing of the proteinaceous factor, or that the CDIF is degraded by enzymatic processes that are accelerated at this temperature.

In that respect, when checking for the involvement of proteases, treatment with protease inhibitor (PI) led to different results regarding different types of recipient cells. In synchronized recipient cells (**Figure 39A**), PI led to a slightly but significantly increased mortality in control samples (CTRL PI), while in recipient cells from the stationary phase no effect on mortality could be seen in control samples. When PI was added to PEF SN prior to incubation of synchronized recipient cells, the mortality was at first decreased (around 20 %) after 4 h incubation in the extract. However, after 24 h incubation, the mortality in presence of PI equaled that of cells treated with regular PEF SN. Recipient cells from the stationary phase (**Figure 39B**) show no delay of mortality in the rapid response. But a slight, albeit not significant decrease of mortality in presence of PI compared to cells treated with regular PEF SN could be observed in the slow response after 24 h. In connection with protease involvement, the delayed manifestation of mortality in recipient cells from a synchronized culture but not from the stationary phase leads to the conclusion that proteases might act in response to the CDIF in the recipient cell. This is more likely than proteases serving as the CDIF generated by donor cells, since then a similar effect would be visible in both types of recipient cells.

To compare another cell disruption method, the supernatant of total cell extract after HPH was investigated and found to contain the cell-death inducing effect as well. The effect of HPH supernatant (HPH SN) was even stronger, especially when monitoring the mortality of recipient cells in the stationary phase. Extract after PEF treatment led to a mortality of 60 % while HPH extract induced over 90 % of recipient cells to die. The even higher cell death after incubation in HPH SN proves that the mechanical cell extraction method liberates the CDIF as well. Since HPH treatment immediately destroys the cell and no cellular response to the treatment is possible, the CDIF must be already present in the donor cell and is not only generated with PEF treatment acting as a signal. With this experiment, PEF treatment related side effects e.g., metallic ions released due to electrode degradation or water electrolysis can be excluded as well. Another information gain is the fact that mechanical disruption does not destroy the CDIF.

When recipient cells are incubated with PEF and HPH extract at 4 °C compared to 23 °C, the cell-death inducing effect is decelerated (**Figure 39CD**). For recipient cells from a synchronized culture (**Figure 39C**), PEF SN induced mortality was less than half of that seen at 23 °C while HPH SN induced mortality was only slightly reduced by cold incubation. Recipient cells in the stationary phase (**Figure 39D**) show an even more pronounced decrease of mortality during incubation in PEF

SN with mortality dropping to values decreased by more than factor 4. At 23 °C, PEF SN causes around 70 % mortality after 24 h incubation while at 4 °C the mortality drops to 15 %. HPH SN induced mortality also shows a decrease by factor 2 when incubating recipient cells in the stationary phase. Also, it can be observed that there was a rapid increase in mortality in the time interval till 4 h, while the incremental mortality in the much longer period between 4 h and 24 h was small (around 10 % for synchronized and around 20 % for stationary phase). These incremental differences are comparable for both temperature conditions. The rapid early phase (0 h to 4 h) of cold incubation can be used for interpretation, to analyze how the drop of temperature (ΔT = - 19 °C) affects the mortality of cells. When calculating the rate reduction of recipient cells from a synchronized culture in response to PEF SN, the mortality rate is reduced by a factor of 2.3 which corresponds to a temperature coefficient (Q_{10}) of ~1.5. For recipient cells in the stationary phase, the rate reduction in response to PEF SN is even higher by a factor of 4.8, corresponding to a Q_{10} of ~2.3. This results in the conclusion that the mortality induced by the CDIF (in PEF SN) is more than a diffusion-driven process since the temperature sensitivity of enzymatically catalyzed reactions involved in plant respiration is often found with a Q_{10} of around 2 (Lambers *et al,* 2008, pp. 127-128) and diffusion-driven processes are defined with a Q_{10} around 1.

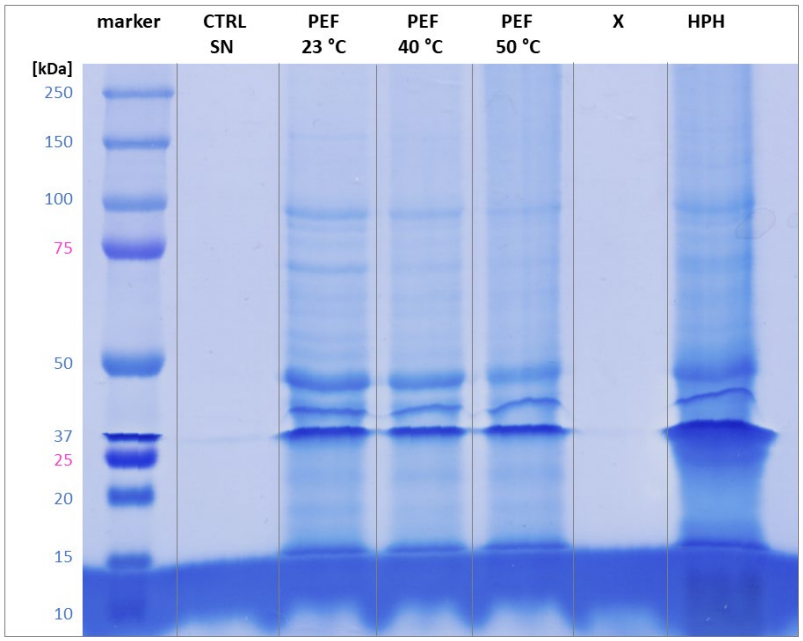

Figure 38 Visualization of protein extracts after heat inactivation. *C. vulgaris* cells from cultures grown under continuous light (7 dpi) were concentrated to a high cell density of 10 mg·ml^{-1}. One part was pulsed with a specific energy of 9.4 J·ml^{-1} and the other part treated with HPH. After centrifugation, the water-soluble extract was treated for 2 h in water baths with temperatures at 23 °C (PEF 23 °C), 40 °C (PEF 40 °C) and 50 °C (PEF 50 °C) and sterile filtrated to remove aggregates prior to sample preparation for SDS PAGE. The samples were separated on a 12 % polyacrylamide gel and subsequently visualized by Coomassie staining. CTRL SN: control without PEF treatment. X: empty lane.

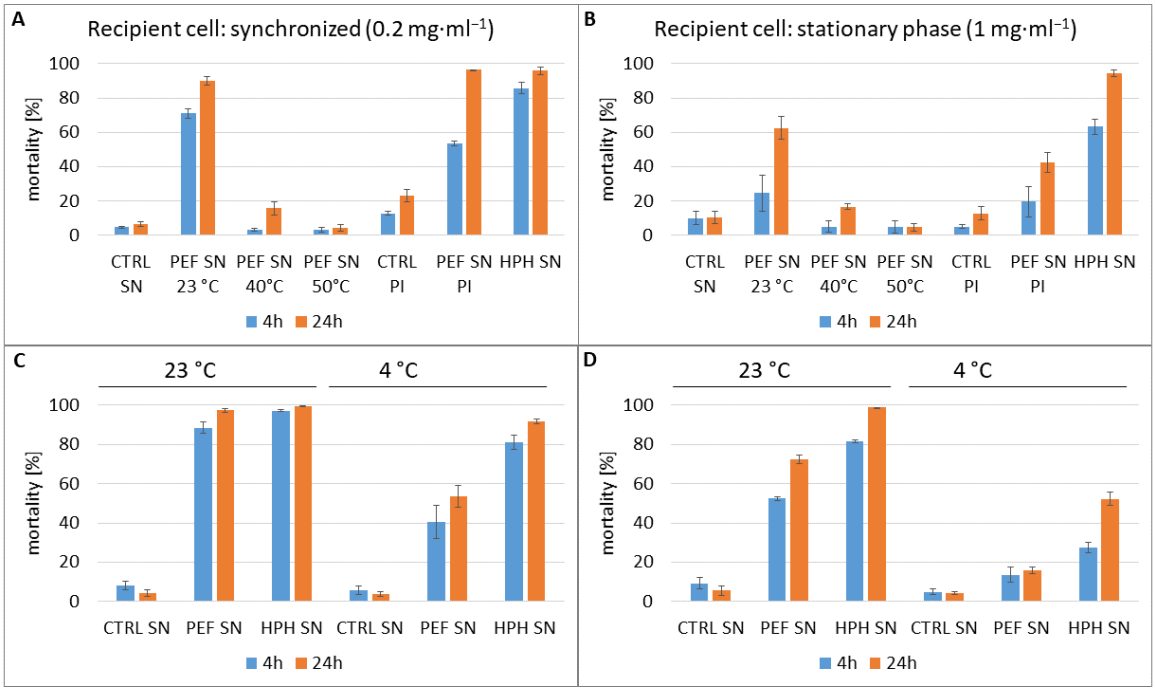

Figure 39 Temperature dependency of the CDIF. *C. vulgaris* from cultures grown under continuous light (7 dpi) were concentrated to a high cell density of 10 mg·ml^{-1}, as donor cells pulsed with a specific energy of 9.4 J·ml^{-1} and incubated for 24 h. After centrifugation, the water-soluble extract in the supernatant (SN) was added to viable recipient cells from a synchronized culture (**AC**, time point 0) or recipient cells grown under continuous light in the stationary phase (**BD**, 7 dpi). Viability was monitored at 4 h and 24 h via FDA assay (50 µM). **AB)** Before addition to live cells, the water-soluble extract was treated for 2 h in water baths with temperatures at 23 °C (PEF SN 23 °C), 40 °C (PEF SN 40 °C) and 50 °C (PEF SN 50 °C). The effect of protease inhibitor cocktail (PI) was tested on control samples (CTRL PI) and samples with PEF supernatant (PEF SN PI), additionally the effect of HPH supernatant (HPH SN) was tested. **CD)** Incubation period after addition of different supernatants was performed either at 23 °C or 4 °C. CTRL SN: recipient cells treated with supernatant from untreated donor cells. Data represent averages and standard errors from three biological replicates. Modified from Krust *et al,* 2022.

So far, previous experiments had been conducted using recipient cells with the original cell density after cultivation. For synchronized cultures, daily dilution leads to low cell density of around 0.2 mg·ml^{-1}, and for cells in the stationary phase (7 dpi) longer cultivation leads to a higher cell density of around 1 mg·ml^{-1}. Since the reception of the CDIF is also of great interest, those differently cultured recipient cells were normalized regarding cell density (**Figure 40**). The mortality induced by PEF and HPH extract is lower when the recipient cells come from the stationary phase as compared to synchronized cells, even when cell density was normalized to 0.2 mg·ml^{-1}. Interestingly, this reduced responsiveness of recipient cells in the stationary phase almost does not change at all, even though the cell density was diluted by factor 5. The effect of PEF SN on recipient cells in the stationary phase with a cell density of 1 mg·ml^{-1} is comparable with the effect on recipient cells with a cell density of 0.2 mg·ml^{-1}. The mortality induced by HPH SN is

even slightly reduced when diluting the cell density of recipient cells in the stationary phase. One point where the two recipient cells differ, is the composition of the cell wall. Recipient cells from a synchronized culture and shortly after autosporulation are enclosed only by a fragile unilaminar layer of cell wall (Yamamoto *et al,* 2004). Recipient cells in the stationary phase cells contain a rigid thick cell wall (Safi *et al,* 2014). One possible explanation could be, that the CDIF has easier access to recipient cells with a fragile cell wall, explaining the lower resistance of recipient cells from a synchronized culture. In conclusion, the CDIF has to cross the cell wall to gain access to the cell membrane, possibly to activate a putative signal-receptor (either membrane-bound or inside the of cell). This result also provides the first hint of possible dependency on the cell cycle stage of the recipient microalgae. From this point on, the cell density of recipient cells was normalized to 0.2 mg for both ways of cultivation.

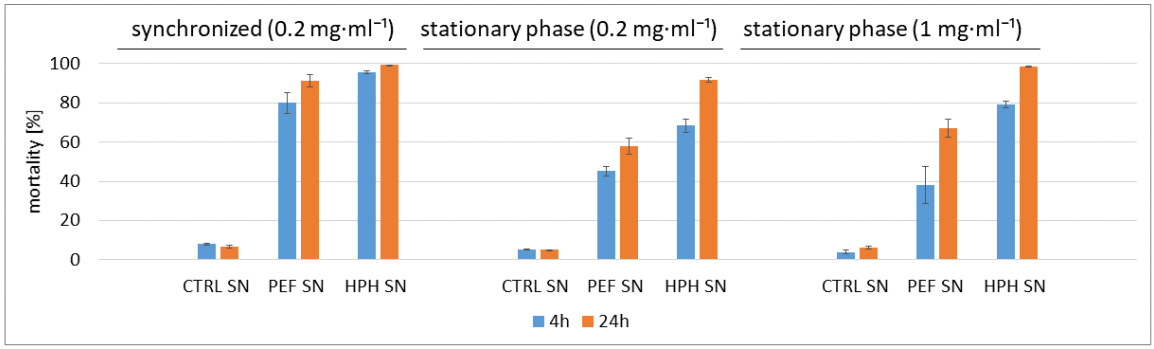

Figure 40 Cell mortality after addition of the CDIF while comparing differently cultivated recipient cells. *C. vulgaris* from cultures grown under continuous light (7 dpi) were concentrated to a high cell density of 10 mg·ml^{-1}, as donor cells pulsed with a specific energy of 9.4 J·ml^{-1} and incubated for 24 h. After centrifugation, the water-soluble extract in the supernatant (SN) was added to viable recipient cells, either synchronized (time point 0), or cultivated under continuous light in the stationary phase at comparable cell density (0.2 mg·ml^{-1}) and at higher cell density (1 mg·ml^{-1}). Viability was monitored at 4 h and 24 h via FDA assay (50 µM). CTRL SN: recipient cells treated with supernatant from untreated donor cells; HPH SN: high-pressure homogenization supernatant. Data represent averages and standard errors from three biological replicates. Modified from Krust *et al,* 2022.

Next, the dose-response relation of the CDIF was tested by diluting PEF extract as well as HPH extract from donor cells. These dilution series were tested on recipient cells from a synchronized culture (**Figure 41A**) as well as from stationary phase (**Figure 41B**) while keeping the cell density of the recipient cells constant. When looking at the recipient cells from a synchronized culture, PEF and HPH extract retain a comparable cell-death inducing effect down to a dilution of ten times. If the extracts are diluted further, the mortality starts to decrease significantly. In the end, for both PEF and HPH SN a dilution of 1:100 yields a mortality that is only insignificantly higher than that seen in untreated control samples. Recipient cells from the stationary phase are affected by PEF SN with even lower concentrations, including a dilution of 1:50. In contrast, HPH SN starts to lose

its cell-death inducing effect already with a dilution of 1:50. For stationary phase recipient cells, both PEF and HPH SN with a dilution of 1:100 cause insignificantly higher mortality than the control samples, same as for recipient cells from a synchronized culture. This dose-dependency experiment strengthens the model of a receptor that accepts the CDIF. At high concentrations of the CDIF this putative receptor can be saturated with a signal while at lower concentrations only partial activation leads to reduced signaling resulting in reduced mortality in the recipient cell.

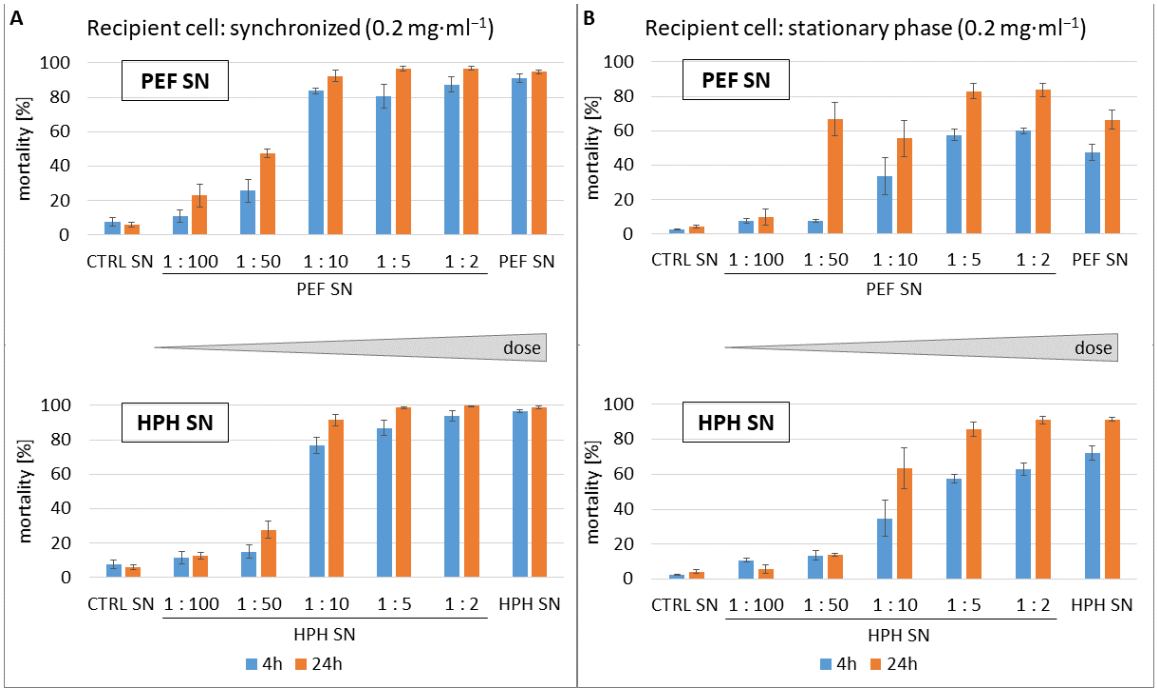

Figure 41 Dilution series of extracts containing the CDIF. *C. vulgaris* from cultures grown under continuous light (7 dpi) were concentrated to a high cell density of 10 mg·ml^{-1} (donor cells), one part pulsed with a specific energy of 9.4 J·ml^{-1} and the other part treated with HPH. After 24 h incubation followed by centrifugation, the water-soluble extract in the supernatant (SN) was diluted with sterile medium in given ratios and added to viable recipient cells from a synchronized culture (**A**, time point 0) or recipient cells grown under continuous light in the stationary phase (**B**, 7 dpi). Viability was monitored at 4 h and 24 h via FDA assay (50 µM). CTRL SN: recipient cells treated with supernatant from untreated donor cells. Data represent averages and standard errors from three biological replicates. Modified from Krust *et al,* 2022.

5.4.3. Generation of the CDIF in the stationary growth phase

So far, the generation of cell-death inducing extract had been achieved using donor cells from cultures grown under continuous light in the stationary phase (7 dpi). The exponential growth phase takes place on 2-3 dpi and with the start of 4 dpi, the stationary phase is reached (**Figure 9**). This experiment was designed to test whether the ability to extract cell-death inducing activity depends on the growth phase of the donor cell. For this purpose, PEF and HPH extracts from donor cells with normalized cell density at different time points of the culture cycle were generated. These extracts were tested on recipient cells from a synchronized culture (**Figure 42A**), as well as

from the stationary phase (**Figure 42B**), with normalized cell density. PEF extracts cause increasing toxicity with the growing age of culture (upper row). PEF SN generated from donor cells at 2 to 3 dpi shows a very small cell-death inducing effect after 24 h incubation with extract, independently of the recipient cell type. When observing mortality of cells treated with PEF SN from the start of the stationary phase at 4 dpi and older, the cell-death inducing effect increases with the age of the donor cells. HPH extract shows a similar tendency (lower row). However, when recipient cells from a synchronized culture are incubated with HPH extract from different growth phases, HPH extract shows significant cell-death inducing activity after 24 h incubation with extract even in the exponential phase (2-3 dpi). This cannot be observed for recipient cells in the stationary phase, where the cell-death inducing activity of HPH SN only starts when the donor cells have reached the stationary phase. The cell-death inducing effect of HPH SN in the exponential phase (**Figure 42A**) shows a delayed rapid response, instead, the slow response develops in a more pronounced way. This might be explained by the assumption that cells in the exponential growth phase generate the CDIF in very low concentrations so it can only be found in total cell extract after HPH treatment and only affects the more sensitive synchronized cells. It could also be possible that there is a compartmentalization of synthesis, so that two or more pro-factors of the CDIF are kept separated and only after HPH treatment the total cell extract combines those. It is also plausible that the CDIF is membrane-bound to prevent accidental self-suicide. This could also prevent extraction by PEF treatment. All in all, both PEF and HPH SN are most potent when donor cells have reached the stationary phase. The characteristic sigmoidal growth curve is caused by mixotrophic cultivation in TAP medium that ultimately leads to limited nutrient supply and mutual shading of the cells resulting in induction of the stationary phase. Physiological and biochemical characteristics vary greatly during the different growth phases (Borowitzka *et al,* 2016, pp. 3-46). These variations include protein levels, lipid, and secondary compound accumulation as well as changes in gene expression. When in the exponential phase, cells are still undergoing division or expansion while in the stationary phase differentiation is initiated. Summing up this experiment, the CDIF is only generated in higher concentrations when donor cells have reached the stationary growth phase. In the exponential phase, the CDIF is generated at very low concentrations that can only be extracted by HPH treatment and only affects synchronized recipient cells.

To gain further insight into the nature of the CDIF, the protein content extracted by PEF treatment and the total protein content in HPH extract were measured during the growth phase of the donor cell (**Table 3**). From these two values, the extraction efficiency can be calculated. The overall protein content as well as the PEF treatment extraction efficiency increased with the progression of the donor cells through the culture cycle. This increase was concomitant with the rise of the

mortality caused by the PEF extract (**Figure 42**). However, the PEF-released protein increase (around 1.6-fold) was not able to account for the much stronger (around 4- to 5-fold) increase of the cell-death activity during the transition from exponential phase to stationary phase.

Table 3 Protein content of HPH and PEF extracts after 24 h incubation measured by Lowry assay. *C. vulgaris* from cultures grown under continuous light at different time points of the growth curve were concentrated to a high cell density and subjected to HPH and PEF treatment. Data represent averages and standard errors from three biological replicates. Modified from Krust *et al,* 2022.

time [dpi]	Total protein (HPH) [% CDW]	Extracted Protein (PEF) [% CDW]	Extraction efficiency [%]
2	44.53 ± 0.30	13.53 ± 0.20	30.4
3	48.13 ± 1.73	13.63 ± 0.65	28.3
4	52.92 ± 2.28	21.98 ± 1.01	41.5
5	52.94 ± 0.21	22.54 ± 0.81	42.6

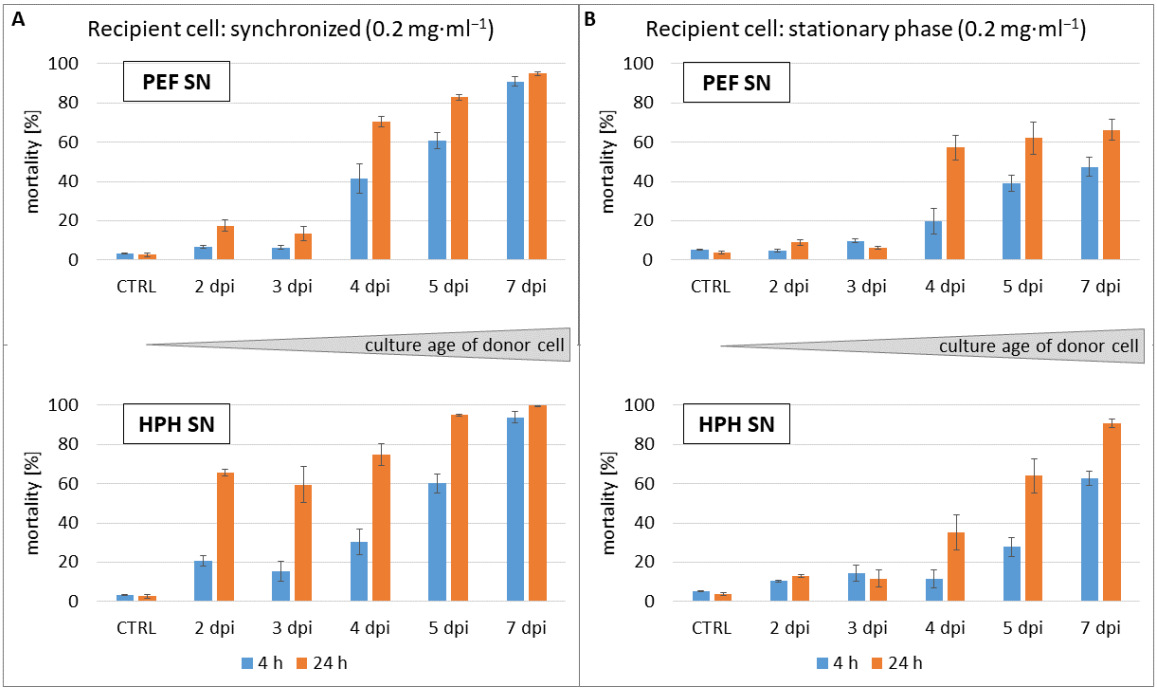

Figure 42 Dependence of the CDIF on culture age of donor cell. *C. vulgaris* from cultures grown under continuous light at different time points of the growth curve were concentrated to a high cell density of 7 mg·ml^{-1} (donor cells), one part pulsed with a specific energy of 8.0 J·ml^{-1} and the other part diluted by factor 2 and treated with HPH. After 24 h incubation followed by centrifugation, the water-soluble extract in the supernatant (SN) was added to viable recipient cells from a synchronized culture (**A**, time point 0) or recipient cells grown under continuous light in the stationary phase (**B**, 7 dpi). Viability was monitored at 4 h and 24 h via FDA assay (50 µM). CTRL SN: recipient cells treated with supernatant from untreated donor cells. Data represent averages and standard errors from three biological replicates. Modified from Krust *et al,* 2022.

For clarification on whether the CDIF is generated depending on the growth phase of the donor cell, another experiment using synchronized cells as donor cells was conducted. Synchronized cells are kept in a perpetual exponential growth phase by diluting the culture continuously. To check for the generation of the CDIF, synchronized cells from two different time points in the synchronization cycle (0 h and 6 h) were used as donor cells, with normalized cell density compared to previous experiments. In parallel, donor cells from the stationary phase were used as a positive control. The extracts from both different donor cell types were tested on recipient cells from a synchronized culture (**Figure 43A**), as well as on recipient cells from the stationary phase (**Figure 43B**), with normalized cell density. The cell-death inducing effect of PEF extract was completely abolished, irrespective of whether PEF treatment was applied to the donor cells from a synchronized culture at 0 h or at 6 h of the cell cycle (lower row). Additionally, the recipient cell type did not make any difference. This led to the conclusion that the synchronized cell culture does not generate the CDIF, at least not in an amount that is extractable by PEF treatment. It would be interesting to analyze HPH extract of the synchronized culture for the existence of the CDIF, since the cell-death inducing activity of donor cells in the exponential phase (2 dpi) could only be detected in HPH extract.

When quantifying the protein content of PEF treated synchronized culture (**Table 4**), it can be observed that PEF extract of donor cells from a synchronized culture only contains 5-7 % CDW protein. This is only roughly one fourth of the protein content when compared to PEF extract of donor cells from stationary phase. The total protein content is predicted to be lower as well (around 20 % CDW when assuming PEF extraction efficiency of 30 %). However, the CDIF might not even be a protein, so protein concentration might not be related to the cell-death inducing effect.

Table 4 Protein content of PEF extracts after 24 h incubation measured by Lowry assay. *C. vulgaris* from cultures grown under continuous light and from synchronized cultures at different time points were concentrated to a high cell density and subjected to PEF treatment. Data represent averages and standard errors from three biological replicates.

	Extracted Protein (PEF) [% CDW]	
	Time point 0 h	**Time point 6 h**
donor cell: stationary phase (7 dpi)	21.06 ± 0.59	21.66 ± 0.76
donor cell: synchronized	6.77 ± 0.54	5.14 ± 0.95

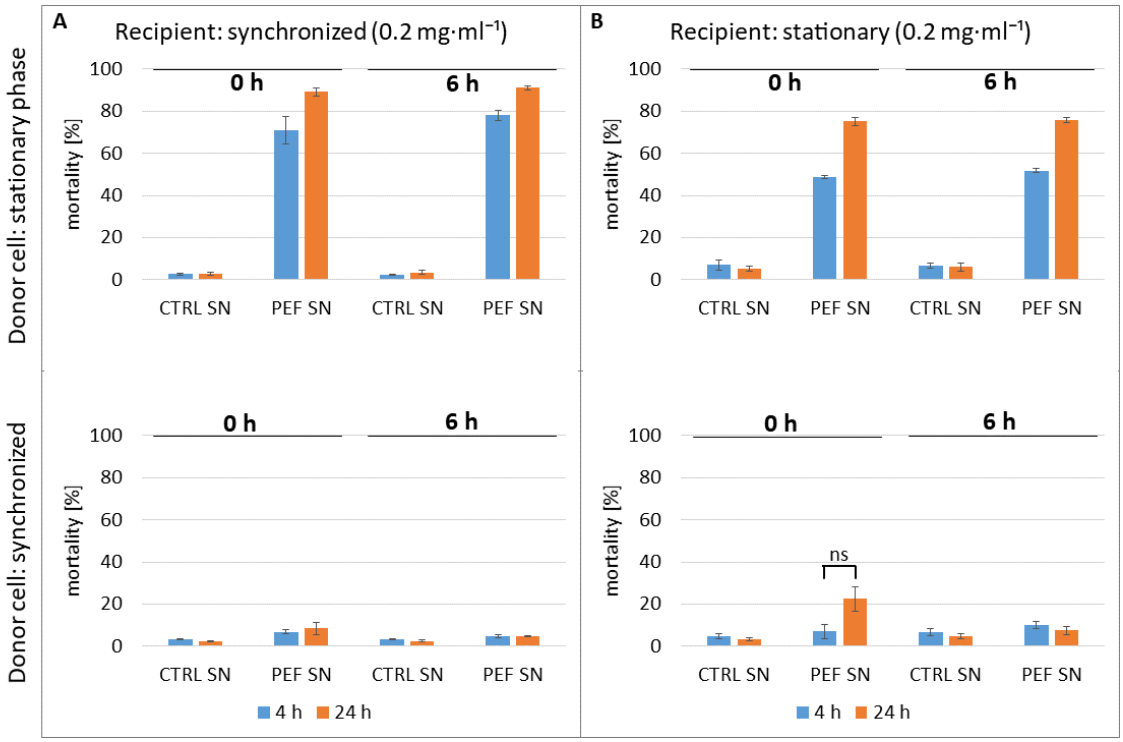

Figure 43 Dependence of the CDIF on cultivation method of donor cell. Upper row: *C. vulgaris* from cultures grown under continuous light were concentrated to a high cell density of 5.7 mg·ml^{-1} (donor cell: stationary phase), lower row: *C. vulgaris* from synchronized cultures were concentrated to a high cell density of 6.3 mg·ml^{-1} (donor cell: synchronized, time points 0 h and 6 h), both high cell density suspensions were pulsed with a specific energy of 8.0 J·ml^{-1}. After 24 h incubation followed by centrifugation, the water-soluble extract in the supernatant (SN) was added to viable recipient cells from a synchronized culture (**A**, time points 0 h and 6 h) or recipient cells grown under continuous light in the stationary phase (**B**, 7 dpi). Viability was monitored at 4 h and 24 h via FDA assay (50 µM). CTRL SN: recipient cells treated with supernatant from untreated donor cells. Data represent averages and standard errors from three biological replicates. Brackets indicate non-significant (ns) differences ($P > 0.05$), using two-sample *t*-test assuming equal variances. Modified from Krust *et al,* 2022.

So far, the generation of cell-death inducing extract had been achieved by incubating PEF treated high cell density suspensions as donor cells for 24 h. To investigate the time-dependent release of the CDIF, a time course varying the incubation time of donor cells after PEF treatment was conducted. The generated extracts were tested on recipient cells from a synchronized culture (**Figure 44A**), as well as from the stationary phase (**Figure 44B**), with normalized cell density. It has to be taken to mind that recipient cells from a synchronized culture are concomitantly maturing in the cell cycle, with the time points 1 h and 24 h incubation time of donor cell in **Figure 44A** corresponding to time point 0 h in the synchronization cycle. The time point 6 h incubation time of donor cell corresponds to time point 6 h in the synchronization cycle of the recipient cell. When looking at the effect on recipient cells from synchronized culture, the release of the CDIF already reaches saturation at 6 h incubation time of donor cell. Longer incubation periods lead to lower mortality in synchronized recipient cells. The effect on recipient cells from the stationary phase

paints a different picture. The maximum effect can also be seen at 6 h incubation time of donor cell, however, longer incubation periods of the donor cell show a saturation and no reduction of mortality. The differences in mortality between 6 h and 8 h incubation time of donor cells are not significant. In conclusion, this experiment shows that the CDIF is released in a time-dependent manner with the highest activity after 6 h incubation. The results from synchronized recipient cells are distorted insofar that reception of the CDIF might additionally be dependent on the cell cycle (see next chapter). In contrast, recipient cells from the stationary phase show saturation of release after 6 h incubation. This time-dependency hints at biological processes in action.

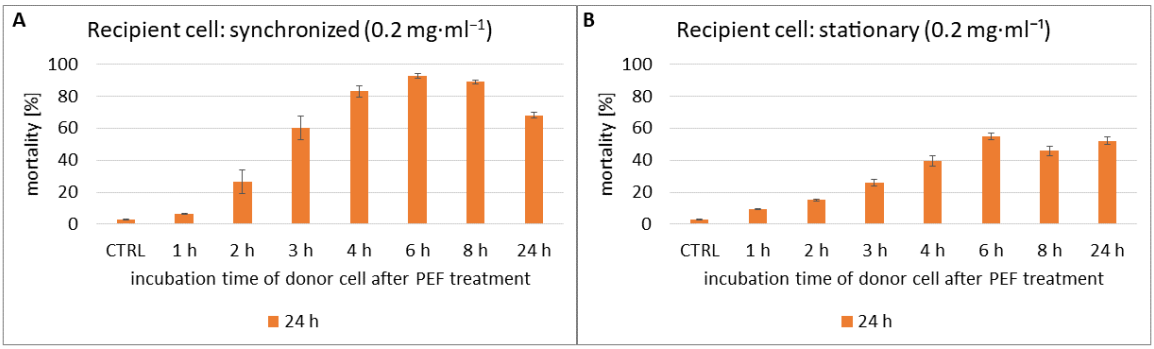

Figure 44 Time course of the CDIF release. *C. vulgaris* cells from cultures grown under continuous light (7 dpi) were concentrated to a high cell density of 6 mg·ml^{-1}, as donor cells pulsed with a specific energy of 9.4 J·ml^{-1} and incubated for 1, 2, 3, 4, 6, 8 and 24 h. After centrifugation, the water-soluble extract in the supernatant (SN) was added to viable recipient cells **A)** from a synchronized culture (time point 0) or **B)** grown under continuous light in the stationary phase (7 dpi). Viability was monitored after an incubation period of 24 h via FDA assay (50 µM). CTRL: recipient cells without exchanging supernatant. Data represent averages and standard errors from three biological replicates.

5.4.4. Reception of the CDIF

After dissection of the generation of the CDIF, a closer look was taken at the reception. In a first step, the specificity of the extract was investigated. It could be demonstrated that already the way of cultivation of *C. vulgaris* – whether the recipient cell is synchronized or in the stationary phase – makes a difference in the magnitude of mortality (**Figure 40**). Next, the effect of the cell-death inducing PEF and HPH extracts from *C. vulgaris* was tested when changing the species of recipient cell to the related species *A. prothothecoides* (**Figure 45A**) and *S. almeriensis* (**Figure 45B**). As negative controls, one part of viable recipient cells was incubated in their original medium (Wu or Arnon) and another part incubated in supernatant generated from non-pulsed *C. vulgaris* donor cells, which corresponds to used TAP cultivation medium. When measuring mortality of recipient cells from related species, the addition of cell-death inducing PEF and HPH extracts does not have any effect at all on these recipient cells. Neither TAP medium itself, nor PEF SN or HPH SN shows any cell-death inducing effect on *A. prothothecoides* and *S. almeriensis*. The fact that the CDIF has no effect on related species shows a clear specificity for *C. vulgaris*. This specificity also excludes

general toxic effects of released compounds as has been proposed for high bicarbonate concentrations (Mandalam & Palsson, 1995) when reaching the stationary phase with high-density suspensions. The described phenomena concerning the CDIF might not involve a defense mechanism, but rather a housekeeping or survival mechanism. One possible hypothesis proposes that the CDIF is involved in an inherent cellular mechanism (like breakage of a mature mother cell wall at autosporulation) set off at the wrong time. Otherwise, the CDIF could be a specific (but normally contained) signal for induction of PCD achieving that part of the cells provide surviving cells with nutrients.

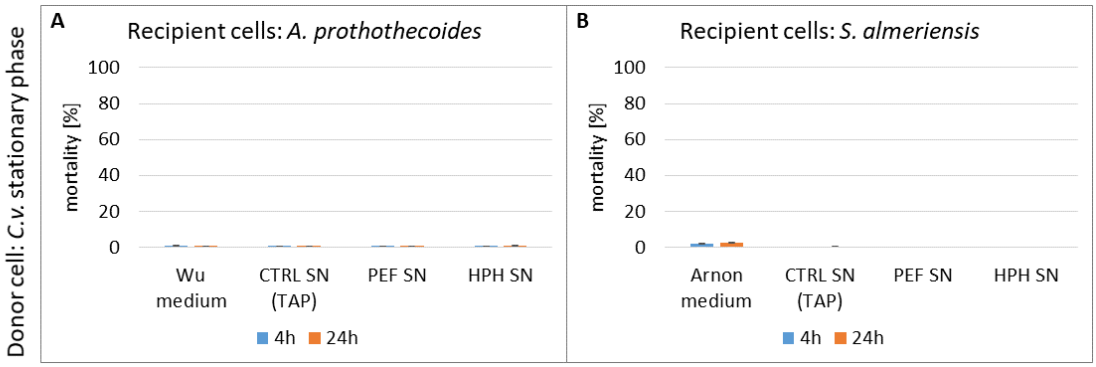

Figure 45 Effect of the CDIF on recipient cells from different microalgae species. *C. vulgaris* from cultures grown under continuous light were concentrated to a high cell density of 10.5 mg·ml^{-1} (donor cell: stationary phase), one part pulsed with a specific energy of 9.4 J·ml^{-1} and the other part treated with HPH. After 24 h incubation followed by centrifugation, the water-soluble extract in the supernatant (SN) was added to viable recipient cells **A**) *Auxenochlorella protothecoides* and **B**) *Scenedesmus almeriensis* (biomass of both species 0.2 mg·ml^{-1}). Viability was monitored at 4 h and 24 h via YO-PRO assay (1 µM). Wu medium (A.p.) and Arnon medium (S.a.) represent the respective controls in own cultivation medium. CTRL SN: recipient cells treated with supernatant from untreated donor cells (TAP medium). Data represent averages and standard errors from two biological replicates.

Another way the reception of the CDIF can be analyzed is by investigating the dependency on the cell cycle. In previous experiments it could already be demonstrated that PEF induced mortality depends on the cell-cycle stage in synchronized cells (**Figure 27**). The experiment was modified insofar, that here the responsiveness of recipient cells in dependency of the cell cycle was tested. Recipient cells were sampled at different stages of the cell cycle and mortality to PEF and HPH extracts monitored after 4 h incubation (**Figure 46A**) or 24 h incubation (**Figure 46B**). In general, it could be observed that the responsiveness of the recipient cells to PEF extract was dependent on the progression of the cell cycle. Just at the onset of the light phase (0 h), shortly after autosporulation, the cells were less sensitive when compared to enlarged cells (6 h, light phase) or compared to cells in the G2 phase (-6 h, dark phase). This could be observed for both the rapid response of 4 h incubation with extract, as well as for the long-term response after 24 h incubation with extract. The fact that the responsiveness to the CDIF depends on the cell cycle stage the same

as PEF induced mortality, is another sign pointing towards the CDIF acting not merely as a non-specific toxin, but as a specific signal. When comparing the behavior of cells in G2 (-6 h in the dark phase), the response to the CDIF results in high mortality while direct PEF treatment causes mortality as low as for cells shortly after autosporulation. Since the cell cycle is similarly controlled in microalgae than in higher plants, with cyclin-dependent kinase CDKB and cyclin B playing essential parts for mitosis (Atkins & Cross, 2018), the CDIF might interfere with mitosis regulation pathways. When taking all prior results into consideration, a model can be composed to differentiate between the behavior of cells in G2. In the first case, direct PEF treatment at low specific energies acts as a mild abiotic stress signal that can be compensated through activation of adaptive gene expression. In the second case, the CDIF released from pulsed cells acts as a biotic signal and activates a different pathway culminating in programmed cell death. In summary, it can be said that the CDIF acts with high specificity and shows dependency on the cell cycle either through different expression levels or different activity. The reception of the CDIF most likely is through a signal-receptor complex leading to the activation of pathways culminating in PCD. Whether the receptor concentration varies over the cell cycle, or whether the processing of the signal is cell-cycle dependent, remains to be elucidated. In contrast, the responsiveness to HPH extract shows no difference when comparing different cell cycle stages of the recipient cells. This could be caused by the heightened sensitivity of synchronized cells to the CDIF in HPH extract even at very low concentrations, as could already be seen in reaction to HPH extract from donor cells in the exponential phase (**Figure 43A**, lower graph).

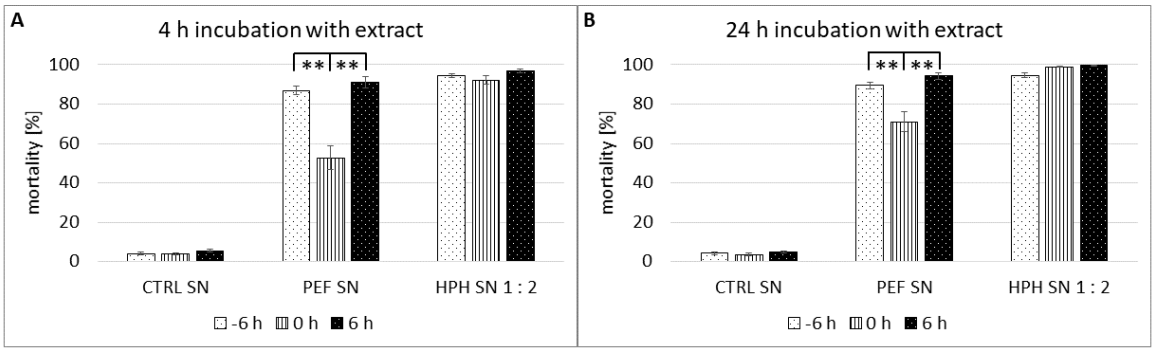

Figure 46 Cell mortality of synchronized recipient cells at different stages of the cell cycle in response to the CDIF. *C. vulgaris* from cultures grown under continuous light (7 dpi) were concentrated to a high cell density of 7.6 mg·ml^{-1} (donor cells), one part pulsed with a specific energy of 9.4 J·ml^{-1} and the other part diluted by factor 2 and treated with HPH. After 24 h incubation followed by centrifugation, the water-soluble extracts were added to live synchronized cells at different times of the cell cycle (-6 = dark, 0 = onset of light, 6 = light) and viability was monitored at 4 h and 24 h via FDA assay (50 µM). Data represent averages and standard errors from at least three biological replicates. Brackets indicate differences that are significant at P ≤ 0.01 (**), using two-sample *t*-test assuming unequal variances. Modified from Krust *et al,* 2022.

5.4.5. Attempt at elucidation of the CDIF

To further elucidate the nature of the CDIF, activity-guided size-exclusion chromatography was performed. When looking at the elution profile after SEC (**Figure 47A**), the protein was separated into over 100 fractions which could be pooled (Pool 1 – 10). Visualization of the strongly diluted pooled fractions (**Figure 47B**) shows faint bands that are not corresponding to size, as would have been expected from SEC. Pool 3 (P3), which had the highest protein content, contains bands from 15 kDa to 100 kDa. The same can be observed in the other lanes. Nevertheless, the pooled fractions were tested for their activity on recipient cells from a synchronized culture (**Figure 47C**). Here, the negative control containing only SEC buffer did not show any cell-death inducing effect while every one of the tested pooled fractions (P1-P7) caused a mortality of 50 % or higher in recipient cells. Interestingly, the fraction containing the highest protein content (P3) showed the least cell-death inducing effect on recipient cells. The highest cell-death inducing effect was caused by pool 6 (P6), Here, the cell-death inducing effect equaled that of fresh PEF extract even though the protein content of the pooled fraction was much lower. In a next step, P6 was defined as containing the most potent activity and concentrated again by ultrafiltration. The concentrated fraction P6 was again visualized (**Figure 47D**) and confirmed to include bands from size 25 kDa to 100 kDa. The diluted fraction shows the most abundant proteins in three sizes: around 28, 34 and 45 kDa. The following MALDI-TOF mass spectroscopy analysis validated a total of 1,000 proteins with a false discovery rate (FDR) of 1 % at the protein and peptide level. The database Chlorophyta (ID 3041, 305,334 entries) from Uniprot was used for the search. Only 1.6 % of these hits were identified for *C. vulgaris* (**Table 5**), the rest recognized proteins in related species. The list is sorted by descending score, which corresponds to the quality of identification.

One of the hits with the highest score detected was the Heat shock protein 70 (Hsp70). In addition to detection for *C. vulgaris,* other hits confirmed presence in 4 related species. Heat shock proteins (Hsp) are proteins that are expressed in response to stress conditions (e.g., heat, oxidative stress) and act as molecular chaperones (1) facilitating de novo folding, (2) preventing aggregation, (3) assisting of translocation into organelles such as the chloroplast as well as (4) degradation of misfolded proteins (Al-Whaibi, 2011; Usman *et al,* 2017). Hsp are part of the adaptive defense mechanism and since previous experiments already classified PEF treatment as an abiotic stress signal, the expression of such a protein makes sense. However, in mammalian cells, Hsp70 has also been shown to act as an extracellular signal (Calderwood *et al,* 2007) which initiates signal transduction in neighboring cells. This would fit nicely into the model concerning the CDIF, making Hsp70 a serious candidate.

Next on the list was the Elongation factor tu (EF-Tu) with additional hits confirmed in 10 related species. This protein transports aminoacyl-tRNA to ribosomes during protein biosynthesis in a GTP-dependent process. Other roles include chaperone activity as protection against aggregation and facilitating renaturation of misfolded proteins, as well as degradation of proteins by the proteasome (Fu *et al,* 2012). Interestingly, the N-terminal part of bacterial EF-Tu acts as a pathogen-associated molecular pattern (PAMP) and elicits plant innate immunity (Kunze *et al,* 2004). It has already been investigated that peptides derived from plant mitochondrial or plastid EF-Tu are inactive PAMPs. However, in bacterial cells, EF-Tu can be exposed on the surface (Harvey *et al,* 2019) in order to interact with membrane receptors. Since EF-Tu already plays a role in stress response, can act as an elicitor in bacterial infection and has been found to be exposed on the surface of cells, a potential role as an extracellular signal seems plausible.

With a similar score to EF-Tu, RuBisCO could be detected in the sample with additional hits in 65 related species. This immense number of hits is most likely caused by the high conservation of the protein and by the fact that the sequence for RuBisCO has been deposited for many related species. It is commonly known that the concentration of RuBisCO can reach up to 50 % of soluble proteins in plant cells (Heldt & Piechulla, 2015, p. 163). However, the RuBisCO concentration in microalgae seems quite low making up only up to 6 % (in *C. reinhardtii* 2 %) in several microalgae species (Losh *et al,* 2013). The release of RuBisCO after PEF has already been confirmed in western blots (Scherer *et al,* 2019), so this hit comes as no surprise. Since another role for RuBisCO apart from carbon fixation is not known, this protein is highly unlikely to act as CDIF. The following proteins, 2-cys peroxiredoxin, thioredoxin reductase and ascorbate peroxidase are all involved as abundant antioxidant proteins. Cellular antioxidant proteins help to control intracellular peroxide levels and prevent oxidative stress damage in cells (microalgal antioxidant pathways reviewed in Tamaki *et al,* 2021). Peroxiredoxin and thioredoxin reductase are additionally involved in redox signaling (Liebthal *et al,* 2018). Both of these enzymes have been identified in *C. vulgaris* (Machida *et al,* 2012) and are suggested to play part in increasing stress tolerance (freezing, heat and oxidative stress). These proteins are one part of an important mechanism in response to stress, but a further role as an extracellular signal is unlikely. The antifreeze proteins and cold-regulated protein 2 could only be detected in *C. vulgaris.* Antifreeze proteins or ice-binding proteins protect cells against freezing at extremely low temperatures by decreasing the freezing point of fluids and inhibiting ice crystallization (Kim *et al,* 2017). Nothing is known about these proteins in *C. vulgaris* except identification and characterization (Liu *et al,* 2011) and their role as CDIF seems unlikely.

With a rather low score, but additionally detected in 7 related species, the “ATP-dependent Clp protease proteolytic subunit” was identified. This protein plays a central role in chloroplast

development and regular functioning and is responsible for the selective removal of misfolded, aggregated, or unwanted proteins. The degradation signal on protein targets is not known yet (Nishimura & van Wijk, 2015). It boasts a highly conserved basic structure with a barrel-like protease core. The proteolytic subunit is the only subunit that is encoded in the chloroplast genome. Depletion of Clp protease shows that this protease is essential for cell viability and gradual depletion leads to an autophagy-like morphology (Ramundo *et al,* 2014). Additionally, there exists a connection with Hsp70 chaperone in *A. thaliana,* where both Hsp70 and Clp protease were found to be required for protection against oxidative stress (Pulido *et al,* 2017). It cannot be excluded that the Clp protease works in cooperation with Hsp70, one serious candidate for the CDIF. However, the chloroplast specific role makes extracellular signaling rather unlikely for involvement as CDIF. Additionally, the protease inhibition of PEF extract would have affected this protein, so this candidate seems unlikely.

Three proteins at the end of the table, Glucose-6-phosphate 1-dehydrogenase, ATP synthase subunit beta and 50S ribosomal protein L12 are all abundant in the PEF SN since they play a vital part in maintaining regular cellular homeostasis. Glucose-6-phosphate 1-dehydrogenase catalyzes the first step of the oxidative pentose-phosphate pathway. ATP synthase subunit beta is a fundamental part of the respiratory chain and the 50S ribosomal protein L12 as part of the ribosomal stalk is essential for accurate translation. All three proteins are unlikely to acts as CDIF. Thiamine thiazole synthase with a very low score is upregulated by abiotic stresses (Li *et al,* 2016). But even if it represents one important mechanism in response to stress, a role as an extracellular signal is unlikely. Cyt f can faintly be detected, this further confirms the western blot results (**Figure 35**). With such a low score it is no wonder that the detection of cyt f after PEF treatment was not possible.

When looking into literature, the CDIF might also play a direct role in the autolytic process via cell wall degradation. While analyzing lipid bioaccessibility, Canelli *et al* (2022) could show the presence of enzymes with hydrolytic activity as well as one protein with calcium binding activity by proteome analysis of PEF extracted proteins. The hydrolytic enzymes are most likely involved in cell wall degradation of the own cell as well as still intact neighbor cells while the calcium binding protein has been proposed to be involved in the cellular response to stress induced by PEF. This opens the possibility of not one CDIF, but several enzymes working in accord. However, the enzymes identified in the work of Canelli *et al* (2022) could not be detected in the proteomic analysis of this thesis.

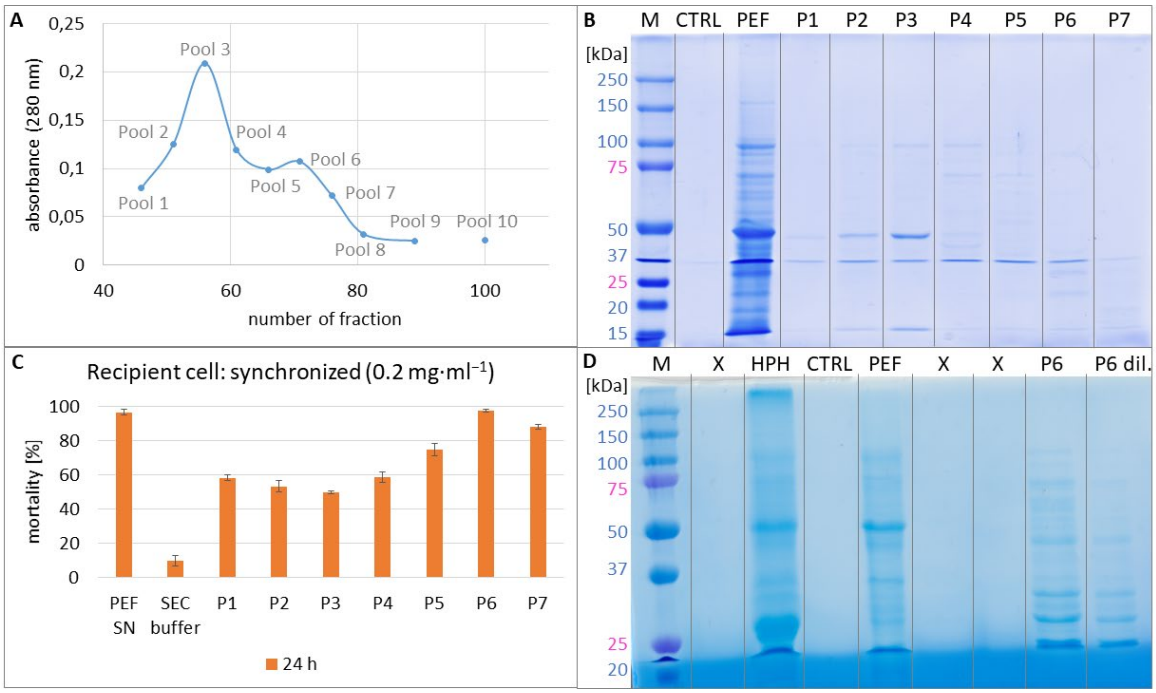

Figure 47 Supervision of SEC fractionation. **A**) Elution profile of sample after pooling of fractions. **B**) Visualization of pooled fractions (P1-P7) on SDS-PAGE, the samples were separated on a 12 % polyacrylamide gel. **C**) The pooled fractions (P1-P7) were added to viable recipient cells from a synchronized culture (time point 0). Viability was monitored after an incubation period of 24 h via FDA assay (50 µM). SEC buffer: size exclusion chromatography buffer as a negative control. **D**) Visualization of concentrated pool 6 (P6) on SDS-PAGE, the samples were separated on a 15 % polyacrylamide gel and subsequently visualized by Coomassie staining. CTRL: control without PEF treatment. X: empty lanes.

Table 5 Excerpt of MALDI TOF MS data, selection of proteins identified for *C. vulgaris* sorted by score.

Accession	Protein name	Localization	Score (quality)	Coverage [%]	MW [Da]	#specific peptides
A9XHZ1_CHLVU	Heat shock protein 70	cytoplasm/ nucleus ?	1051.278	45.64	70833	13
EFTU_CHLVU	Elongation factor Tu, chloroplastic	chloroplast	490.277	39.61	44911	9
RBL_CHLVU	RuBisCO	chloroplast	409.003	30.11	52569	3
K4PW22_CHLVU	2-cys peroxiredoxin	?	256.522	38.91	25838	7
B9ZYY5_CHLVU	Thioredoxin reductase	cytoplasm	222.856	16.07	56749	4
A9XHY8_CHLVU	Antifreeze protein	?	172.885	50.96	10776	5
CLPP_CHLVU	ATP-dependent Clp protease	chloroplast	108.327	19.4	22438	3
Q8LNZ7_CHLVU	Glucose-6-phosphate 1-dehydrogenase	cytoplasm	83.645	9.6	58639	4
G0YUY1_CHLVU	Cold-regulated protein 2	?	58.894	12.1	13847	1
A9XHZ3_CHLVU	Antifreeze protein	?	58.367	15.73	18683	2
ATPB_CHLVU	ATP synthase subunit beta	chloroplast	55.262	7.9	51644	1
Q4QSA5_CHLVU	Ascorbate peroxidase	?	43.069	17.8	29163	2
RK12_CHLVU	50S ribosomal protein L12	chloroplast	40.912	17.56	13712	3
D2KTU8_CHLVU	Glucose-6-phosphate 1-dehydrogenase	?	39.524	6.02	66940	3
A9XHY7_CHLVU	Thiamine thiazole synthase	chloroplast	26.745	7.35	36265	1
CYF_CHLVU	Cytochrome f	chloroplast	17.433	3.49	34213	1

5.4.6. Working model regarding the CDIF

When thinking about the evolutionary context of the CDIF putatively contributing to PCD, the biological function of PCD has to be considered first. Even if PCD seems counter-intuitive in unicellular algae, as mentioned in chapter 2.3.2, there are several evolutionary advantages to be considered. For the case of vigorous clonal growth, PCD would provide a selective advantage when conditions become limiting, since in a clonal organism, "altruistic" behavior would undergo kin selection. Even though *Chlorella* spp. has been proposed to have lost sexuality, it still has retained the meiotic genes (Fučíková *et al,* 2015) and therefore, autosporulation kind of represents a remnant of gametogenesis. The collective suicide of older cells for the benefit of enhanced gametogenesis would then be a manifestation of facultative sexuality, which is widespread in many algae including *C. reinhardtii* (Lachapelle & Bell, 2012). In this context, the role of the CDIF could be a specific signal for the induction of PCD in adverse conditions, achieving that part of the cells provide surviving cells with nutrients. So now the question remains: what exactly is this signal called CDIF?

When assuming that the CDIF is a lipid-derivative compound, it could be linked to small aldehydes connected to plant defense, called C_6 green leave volatiles (GLVs). GLVs such as *cis*-3-hexenal have been shown to cause PCD via actin disruption in grapevine cells (Akaberi *et al,* 2018). As mentioned in chapter 2.3.2, acetic acid leads to PCD in *C. reinhardtii* while generating also the GLV hexenal, among other VOCs. There, VOCs have been proposed to act as infochemicals involved in cell-to-cell communication (Zuo *et al,* 2012). Such a mobile signal would fit into the context of what is known so far about the CDIF. However, a gas-chromatographic analysis of the gaseous phase after PEF treatment was only able to produce contradictory results with no robust qualitative result. Additionally, degassing of the sample to remove potential VOCs did not lead to a reduction of the cell-death inducing activity. Therefore, the hypothesis of the CDIF as lipid-derived VOC was rejected.

The next option puts the CDIF into the category of peptides. Heat-inactivation and temperature dependency both match this concept. This could involve one short peptide acting as a signal in the same manner as the cell-penetrating peptide Bp100 that can be used as a transporter into living cells while interfering with the integrity of the cell by actin freezing (Eggenberger *et al,* 2017). But this mode of action, i.e., affecting cell homeostasis, would not necessarily be specific to *C. vulgaris*. The experiment showing lack of response in other microalgae species (**Figure 45**) weakens this hypothesis. Alternatively, the CDIF could involve one or several proteins with a specific function or working on an enzymatic basis. The protein quantification in **Table 3** and **Table 4** shows that the total protein content is not proportional to the activity, however, this observation makes sense

since the CDIF would only make up a small fraction of the total protein in the sample. Visualization of active fractions **(Figure 47BD**) classifies the candidates in the size range of most likely 25 – 50 kDa.

It has been proposed in literature that autolysis could be a new enzymatic alternative for microalgae cell wall disruption (Demuez *et al,* 2015). In that scenario the cell is being disrupted by the action of its own enzymes. This has been demonstrated to be effective in *C. reinhardtii* using autolysin extract for pretreatment (Sierra *et al,* 2017). Autolysins as cell-wall lytic enzymes were found to be (hydroxy)proline-specific proteases predominantly attacking selected domains within cell walls of *C. reinhardtii* zoosporangia or gametes (Jaenicke *et al,* 1987). Since the cell wall composition is species-dependent and even used for taxonomy (Alhattab *et al,* 2019; Takeda, 1993), the specificity of the CDIF only acting on *C. vulgaris* could be explained. *Chlorella* spp. cell walls have been shown to be sensitive to chitinases due to the presence of a chitin-like glycan (Kapaun & Reisser, 1995; Gerken *et al,* 2013; Canelli *et al,* 2021). Therefore, the CDIF might be one or more enzymes involved in the chitin metabolism. These rather uncommon genes most likely have been acquired by horizontal gene transfer from algal viruses (Blanc *et al,* 2010) and include two chitinases needed for degradation of the cell wall, e.g., during autosporulation. The proteome analysis of PEF SN did not detect any proteins involved in the chitin metabolism. However, the corresponding genes and proteins have not been identified for *C. vulgaris* yet. The work of Canelli *et al,* 2021 investigated enzymatic pretreatment of heterotrophically cultivated *C. vulgaris* for improvement of bioaccessibility. They identified chitinases as causing the highest total carbon and total nitrogen release into the supernatant while preserving oxidative stability, proofing the high efficiency of this enzyme.

Based on these findings, we claim that the CDIF is one or multiple enzymes from the class of chitinases involved in cell wall degradation by attacking chitin-like structures. This working model can explain the results seen in this work. As mentioned above, heat inactivation, as well as temperature dependency with lower toxicity at 4 °C, match well the general properties of enzyme action. The protease inhibition did not affect the CDIF since it does not involve proteolytic activity. HPH extract acting with higher potency would be attributed to higher concentrations of the enzyme. This might additionally be combined with improved working conditions such as lower pH due to a larger number of free amino and nucleic acids generated by pressure disruption. Now, when looking at the comparison of differently cultured recipient cells (**Figure 40**), the reduced effect of the CDIF on cells in the stationary phase can be clearly explained. Since the cell wall is already much thicker with more chitin-like structures, degradation requires more time. The dose-response of recipient cells to the CDIF (**Figure 41**) requires additional explanation, where the

enzymatic work is combined with a signaling component (of the enzyme itself) that might only work once the cell wall has been breached. This would require longer in recipient cells from stationary phase and is mirrored in the slower incremental response from time point 4 h to 24 h. Once inside, the CDIF might trigger positive feedback by recruiting more CDIF from the cell itself and the cell would start its own autolysis in addition to affecting neighboring cells. When looking at the generation of the CDIF (**Figure 42** and **Figure 43**), the most striking observation is the fact that PEF extract from cells in the exponential phase does not contain the CDIF. Apparently, in the exponential phase the CDIF is only generated at very low concentrations or strongly attached to intracellular structures preventing externalization and release is tightly regulated (extractable exclusively by HPH treatment). Cell wall degrading enzymes are necessary during division for induction of autosporulation, where the cell wall of the mother cell ruptures to release daughter cells (Yamamoto *et al,* 2004). It is possible that this tight regulation also is responsible for the increased sensitivity of synchronized cells as recipient cells since already low concentrations might set off the cell wall rupturing process. When looking at the reception of the CDIF at different stages of the cell cycle (**Figure 46**), different sensitives due to cell cycle stage with reduced mortality shortly after autosporulation are visible for the PEF extract. This reduced mortality following autosporulation fits right in with this working model, since daughter cells during autosporulation need to be immune to the mother cell wall rupture. One possible explanation could be that affected cell wall regions such as chitin-like structures are not built up yet in young daughter cells.

With the CDIF being involved in cell wall weakening, it would already be effective during the incubation period of the donor cell and support component externalization from PEF treated cells by enzymatic autolysis (**Figure 48**). Afterward, the water-soluble extract containing the CDIF would still contain the active factor and when incubating fresh, untreated recipient cells, the enzyme would start to degrade the cell wall of otherwise undamaged cells as a first external effect as well as potentially triggering PCD processes as an internal signal in the recipient cells.

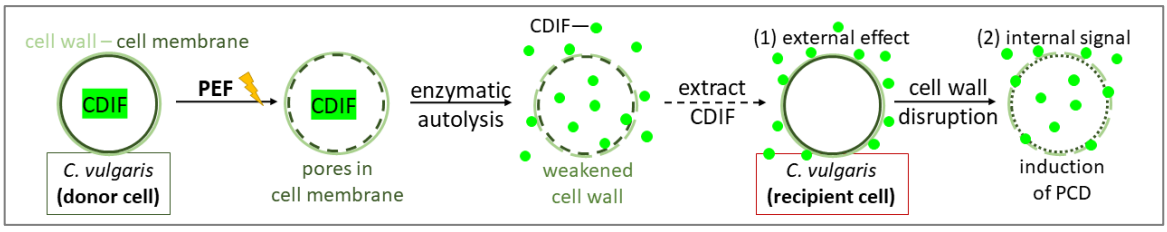

Figure 48 Working model concerning the mode of action regarding the cell-death inducing factor (CDIF). *C. vulgaris* are concentrated to a high cell density and pulsed as donor cells (PEF). The cell integrity is damaged due to pores in the cell membrane and after enzymatic autolysis processes the cell wall is partially degraded due to the work of the CDIF. The water-soluble extract containing CDIF is added to viable recipient cells, causing (1) an external effect of cell wall degradation and after internalization, the CDIF can act as (2) internal signal triggering PCD.

5.5. Improvement of protein extraction efficiency in *C. vulgaris*

In the previous chapters, it could be demonstrated that mortality in response to PEF treatment involves active biological processes rather than being a merely physical process. In consequence, for the improvement of protein extraction efficiency in *C. vulgaris*, it might be sufficient to trigger these biological processes at a low energy input and utilize the synergy of autolytic and biophysical permeabilization of the cell boundary. This hypothesis was tested by analyzing the dose-response relation of PEF induced mortality (**Figure 49A**) and protein extraction efficiency (**Figure 49B**) while varying the specific energy, within a range between 0.8 to 8 $J \cdot ml^{-1}$. The cell suspensions were concentrated to a medium cell density. As already shown in **Figure 36**, PEF induced mortality at low specific energies (0.8 – 2.4 $J \cdot ml^{-1}$) and at concentrated cell density increases over incubation time. For specific energies greater than or equal to 3.2 $J \cdot ml^{-1}$, the PEF induced mortality is already close to 100 % at the earliest time point. When looking at the energy dose-response relation for protein recovery, protein extraction efficiency was already reaching saturation for the second-lowest tested energy input (1.6 $J \cdot ml^{-1}$). The efficiency achieved with this very low specific energy was virtually identical to that seen with the highest energy (8 $J \cdot ml^{-1}$), although the energy input was reduced to only 20 %. The protein extraction efficiency of 18 % CDW constitutes almost half of the total protein content when compared to HPH extract. For the lowest tested energy input (0.8 $J \cdot ml^{-1}$), the PEF induced mortality reaches around 50 % after 24 h incubation. The protein extraction efficiency after 24 h incubation is smaller than for higher specific energies, but still reaches two third of the maximum of PEF extracted protein.

There is one major advantage that can be drawn from this experiment: energy reduction of the extraction step. The fact that protein extraction is possible even at a 100-fold reduction of the established energy (150 $J \cdot ml^{-1}$) supports the use of lower energies while still achieving the same result. This avoids complications that come with higher energies, such as a rise in temperature resulting in possible degradation of valuable compounds. This experiment further strengthens the hypothesis of PEF treatment acting as abiotic stress signal inducing PCD processes responsible for autolytic processes breaking down the cell, which has been proposed previously (Scherer *et al,* 2019). This hypothesis can now be complemented with our working model (**Figure 48**) to include the effect of the CDIF as cell wall degrading enzymes (chitinases) working in concert with autolytic processes. Autolytic processes only include the damaged cell itself, however, when stressed and/or dying cells emit the CDIF this also begins to affect neighboring cells that otherwise would have stayed viable after treatment. Taking this model into consideration, a novel biotechnological strategy based on sustainable microalgae cultivation combined with energy-efficient extraction via PEF can be devised (**Figure 50**).

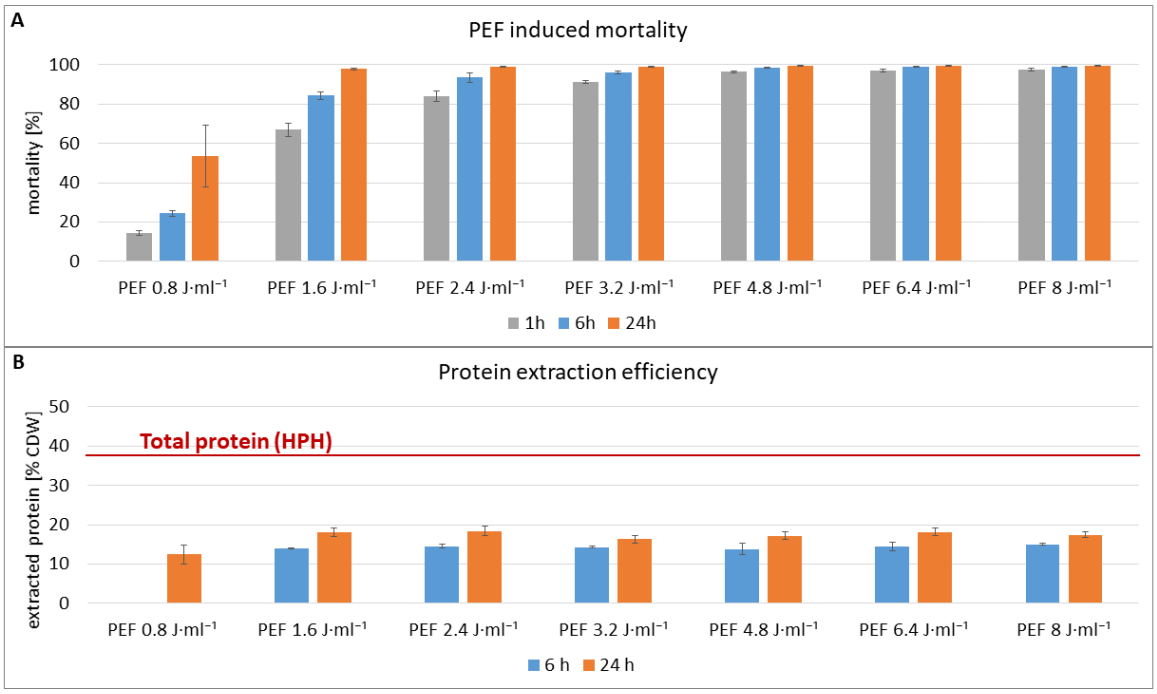

Figure 49 Protein extraction efficiency in dependence of the energy input. *C. vulgaris* from cultures grown under continuous light (7 dpi) were concentrated to a medium cell density of 4.7 mg·ml^{-1}, one part pulsed with different specific energies in the range of 0.8 to 8 J·ml^{-1} and the other part subjected to HPH treatment. **A)** Viability of cell suspensions was monitored at 1 h, 4 h and 24 h via FDA assay (50 µM). **B)** Protein concentration of total protein in HPH extract (red line) and PEF extracts was measured in the supernatant after centrifugation by Lowry assay. Data represent averages and standard errors from three biological replicates.

In a first step, microalgae are cultivated optimally while utilizing direct sunlight and excess carbon dioxide. Next, the biomass is subjected to low-energy PEF treatment. An extended incubation period allows both autolytic processes as well as feedback of the CDIF to take place. Afterward, first water-soluble proteins and subsequently lipids can be extracted in a cascade process as introduced in chapter 1 (**Figure 1**). The final products of this value chain include protein for use in the food industry, as well as biodiesel and biogas as energy sources. With this concept in place, there is no waste of energy on drying of the biomass or high treatment energies while still providing first products safe for consumption and secondly carbon neutral biodiesel. Additionally, when recycling residual biomass via thermochemical conversion or anaerobic fermentation is implemented, the whole process should be sustainable for industrial application. Furthermore, since the major steps of microalgae cultivation as well as extraction by PEF technology are easily scalable, the range of applications runs from small-scale concepts to large facilities. An exciting application would be the utilization of microalgae in spacecrafts as source for oxygen enrichment while also providing edible biomass. Large applications already include wastewater treatment, however, here the application as a food source must obviously be excluded. The range of possible applications, when only considering *C. vulgaris* as biomass, is already huge. However, what is still

missing for the jump from niche to general usage is social acceptance in western society for algae as food products. But at least the recognition and positive image of microalgae is growing: the bioenergy façade of “BIQ Das Algenhaus” in Hamburg is able to produce heat and biomass concomitantly (Kerner *et al,* 2019), integrating microalgae right in the heart of a city. It would be desirable that the results of this work promote a wider utilization of microalgae as a future resource for food, feed, and transportation fuels.

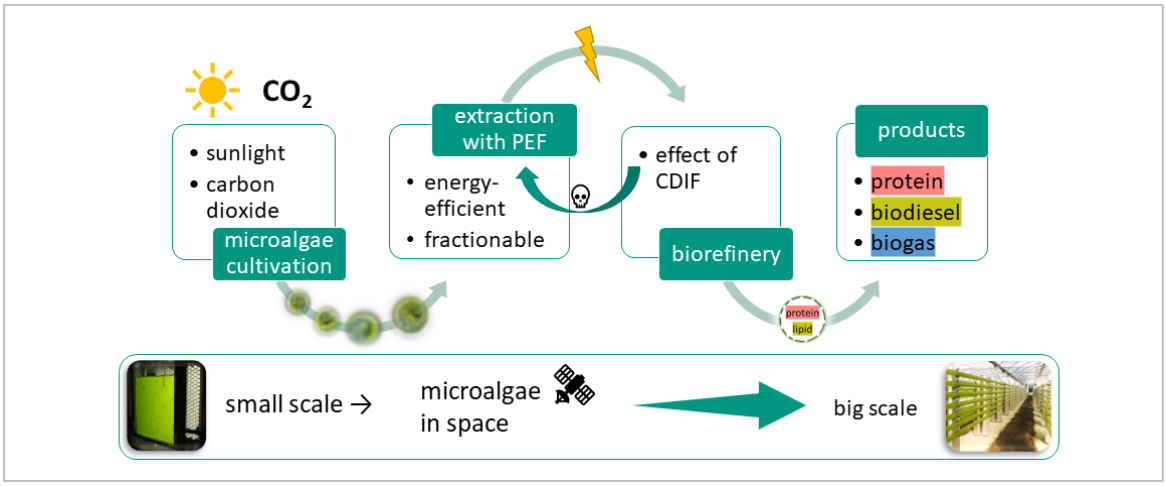

Figure 50 Biorefinery concept based on sustainable microalgae cultivation. Energy-efficient extraction with PEF treatment combined with incubation period to take advantage of the cell-death inducing factor (CDIF) results in end products of protein for food industry as well as biodiesel and biogas as energy sources. Applicable from small to big scale.

5.6. Conclusion

In summary, it could be demonstrated that an interdisciplinary approach allowed research progress on identification of a cell-death inducing factor and its properties. Investigations of biological and biochemical processes triggered by pulse exposure and analysis of autolytic and signaling processes occurring during the microalgae incubation period led to a more thorough understanding of PEF assisted protein extraction and its kinetics. Physical PEF treatment parameters, i.e., electric field strength and specific treatment energy, were adjusted for minimum energy demand at maximum protein yield. This allowed the realization of optimized biotechnological workflows for Spirulina and *C. vulgaris*. When including the identified auto-enzymatic processes into the processing scheme, a major energy reduction up to a factor of 100 could be established for PEF assisted protein extraction from *C. vulgaris*.

In a first step, the effect of PEF treatment on the model organism Spirulina was examined. Particular attention was paid to the post-PEF incubation period. It could be shown that electroextraction of the valuable pigment C-PC and proteins from Spirulina is possible at high purity and stability with an optimized protocol using homogenous cell suspensions and stable pH-buffers (pH 6 or pH 8). The extraction efficiency was energy-dependent and exhibited a maximum after a 24 h post-PEF incubation period. At lower treatment energies, extraction efficiency is related to post-PEF autolytic processes during the incubation period. With the optimized extraction protocol, PEF treatment can be suggested as preferential downstream processing method to produce C-PC from Spirulina with high purity at low energy demand.

The main part of this thesis focused on advancing the knowledge of biological aspects of PEF treatment and subsequent cell death in the model organism *C. vulgaris*. For this purpose, cell cycle synchronization and reliable viability cell sorting techniques provided the necessary tools to dissect cell death responses due to the PEF treatment. It became apparent that PEF treatment can act as an abiotic stress signal. In synchronized *C. vulgaris* cell culture shortly after cell division, the stress signal manifests via ROS burst after low energy PEF treatment and PEF induced mortality rises when inhibiting enzymatic oxidative burst. Furthermore, PEF induced mortality could be shown to be generally dependent on progression through the cell cycle. Neither cytochrome c nor cytochrome f release could be detected after PEF treatment. In a biotechnological context, this knowledge can be used to optimize microalgae processing: PEF treatment can be applied to trigger a signaling pathway at low energy expenditure leading to PCD related self-autolytic processes in the microalgae instead of using the blunt force of high energy treatment.

Unexpectedly, PEF treatment extracted a cell-death inducing factor from *C. vulgaris* that caused cell death of cells which were not PEF treated previously. This CDIF was specific to *C. vulgaris* and did not kill other microalgae species. In an evolutionary context, the CDIF might have played part in cellular homeostasis by regulating autosporulation or by inducing PCD in old cultures as nutrition of young cells. The working model classifies the CDIF as one or multiple enzymes involved in cell wall degradation as well as internal signaling, most probable a chitinase. Combination of self-autolytic processes with the CDIF provides the opportunity to develop PEF treatment of *C. vulgaris* to an energy-efficient cell disruption method for biorefinery concepts.

6. Outlook – In search of the CDIF

The outcome of PEF treatment and electroporation in all fields (medicine included) has more and more left behind the concept of merely porating the cell membrane, and effects such as lipid oxidation, protein denaturation and even cytoskeleton disruption have gotten more into focus (Balantič *et al,* 2021). When narrowing down to plant cells, PEF treatment inducing stress responses has been indicated in many studies and PEF treatment has even been classified as an abiotic stressor (Balasa, 2020), same as in this thesis. Since the stress response of ROS generation was already shown in cells from a synchronized culture (**Figure 28**), future studies should test the presence of ROS while comparing different cell stages in *C. vulgaris*. This can be done while still working with a synchronized culture by using different time points during the cell cycle, or in comparison with cells in the stationary phase. Additionally, it would be very interesting to conduct a time course of ROS generation after PEF treatment, since so far only 3 h after treatment was analyzed. This can be combined again with inhibition of NADPH oxidase, to see whether the generation of ROS can be partially suppressed (since ROS can also be generated by the electric pulses itself). When applying low energy pulses, the ROS-scavenging activity can also be studied to further investigate the role of PEF treatment acting as an abiotic stress signal. For this purpose, free radical-scavenging activity combined with antioxidant enzyme activity (e.g., catalase, peroxidase, glutathione reductase and superoxide dismutase) can be measured. Since the experiment aimed at analyzing the effect of calcium signaling via inhibition did not give any significant results (**Figure 30**), the influence of calcium influx can be tested with artificial calcium influx. This can be achieved by adding a calcium ionophore to the cells prior to PEF treatment.

One of the first indicators posing the challenge to investigate the biological response and cell death due to electroporation in *C. vulgaris* was the presence of post-PEF DNA laddering (Scherer *et al,* 2019). Even though the significance of DNA laddering is ambivalent and can point towards both PCD and necrosis, it would be interesting to analyze post-PEF DNA residues in a synchronized culture. Another way of discriminating between PCD and necrosis is the involvement of metacaspases. Since the structure is universally conserved, the antibody raised against human caspase 3 is able to recognize the corresponding metacaspase in *Chlorella* sp. (Zuppini *et al,* 2010). Western blotting in addition to measuring caspase-3-like activity after PEF treatment at survival threshold should provide some clarity in respect to the classification of post-PEF cell death.

Regarding the CDIF, identification is of the topmost priority. For that purpose, the protein levels can be compared by performing two-group analyses, e.g., by analyzing two PEF extracts in comparison: (1) extract containing CDIF (culture age of donor cell 7 dpi) and (2) extract without the CDIF (culture age of donor cell 2 dpi). However, the HPH extract of 2 dpi donor cells already

showed cell-death inducing activity (**Figure 42**), so it might be more convenient to use synchronized cultures as donor cells without the CDIF. For synchronized cultures it is not known whether the total cell extract (after HPH) also contains low concentrations of the CDIF, that could not be extracted by PEF treatment. Therefore, one more experiment should be to test the presence of the CDIF in HPH extract of a synchronized culture. The already performed preliminary elucidation gave two interesting, identified candidates: Hsp70 and EF-Tu (chapter 5.4.5). Literature research in combination with data interpretation led to the working model proposing the CDIF to be a chitinase. In that context it is again important to highlight the lack of annotated proteome sequence data for *C. vulgaris*. This means that the real CDIF might not be identified and annotated yet. Consequently, hunting this factor becomes even more difficult. The putative candidates Hsp70, EF-Tu and chitinase can still be tested for their activity as pure compounds. Additionally, the cell residue after PEF treatment of donor cells in the stationary phase can be analyzed for gene expression with quantitative real-time PCR. The primers for the genes need to be designed carefully using the sequence information of either *C. vulgaris* for Hsp70 and EF-Tu, or *C. variabilis* for the chitinase. Actin can be used as housekeeping gene for normalization. Gene expression of these transcripts can also be monitored in untreated donor cells with samples ranging from the exponential growth (2 dpi) phase to the stationary growth phase (7 dpi).

Assuming the CDIF is a protein, the list of candidates can also be narrowed down via iterative protein precipitation (e.g., ammonium sulfate). Further elucidation can be achieved by combination of activity guided fractionation with cation-exchange chromatography followed by HPLC-MS. This has been shown to be successful for identification of a wheat protein inhibiting yeast cells, where the result was validated using recombinant expression of the identified thaumatin-like protein (van der Maelen *et al,* 2019). The identified CDIF can similarly be validated using recombinant expression, *C. vulgaris* can be transformed via electroporation (Chow & Tung, 1999). After identification of the CDIF this knowledge can be utilized, on the one hand, to thoroughly investigate the working mode of the CDIF on recipient cells. On the other hand, it can be used to optimize cultivation of *C. vulgaris* for high accumulation of the CDIF while simultaneously improving the biotechnological processing step for biorefinery concepts.

When looking at the recipient cells, the involved pathways leading to cell death should be further dissected as well. Here, the involvement of the MAP kinase cascade seems likely. This can be tested by specific inhibition of this pathway while incubating the recipient cell with extract containing CDIF. It has already been demonstrated in this work that the reception of the CDIF depends on the cell cycle (**Figure 46**). Whether this is caused by varying concentration of the receptor during progression through the cell cycle or by varying transduction of the signal, however, is not clear.

One possible experiment to clarify would be recording dose–response curves during progression through the cell cycle. If the response is shifted with respect to its threshold, this would support a receptor modulation. When the response is not shifting, but showing a change in amplitude, a transductor modulation is in place (Toyomasu *et al,* 1994).

When looking into literature more broadly, a comparison of the CDIF to the bystander effect known from radiation and electroporation for cancer therapy (mammalian cells) can be drawn. Here it could be shown that treated cells release signals which cause damage to nearby, unirradiated or non-electroporated cells. (Prevc *et al,* 2016; Ruzgys *et al,* 2021). Similar effects seem to be found again and again and always are defined with a new name, which makes it hard to take notice of those studies. In the same manner, a connection to algal organic matter (AOM) can be drawn. It was investigated that during cultivation, microalgae can excrete up to 17 % of fixed carbon in the form of proteins, nucleic acids, lipids and small molecules, but mostly charged or neutral polysaccharides. AOM interferes with flocculation-based harvesting methods (Vandamme *et al,* 2012). With this knowledge in mind, the polysaccharide fraction of PEF extract should be separated and additionally investigated for cell-death inducing activity.

Another very important question pertains to the specificity of the CDIF for *C. vulgaris*. Is there something similar to the CDIF in related microalgae species? The PEF extract of *C. vulgaris* donor cells had no effect on *A. prothothecoides* and *S. almeriensis* (**Figure 45**), but the PEF extract of those species as donor cells had not been tested. Since the rigid cell wall of microalgae is the obstacle that needs to be overcome for biotechnological disruption methods, a universally applicable technique is preferable.

The advantages of direct PEF treatment to optimize extraction efficiency both in *C. vulgaris* and in Spirulina have been thoroughly discussed in this work. The additional advantage of lowering energy costs by incubating PEF treated biomass to trigger both autolytic process and feedback of the CDIF was proposed as well. In conclusion, it can be said that every species and even every strain boasts different rigid cell wall structures, so disruption processes need to be adjusted accordingly. The direct impact of PEF treatment on the permeability and structure of the cell wall could already be demonstrated in the model organism *C. reinhardtii* (Bensalem *et al,* 2020). The advantage of utilizing PEF treatment combined with the CDIF as signal and/or autolytic enzymes lies in species selective extraction. The fact that incubation periods are necessary to trigger effects such as enzymatic activity after electroporation, fortunately, has become more widely known (Martínez *et al,* 2020). The discovery of the CDIF in *C. vulgaris*, as well as improvement of extraction protocols for C-PC electroextraction from Spirulina, hopefully helps biotechnology in advancing the extraction of valuable compounds.

7. Appendix

Supplementary Table 1 Preparation protocol for 1× TAP medium with corresponding buffer compositions

weight or volume	compound	final concentration
TAP medium 1× (final volume: 5 l, adjust to pH 7.0 with HCl)		
12.1 g	Tris	0.02 M
50 ml	TAP salts 100×	1×
4.7 ml	potassium phosphate buffer	0.001 M
50 ml	Hutner's trace elements 100×	1×
5 ml	acetic acid	0.001 % (v/v)
TAP salts 100× (final volume 1 l)		
37.5 g	NH_4Cl	0.7 M
10 g	$MgSO_4 \cdot 7H_2O$	40 mM
5 g	$CaCl_2 \cdot 2H_2O$	34 mM
potassium phosphate buffer (final volume 250 ml)		
28.8 g	K_2HPO_4	0.66 M
14.4 g	KH_2PO_4	0.42 M
Hutner's trace elements 100× (final volume 1 l) (Hutner *et al,* 1950)		
5.00 g	EDTA Disodium	15 mM
1.14 g	H_3BO_3	18 mM
2.20 g	$ZnSO_4 \cdot 7H_2O$	7.6 mM
0.51 g	$MnCl_2 \cdot 4H_2O$	2.6 mM
0.50 g	$FeSO_4 \cdot 7H_2O$	1.8 mM
0.16 g	$CoCl_2 \cdot 6H_2O$	0.67 mM
0.16 g	$CuSO_4 \cdot 5H_2O$	0.64 mM
0.11 g	$(NH_4)6Mo_7O_{24} \cdot 4H_2O$	89 µM

Supplementary Table 2 Preparation protocol for Full Zarouk medium (Aiba & Ogawa, 1977)

weight or volume	compound	final concentration
solution I (final volume 1 l)		
27.22 g	$NaHCO_3$	324 mM
8.06 g	Na_2CO_3	76 mM
1.00 g	K_2HPO_4	5.7 mM
solution II (final volume 1 l)		
5.00 g	$NaNO_3$	59 mM
2.00 g	K_2SO_4	11.5 mM
2.00 g	NaCl	34 mM
0.40 g	$MgSO_4 \cdot 7H_2O$	1.6 mM
0.08 g	$CaCl_2 \cdot 2H_2O$	559 µM
0.02 g	$FeSO_4.7H_2O$	72 µM
0.16 g	EDTA Disodium	476 µM
10 ml	Hutner's trace elements 100× (**Supplementary Table 1**)	1×

References

Affenzeller MJ, Darehshouri A, Andosch A, Lütz C, Lütz-Meindl U (2009) Salt stress-induced cell death in the unicellular green alga Micrasterias denticulata. *J Exp Bot* 60: 939–954

Aiba S, Ogawa T (1977) Assessment of Growth Yield of a Blue--green Alga, Spirulina platensis, in Axenic and Continuous Culture. *Journal of General Microbiology* 102: 179–182

Akaberi S, Gusbeth C, Silve A, Senthilnathan DS, Navarro-López E, Molina-Grima E, Müller G, Frey W (2019) Effect of pulsed electric field treatment on enzymatic hydrolysis of proteins of Scenedesmus almeriensis. *Algal Research* 43: 101656

Akaberi S, Krust D, Müller G, Frey W, Gusbeth C (2020) Impact of incubation conditions on protein and C-Phycocyanin recovery from Arthrospira platensis post- pulsed electric field treatment. *Bioresour Technol* 306: 123099

Akaberi S, Wang H, Claudel P, Riemann M, Hause B, Hugueney P, Nick P (2018) Grapevine fatty acid hydroperoxide lyase generates actin-disrupting volatiles and promotes defence-related cell death. *J Exp Bot* 69: 2883–2896

Alhattab M, Kermanshahi-Pour A, Brooks MS-L (2019) Microalgae disruption techniques for product recovery: influence of cell wall composition. *J Appl Phycol* 31: 61–88

Ali SK, Saleh AM (2012) Spirulina - an overview. *International Journal of Pharmacy and Pharmaceutical Sciences* 4: 9–15

Allen RF (1923) A Cytological Study of Infection of Baart and Kanred Wheats By Puccinia graminis tritici. *Journal of Agricultural Research* XXIII: 131–151

Al-Whaibi MH (2011) Plant heat-shock proteins: A mini review. *Journal of King Saud University - Science* 23: 139–150

Andosch A, Affenzeller MJ, Lütz C, Lütz-Meindl U (2012) A freshwater green alga under cadmium stress: ameliorating calcium effects on ultrastructure and photosynthesis in the unicellular model Micrasterias. *J Plant Physiol* 169: 1489–1500

André FM, Rassokhin MA, Bowman AM, Pakhomov AG (2010) Gadolinium blocks membrane permeabilization induced by nanosecond electric pulses and reduces cell death. *Bioelectrochemistry* 79: 95–100

Aravind L, Koonin EV (2002) Classification of the caspase-hemoglobinase fold: detection of new families and implications for the origin of the eukaryotic separins. *Proteins* 46: 355–367

Arnon DI, McSwain BD, Tsujimoto HY, Wada K (1974) Photochemical activity and components of membrane preparations from blue-green algae. I. Coexistence of two photosystems in relation to chlorophyll a and removal of phycocyanin. *Biochimica et Biophysica Acta (BBA) - Bioenergetics* 357: 231–245

Atkins KC, Cross FR (2018) Interregulation of CDKA/CDK1 and the Plant-Specific Cyclin-Dependent Kinase CDKB in Control of the Chlamydomonas Cell Cycle. *Plant Cell* 30: 429–446

Bai F, Gusbeth C, Frey W, Nick P (2017a) Nanosecond pulsed electric fields trigger cell differentiation in Chlamydomonas reinhardtii. *Biochim Biophys Acta Biomembr* 1859: 651–661

Bai F, Gusbeth C, Frey W, Nick P (2020) Nanosecond pulsed electric fields modulate the expression of the astaxanthin biosynthesis genes psy, crtR-b and bkt 1 in Haematococcus pluvialis. *Sci Rep* 10: 15508

Bai M-D, Hsu H-J, Wu S-I, Lu W-C, Wan H-P, Chen J-C (2017b) Cell disruption of Chlorella vulgaris using active extracellular substances from Bacillus thuringiensis ITRI-G1 is a programmed cell death event. *J Appl Phycol* 29: 1307–1315

Balantič K, Miklavčič D, Križaj I, Kramar P (2021) The good and the bad of cell membrane electroporation. *Acta Chimica Slovenica* 68: 753–764

Balasa A (2020) Stress Response of Plants, Metabolite Production due to Pulsed Electric Fields. In *Handbook of Electroporation,* Miklavcic D (ed) pp. 1–13. Cham: Springer International Publishing; Imprint: Springer

Batista Napotnik T, Polajžer T, Miklavčič D (2021) Cell death due to electroporation - A review. *Bioelectrochemistry* 141: 107871

Beijerinck MW (1890) Culturversuche mit Zoochlorellen, Lichenengonidien und anderen niederen Algen. *Bot. Ztg.* 48: 725-772,781-788

Bennett A, Bogorad L (1973) Complementary chromatic adaptation in a filamentous blue-green alga. *J Cell Biol* 58: 419–435

Bensalem S, Pareau D, Cinquin B, Français O, Le Pioufle B, Lopes F (2020) Impact of pulsed electric fields and mechanical compressions on the permeability and structure of Chlamydomonas reinhardtii cells. *Sci Rep* 10: 2668

Berghöfer T, Eing C, Flickinger B, Hohenberger P, Wegner LH, Frey W, Nick P (2009) Nanosecond electric pulses trigger actin responses in plant cells. *Biochem Biophys Res Commun* 387: 590–595

Berns DS, MacColl R (1989) Phycocyanin in physical chemical studies. *Chemical Reviews* 89: 807–825

Bhowmick S, Mazumdar A, Moulick A, Adam V (2020) Algal metabolites: An inevitable substitute for antibiotics. *Biotechnology Advances* 43: 107571

Bidle KD (2016) Programmed Cell Death in Unicellular Phytoplankton. *Curr Biol* 26: R594-R607

Bidle KD, Falkowski PG (2004) Cell death in planktonic, photosynthetic microorganisms. *Nat Rev Microbiol* 2: 643–655

Blanc G, Duncan G, Agarkova I, Borodovsky M, Gurnon J, Kuo A, Lindquist E, Lucas S, Pangilinan J, Polle J et al (2010) The Chlorella variabilis NC64A genome reveals adaptation to photosymbiosis, coevolution with viruses, and cryptic sex. *Plant Cell* 22: 2943–2955

Borowitzka MA, Beardall J, Raven JA (2016) *The Physiology of Microalgae.* Cham: Springer International Publishing

Buckow R, Ng S, Toepfl S (2013) Pulsed Electric Field Processing of Orange Juice: A Review on Microbial, Enzymatic, Nutritional, and Sensory Quality and Stability. *Compr Rev Food Sci Food Saf* 12: 455–467

Burke RC, Bardet SM, Carr L, Romanenko S, Arnaud-Cormos D, Leveque P, O'Connor RP (2017) Nanosecond pulsed electric fields depolarize transmembrane potential via voltage-gated K+, Ca2+ and TRPM8 channels in U87 glioblastoma cells. *Biochimica et Biophysica Acta (BBA) - Biomembranes* 1859: 2040–2050

Calderwood SK, Mambula SS, Gray PJ, Theriault JR (2007) Extracellular heat shock proteins in cell signaling. *FEBS Letters* 581: 3689–3694

Candiano G, Bruschi M, Musante L, Santucci L, Ghiggeri GM, Carnemolla B, Orecchia P, Zardi L, Righetti PG (2004) Blue silver: a very sensitive colloidal Coomassie G-250 staining for proteome analysis. *Electrophoresis* 25: 1327–1333

Canelli G, Kuster I, Jaquenod L, Buchmann L, Murciano Martínez P, Rohfritsch Z, Dionisi F, Bolten CJ, Nanni P, Mathys A (2022) Pulsed electric field treatment enhances lipid bioaccessibility while preserving oxidative stability in Chlorella vulgaris. *Innovative Food Science & Emerging Technologies* 75: 102897

Canelli G, Murciano Martínez P, Maude Hauser B, Kuster I, Rohfritsch Z, Dionisi F, Bolten CJ, Neutsch L, Mathys A (2021) Tailored enzymatic treatment of Chlorella vulgaris cell wall leads to effective disruption while preserving oxidative stability. *LWT* 143: 111157

Carroll JW, Thomas J, Dunaway C, O'Kelley JC (1970) Light induced synchronization of algal species that divide preferentially in darkness. *Photochem Photobiol* 12: 91–98

Cecchin M, Marcolungo L, Rossato M, Girolomoni L, Cosentino E, Cuine S, Li-Beisson Y, Delledonne M, Ballottari M (2019) Chlorella vulgaris genome assembly and annotation reveals the molecular basis for metabolic acclimation to high light conditions. *Plant J* 100: 1289–1305

Chang X, Riemann M, Liu Q, Nick P (2015) Actin as deathly switch? How auxin can suppress cell-death related defence. *PLoS ONE* 10: e0125498

Chioccioli M, Hankamer B, Ross IL (2014) Flow cytometry pulse width data enables rapid and sensitive estimation of biomass dry weight in the microalgae Chlamydomonas reinhardtii and Chlorella vulgaris. *PLoS ONE* 9: e97269

Chow K-C, Tung WL (1999) Electrotransformation of Chlorella vulgaris. *Plant Cell Reports* 18: 778–780

Coustets M, Joubert-Durigneux V, Hérault J, Schoefs B, Blanckaert V, Garnier J-P, Teissié J (2015) Optimization of protein electroextraction from microalgae by a flow process. *Bioelectrochemistry* 103: 74–81

Delemotte L, Tarek M (2012) Molecular dynamics simulations of lipid membrane electroporation. *J Membrane Biol* 245: 531–543

DellaGreca M, Zarrelli A, Fergola P, Cerasuolo M, Pollio A, Pinto G (2010) Fatty acids released by Chlorella vulgaris and their role in interference with Pseudokirchneriella subcapitata: experiments and modelling. *J Chem Ecol* 36: 339–349

Demuez M, Mahdy A, Tomás-Pejó E, González-Fernández C, Ballesteros M (2015) Enzymatic cell disruption of microalgae biomass in biorefinery processes. *Biotechnol Bioeng* 112: 1955–1966

Dong Z, Saikumar P, Weinberg JM, Venkatachalam MA (1997) Internucleosomal DNA cleavage triggered by plasma membrane damage during necrotic cell death. Involvement of serine but not cysteine proteases. *Am J Pathol* 151: 1205–1213

Dower WJ, Miller JF, Ragsdale CW (1988) High efficiency transformation of E. coli by high voltage electroporation. *Nucleic Acids Res* 16: 6127–6145

Ebihara L, Hall JE, MacDonald RC, McIntosh TJ, Simon SA (1979) Effect of benzyl alcohol on lipid bilayers. A comparisons of bilayer systems. *Biophys J* 28: 185–196

Eggenberger K, Sanyal P, Hundt S, Wadhwani P, Ulrich AS, Nick P (2017) Challenge Integrity: The Cell-Penetrating Peptide BP100 Interferes with the Auxin-Actin Oscillator. *Plant and Cell Physiology* 58: 71–85

Eing C, Bonnet S, Pacher M, Puchta H, Frey W (2009) Effects of Nanosecond Pulsed Electric Field Exposure on Arabidopsis thaliana. *IEEE Trans. Dielect. Electr. Insul.* 16: 1322–1328

Eing C, Goettel M, Straessner R, Gusbeth C, Frey W (2013) Pulsed Electric Field Treatment of Microalgae—Benefits for Microalgae Biomass Processing. *IEEE Trans. Plasma Sci.* 41: 2901–2907

Fernández-Rojas B, Hernández-Juárez J, Pedraza-Chaverri J (2014) Nutraceutical properties of phycocyanin. *Journal of Functional Foods* 11: 375–392

Flickinger B, Berghöfer T, Hohenberger P, Eing C, Frey W (2010) Transmembrane potential measurements on plant cells using the voltage-sensitive dye ANNINE-6. *Protoplasma* 247: 3–12

Franklin DJ, Brussaard CP, Berges JA (2006) What is the role and nature of programmed cell death in phytoplankton ecology? *European Journal of Phycology* 41: 1–14

Franklin-Tong VE, Gourlay CW (2008) A role for actin in regulating apoptosis/programmed cell death: evidence spanning yeast, plants and animals. *Biochem J* 413: 389–404

Frey W, Flickinger B, Berghoefer T, Eing C, Liu Q, Nick P (2011) Electropermeabilization versus nsPEF-Stimulation – Pulsed Electric Fields can Stimulate the Growth of Plants and Fungi. *European Bioelectromagnetics Association*

Frey W, Gusbeth C, Schwartz T (2013) Inactivation of Pseudomonas putida by pulsed electric field treatment: a study on the correlation of treatment parameters and inactivation efficiency in the short-pulse range. *J Membrane Biol* 246: 769–781

Fu J, Momčilović I, Prasad PVV (2012) Roles of Protein Synthesis Elongation Factor EF-Tu in Heat Tolerance in Plants. *Journal of Botany* 2012: 1–8

Fučíková K, Pažoutová M, Rindi F (2015) Meiotic genes and sexual reproduction in the green algal class Trebouxiophyceae (Chlorophyta). *J Phycol* 51: 419–430

Gerken HG, Donohoe B, Knoshaug EP (2013) Enzymatic cell wall degradation of Chlorella vulgaris and other microalgae for biofuels production. *Planta* 237: 239–253

Gianulis EC, Pakhomov AG (2015) Gadolinium modifies the cell membrane to inhibit permeabilization by nanosecond electric pulses. *Archives of Biochemistry and Biophysics* 570: 1–7

Gille A, Trautmann A, Posten C, Briviba K (2015) Bioaccessibility of carotenoids from Chlorella vulgaris and Chlamydomonas reinhardtii. *Int J Food Sci Nutr* 67: 507–513

Goettel M, Eing C, Gusbeth C, Straessner R, Frey W (2013) Pulsed electric field assisted extraction of intracellular valuables from microalgae. *Algal Research* 2: 401–408

Guan P, Shi W, Riemann M, Nick P (2021) Dissecting the membrane-microtubule sensor in grapevine defence. *Hortic Res* 8: 260

Guittet A, Poignard C, Gibou F (2017) A Voronoi Interface approach to cell aggregate electropermeabilization. *Journal of Computational Physics* 332: 143–159

Gusbeth C, Frey W, Volkmann H, Schwartz T, Bluhm H (2009) Pulsed electric field treatment for bacteria reduction and its impact on hospital wastewater. *Chemosphere* 75: 228–233

Hadjoudja S, Vignoles C, Deluchat V, Lenain J-F, Le Jeune A-H, Baudu M (2009) Short term copper toxicity on Microcystis aeruginosa and Chlorella vulgaris using flow cytometry. *Aquat Toxicol* 94: 255–264

Hamilton WD (1964) The genetical evolution of social behaviour. I. *Journal of Theoretical Biology* 7: 1–16

Hampl W, Altmann H, Biebl R (1971) Unterschiede und Beeinflussung der Erholungskapazität von Chlorellazellen in Verschiedenen Stadien des Zellzyklus. *Radiation Botany* 11: 201–207

Han G-Z (2017) Evolution of jasmonate biosynthesis and signaling mechanisms. *J Exp Bot* 68: 1323–1331

Harvey KL, Jarocki VM, Charles IG, Djordjevic SP (2019) The Diverse Functional Roles of Elongation Factor Tu (EF-Tu) in Microbial Pathogenesis. *Front. Microbiol.* 10: 2351

Heath RL, Packer L (1968) Photoperoxidation in isolated chloroplasts. *Archives of Biochemistry and Biophysics* 125: 189–198

Heldt HW, Piechulla B (2015) *Pflanzenbiochemie.* Berlin, Heidelberg: Springer Berlin Heidelberg

Hofmann F, Ohnimus H, Scheller C, Strupp W, Zimmermann U, Jassoy C (1999) Electric field pulses can induce apoptosis. *J Membr Biol* 169: 103–109

Hoham RW, Remias D (2020) Snow and Glacial Algae: A Review1. *J. Phycol.* 56: 264–282

Houghton JD (1996) Haems and bilins. In *Natural Food Colorants,* Hendry GAF, Houghton JD (eds) pp. 157–196. Dordrecht: Springer-Science+Business Media B.V

Hutner SH, Provasoli L, Schatz A, Haskins CP (1950) Some Approaches to the Study of the Role of Metals in the Metabolism of Microorganisms. *Proceedings of the American Philosophical Society* 94: 152–170

Ismail A, Takeda S, Nick P (2014) Life and death under salt stress: same players, different timing? *J Exp Bot* 65: 2963–2979

Jaenicke L, Kuhne W, Spessert R, Wahle U, Waffenschmidt S (1987) Cell-wall lytic enzymes (autolysins) of Chlamydomonas reinhardtii are (hydroxy)proline-specific proteases. *Eur J Biochem* 170: 485–491

Jones AM (2001) Programmed cell death in development and defense. *Plant Physiol* 125: 94–97

Kadereit JW, Körner C, Nick P, Sonnewald U (2021) *Strasburger – Lehrbuch der Pflanzenwissenschaften.* Berlin, Heidelberg: Springer Berlin Heidelberg; Imprint: Springer Spektrum

Kanduser M, Sentjurc M, Miklavcic D (2006) Cell membrane fluidity related to electroporation and resealing. *Eur Biophys J* 35: 196–204

Kapaun E, Reisser W (1995) A chitin-like glycan in the cell wall of a Chlorella sp. (Chlorococcales, Chlorophyceae). *Planta* 197: 577–582

Kerner M, Gebken T, Sundarrao I, Hindersin S, Sauss D (2019) Development of a control system to cover the demand for heat in a building with algae production in a bioenergy façade. *Energy and Buildings* 184: 65–71

Kerr JF, Wyllie AH, Currie AR (1972) Apoptosis: a basic biological phenomenon with wide-ranging implications in tissue kinetics. *Br J Cancer* 26: 239–257

Kessler E (1992) Chlorella. *Naturwissenschaften* 79: 260–265

Kim M, Gwak Y, Jung W, Jin E (2017) Identification and Characterization of an Isoform Antifreeze Protein from the Antarctic Marine Diatom, Chaetoceros neogracile and Suggestion of the Core Region. *Mar Drugs* 15

Klemenčič M, Funk C (2018) Structural and functional diversity of caspase homologues in non-metazoan organisms. *Protoplasma* 255: 387–397

Kodama Y, Sumita H (2022) The ciliate Paramecium bursaria allows budding of symbiotic Chlorella variabilis cells singly from the digestive vacuole membrane into the cytoplasm during algal reinfection. *Protoplasma* 259: 117–125

Kotnik T (2020) Cell in Electric Field - Induced Transmembrane Voltage. In *Electroporation-Based Technologies and Treatments,* Kramar P, Miklavčič D (eds)

Kotnik T, Frey W, Sack M, Haberl Meglič S, Peterka M, Miklavčič D (2015) Electroporation-based applications in biotechnology. *Trends Biotechnol* 33: 480–488

Kotnik T, Pucihar G, Miklavcic D (2010) Induced transmembrane voltage and its correlation with electroporation-mediated molecular transport. *J Membrane Biol* 236: 3–13

Kotnik T, Rems L, Tarek M, Miklavčič D (2019) Membrane Electroporation and Electropermeabilization: Mechanisms and Models. *Annu Rev Biophys* 48: 63–91

Kramar P, Miklavčič D (eds) (2020) *Electroporation-Based Technologies and Treatments*

Krust D (2018) *Identication and localization of extracted proteins from the microalgae Chlorella vulgaris.* Masterarbeit der Fakultät für Chemie und Biowissenschaften. Karlsruhe

Krust D, Gusbeth C, Müller AS, Scherer D, Müller G, Frey W, Nick P (2022) Biological signalling supports biotechnology – Pulsed electric fields extract a cell-death inducing factor from Chlorella vulgaris. *Bioelectrochemistry* 143: 107991

Kühn S, Liu Q, Eing C, Frey W, Nick P (2013) Nanosecond electric pulses affect a plant-specific kinesin at the plasma membrane. *J Membr Biol* 246: 927–938

Kunze G, Zipfel C, Robatzek S, Niehaus K, Boller T, Felix G (2004) The N terminus of bacterial elongation factor Tu elicits innate immunity in Arabidopsis plants. *Plant Cell* 16: 3496–3507

Kuthanova A, Opatrny Z, Fischer L (2008) Is internucleosomal DNA fragmentation an indicator of programmed death in plant cells? *J Exp Bot* 59: 2233–2240

Lachapelle J, Bell G (2012) Evolutionary rescue of sexual and asexual populations in a deteriorating environment. *Evolution* 66: 3508–3518

Laemmli UK (1970) Cleavage of structural proteins during the assembly of the head of bacteriophage T4. *Nature* 227: 680–685

Lambers H, Chapin FS, Pons TL (2008) *Plant Physiological Ecology.* New York, NY: Springer New York

Lee RE (2018) *Phycology.* Cambridge, New York, Melbourne, Delhi, Singapore: Cambridge University Press

Lewis LA, Lewis PO (2005) Unearthing the molecular phylodiversity of desert soil green algae (Chlorophyta). *Syst Biol* 54: 936–947

Li C-L, Wang M, Wu X-M, Chen D-H, Lv H-J, Shen J-L, Qiao Z, Zhang W (2016) THI1, a Thiamine Thiazole Synthase, Interacts with Ca2+-Dependent Protein Kinase CPK33 and Modulates the S-Type Anion Channels and Stomatal Closure in Arabidopsis. *Plant Physiol* 170: 1090–1104

Li J-Y, Jiang A-L, Zhang W (2007) Salt Stress-induced Programmed Cell Death in Rice Root Tip Cells. *J Integrative Plant Biology* 49: 481–486

Liebthal M, Maynard D, Dietz K-J (2018) Peroxiredoxins and Redox Signaling in Plants. *Antioxid Redox Signal* 28: 609–624

Liu X, Wang Y, Gao H, Xu X (2011) Identification and characterization of genes encoding two novel LEA proteins in Antarctic and temperate strains of Chlorella vulgaris. *Gene* 482: 51–58

Lorenzen H, Hesse M (1974) Synchronous Cultures. In *Algal physiology and biochemistry,* Stewart WDP (ed) pp. 894–908. Oxford: Blackwell

Losh JL, Young JN, Morel FMM (2013) Rubisco is a small fraction of total protein in marine phytoplankton. *New Phytologist* 198: 52–58

Maccarrone M, Bladergroen MR, Rosato N, Finazzi Agrò AF (1995) Role of lipid peroxidation in electroporation-induced cell permeability. *Biochem Biophys Res Commun* 209: 417–425

Machida T, Ishibashi A, Kirino A, Sato J, Kawasaki S, Niimura Y, Honjoh K, Miyamoto T (2012) Chloroplast NADPH-dependent thioredoxin reductase from Chlorella vulgaris alleviates environmental stresses in yeast together with 2-Cys peroxiredoxin. *PLOS ONE* 7: e45988

Mandalam RK, Palsson BO (1995) Chlorella vulgaris (Chlorellaceae) does not secrete autoinhibitors at high cell densities. *American Journal of Botany* 82: 955–963

Marino D, Dunand C, Puppo A, Pauly N (2012) A burst of plant NADPH oxidases. *Trends in Plant Science* 17: 9–15

Martínez JM, Delso C, Aguilar D, Cebrián G, Álvarez I, Raso J (2018a) Factors influencing autolysis of Saccharomyces cerevisiae cells induced by pulsed electric fields. *Food Microbiol* 73: 67–72

Martínez JM, Delso C, Álvarez I, Raso J (2020) Pulsed electric field-assisted extraction of valuable compounds from microorganisms. *Compr Rev Food Sci Food Saf* 19: 530–552

Martínez JM, Delso C, Angulo J, Álvarez I, Raso J (2018b) Pulsed electric field-assisted extraction of carotenoids from fresh biomass of Rhodotorula glutinis. *Innovative Food Science & Emerging Technologies* 47: 421–427

McLuskey K, Mottram JC (2015) Comparative structural analysis of the caspase family with other clan CD cysteine peptidases. *Biochem J* 466: 219–232

Mittler R, Vanderauwera S, Suzuki N, Miller G, Tognetti VB, Vandepoele K, Gollery M, Shulaev V, van Breusegem F (2011) ROS signaling: the new wave? *Trends in Plant Science* 16: 300–309

Morton WM, Ayscough KR, McLaughlin PJ (2000) Latrunculin alters the actin-monomer subunit interface to prevent polymerization. *Nat Cell Biol* 2: 376–378

Nick P (2013) Microtubules, signalling and abiotic stress. *The Plant Journal* 75: 309–323

Nick P (2018) Destroy to create. *Protoplasma* 255: 1–2

Nishimura K, van Wijk KJ (2015) Organization, function and substrates of the essential Clp protease system in plastids. *Biochim Biophys Acta* 1847: 915–930

Notman R, Noro M, O'Malley B, Anwar J (2006) Molecular basis for dimethylsulfoxide (DMSO) action on lipid membranes. *Journal of the American Chemical Society* 128: 13982–13983

Nuñez A, Savary BJ, Foglia TA, Piazza GJ (2002) Purification of lipoxygenase from Chlorella: production of 9- and 13-hydroperoxide derivatives of linoleic acid. *Lipids* 37: 1027–1032

O'Donnell BV, Tew DG, Jones OT, England PJ (1993) Studies on the inhibitory mechanism of iodonium compounds with special reference to neutrophil NADPH oxidase. *Biochem J* 290 (Pt 1): 41–49

Oleskin AV, Botvinko V, Tsavkelova EA (2000) Colonial organization and intercellular communication in microorganisms. *Microbiology* 69: 249–265

Papachristou I, Akaberi S, Silve A, Navarro-López E, Wüstner R, Leber K, Nazarova N, Müller G, Frey W (2021) Analysis of the lipid extraction performance in a cascade process for Scenedesmus almeriensis biorefinery. *Biotechnol Biofuels* 14: 20

Papachristou I, Silve A, Jianu A, Wüstner R, Nazarova N, Müller G, Frey W (2020) Evaluation of pulsed electric fields effect on the microalgae cell mechanical stability through high pressure homogenization. *Algal Research* 47: 101847

Parniakov O, Barba FJ, Grimi N, Marchal L, Jubeau S, Lebovka N, Vorobiev E (2015) Pulsed electric field and pH assisted selective extraction of intracellular components from microalgae Nannochloropsis. *Algal Research* 8: 128–134

Patel A, Mishra S, Pawar R, Ghosh PK (2005) Purification and characterization of C-Phycocyanin from cyanobacterial species of marine and freshwater habitat. *Protein Expr Purif* 40: 248–255

Pauly H, Schwan HP (1959) Über die Impedanz einer Suspension von kugelförmigen Teilchen mit einer Schale. *Zeitschrift für Naturforschung B* 14: 125–131

Pavlin M, Pavselj N, Miklavcic D (2002) Dependence of induced transmembrane potential on cell density, arrangement, and cell position inside a cell system. *IEEE Trans Biomed Eng* 49: 605–612

Petrov V, Hille J, Mueller-Roeber B, Gechev TS (2015) ROS-mediated abiotic stress-induced programmed cell death in plants. *Front Plant Sci* 6

Pratt R, Daniels TC, Eiler JJ, Gunnison JB, Kumler WD, Oneto JF, Strait LA, Spoehr HA, Hardin GJ, Milner HW et al (1944) Chlorellin, an Antibacterial Substance from Chlorella. *Science (Washington):* 351–352

Prevc A, Bedina Zavec A, Cemazar M, Kloboves-Prevodnik V, Stimac M, Todorovic V, Strojan P, Sersa G (2016) Bystander Effect Induced by Electroporation is Possibly Mediated by Microvesicles and Dependent on Pulse Amplitude, Repetition Frequency and Cell Type. *J Membrane Biol* 249: 703–711

Pucihar G, Kotnik T, Teissié J, Miklavčič D (2007) Electropermeabilization of dense cell suspensions. *Eur Biophys J* 36: 173–185

Pulido P, Llamas E, Rodriguez-Concepcion M (2017) Both Hsp70 chaperone and Clp protease plastidial systems are required for protection against oxidative stress. *Plant Signaling & Behavior* 12: e1290039

Ramundo S, Casero D, Mühlhaus T, Hemme D, Sommer F, Crèvecoeur M, Rahire M, Schroda M, Rusch J, Goodenough U et al (2014) Conditional Depletion of the Chlamydomonas Chloroplast ClpP Protease Activates Nuclear Genes Involved in Autophagy and Plastid Protein Quality Control. *Plant Cell* 26: 2201–2222

Reape TJ, Molony EM, McCabe PF (2008) Programmed cell death in plants: distinguishing between different modes. *J Exp Bot* 59: 435–444

Regel RH, Ferris JM, Ganf GG, Brookes JD (2002) Algal esterase activity as a biomeasure of environmental degradation in a freshwater creek. *Aquatic Toxicology* 59: 209–223

Rieder A, Schwartz T, Schön-Hölz K, Marten S-M, Süss J, Gusbeth C, Kohnen W, Swoboda W, Obst U, Frey W (2008) Molecular monitoring of inactivation efficiencies of bacteria during pulsed electric field treatment of clinical wastewater. *Journal of Applied Microbiology* 105: 2035–2045

Rosello Sastre R, Posten C (2010) Die vielfältige Anwendung von Mikroalgen als nachwachsende Rohstoffe. *Chemie Ingenieur Technik* 82: 1925–1939

Roy P, Roy SK, Mitra A, Kulkarni AP (1994) Superoxide generation by lipoxygenase in the presence of NADH and NADPH. *Biochimica et Biophysica Acta (BBA) - Lipids and Lipid Metabolism* 1214: 171–179

Ruzgys P, Barauskaitė N, Novickij V, Novickij J, Šatkauskas S (2021) The Evidence of the Bystander Effect after Bleomycin Electrotransfer and Irreversible Electroporation. *Molecules* 26: 6001

Sack M, Sigler J, Frenzel S, Eing C, Arnold J, Michelberger T, Frey W, Attmann F, Stukenbrock L, Müller G (2010) Research on Industrial-Scale Electroporation Devices Fostering the Extraction of Substances from Biological Tissue. *Food Eng. Rev.* 2: 147–156

Safaei M, Maleki H, Soleimanpour H, Norouzy A, Zahiri HS, Vali H, Noghabi KA (2019) Development of a novel method for the purification of C-phycocyanin pigment from a local cyanobacterial strain Limnothrix sp. NS01 and evaluation of its anticancer properties. *Sci Rep* 9: 1–16

Safi C, Zebib B, Merah O, Pontalier P-Y, Vaca-Garcia C (2014) Morphology, composition, production, processing and applications of Chlorella vulgaris: A review. *Renewable and Sustainable Energy Reviews* 35: 265–278

Saldaña G, Álvarez I, Condón S, Raso J (2014) Microbiological aspects related to the feasibility of PEF technology for food pasteurization. *Critical Reviews in Food Science and Nutrition* 54: 1415–1426

Sangwan V, Orvar BL, Beyerly J, Hirt H, Dhindsa RS (2002) Opposite changes in membrane fluidity mimic cold and heat stress activation of distinct plant MAP kinase pathways. *Plant J* 31: 629–638

Saulis G (2010) Electroporation of Cell Membranes: The Fundamental Effects of Pulsed Electric Fields in Food Processing. *Food Eng. Rev.* 2: 52–73

Saulis G, Satkauskas S, Praneviciūte R (2007) Determination of cell electroporation from the release of intracellular potassium ions. *Anal Biochem* 360: 273–281

Schenk PM, Thomas-Hall SR, Stephens E, Marx UC, Mussgnug JH, Posten C, Kruse O, Hankamer B (2008) Second Generation Biofuels: High-Efficiency Microalgae for Biodiesel Production. *Bioenerg. Res.* 1: 20–43

Scherer D (2019) *Pulsed electric field (PEF)-assisted protein recovery from microalgae biomass for food and feed applications.* Dissertation. Karlsruhe

Scherer D, Krust D, Frey W, Mueller G, Nick P, Gusbeth C (2019) Pulsed electric field (PEF)-assisted protein recovery from Chlorella vulgaris is mediated by an enzymatic process after cell death. *Algal Research* 41: 101536

Senger H, Pfau J, Werthmüller K (1972) Continuous Automatic Cultivation of Homocontinuous and Synchronized Microalgae. In *Methods in cell physiology: Volume V,* Prescott DM (ed) pp. 301–323. New York: Academic Press

Shimogawara K, Fujiwara S, Grossman A, Usuda H (1998) High-efficiency transformation of Chlamydomonas reinhardtii by electroporation. *Genetics* 148: 1821–1828

Sierra LS, Dixon CK, Wilken LR (2017) Enzymatic cell disruption of the microalgae Chlamydomonas reinhardtii for lipid and protein extraction. *Algal Research* 25: 149–159

Silve A, Kian CB, Papachristou I, Kubisch C, Nazarova N, Wüstner R, Leber K, Strässner R, Frey W (2018a) Incubation time after pulsed electric field treatment of microalgae enhances the efficiency of extraction processes and enables the reduction of specific treatment energy. *Bioresour Technol* 269: 179–187

Silve A, Papachristou I, Wüstner R, Sträßner R, Schirmer M, Leber K, Guo B, Interrante L, Posten C, Frey W (2018b) Extraction of lipids from wet microalga Auxenochlorella protothecoides using pulsed electric field treatment and ethanol-hexane blends. *Algal Research* 29: 212–222

Silve A, Poignard C, Sack M, Straessner R, Frey W (2016) Study of Transmembrane Voltage Kinetics during 100 µs Pulse Using Voltage Sensitive Dyes. In *1st World Congress on Electroporation and Pulsed Electric Fields in Biology, Medicine and Food and Environmental Technologies: Portoroz, Slovenia, September 6 -10 2015,* Jarm T (ed) pp. 147–150. Singapore: Springer Singapore Pte. Limited

Simonis P, Kersulis S, Stankevich V, Kaseta V, Lastauskiene E, Stirke A (2017) Caspase dependent apoptosis induced in yeast cells by nanosecond pulsed electric fields. *Bioelectrochemistry* 115: 19–25

Sirisha VL, Sinha M, D'Souza JS (2014) Menadione-induced caspase-dependent programmed cell death in the green chlorophyte Chlamydomonas reinhardtii. *J Phycol* 50: 587–601

Smertenko A, Franklin-Tong VE (2011) Organisation and regulation of the cytoskeleton in plant programmed cell death. *Cell Death Differ* 18: 1263–1270

Swarbreck SM, Colaço R, Davies JM (2013) Plant calcium-permeable channels. *Plant Physiol* 163: 514–522

Takeda H (1993) Taxonomical assignment of chlorococal algae from their cell wall composition. *Phytochemistry* 34: 1053–1055

Tamaki S, Mochida K, Suzuki K (2021) Diverse Biosynthetic Pathways and Protective Functions against Environmental Stress of Antioxidants in Microalgae. *Plants (Basel)* 10: 1250

Tarek M (2020) Molecular Dynamics Simulations of Lipid Membranes Electroporation. In *Electroporation-Based Technologies and Treatments,* Kramar P, Miklavčič D (eds) pp. 73–104

Testerink C, Munnik T (2005) Phosphatidic acid: a multifunctional stress signaling lipid in plants. *Trends in Plant Science* 10: 368–375

Testerink C, Munnik T (2011) Molecular, cellular, and physiological responses to phosphatidic acid formation in plants. *J Exp Bot* 62: 2349–2361

Thompson JR, Register E, Curotto J, Kurtz M, Kelly R (1998) An improved protocol for the preparation of yeast cells for transformation by electroporation. *Yeast* 14: 565–571

Toepfl S, Mathys A, Heinz V, Knorr D (2006) Review: Potential of High Hydrostatic Pressure and Pulsed Electric Fields for Energy Efficient and Environmentally Friendly Food Processing. *Food Reviews International* 22: 405–423

Toyomasu T, Yamane H, Murofushi N, Nick P (1994) Phytochrome inhibits the effectiveness of gibberellins to induce cell elongation in rice. *Planta* 194: 256–263

Usman MG, Rafii MY, Martini MY, Yusuff OA, Ismail MR, Miah G (2017) Molecular analysis of Hsp70 mechanisms in plants and their function in response to stress. *Biotechnol Genet Eng Rev* 33: 26–39

van der Maelen E, Rezaei MN, Struyf N, Proost P, Verstrepen KJ, Courtin CM (2019) Identification of a Wheat Thaumatin-like Protein That Inhibits Saccharomyces cerevisiae. *J Agric Food Chem* 67: 10423–10431

van Doorn WG (2011) Classes of programmed cell death in plants, compared to those in animals. *J Exp Bot* 62: 4749–4761

Vandamme D, Foubert I, Fraeye I, Muylaert K (2012) Influence of organic matter generated by Chlorella vulgaris on five different modes of flocculation. *Bioresour Technol* 124: 508–511

Vavilala SL, Gawde KK, Sinha M, D'Souza JS (2015) Programmed cell death is induced by hydrogen peroxide but not by excessive ionic stress of sodium chloride in the unicellular green alga Chlamydomonas reinhardtii. *European Journal of Phycology* 50: 422–438

Velikova V, Yordanov I, Edreva A (2000) Oxidative stress and some antioxidant systems in acid rain-treated bean plants. *Plant Science* 151: 59–66

Vonshak A (1997) *Spirulina platensis (Arthrospira): Physiology, cell-biology, and biotechnology.* London, Bristol PA: Taylor & Francis

Wang L, Nick P (2017) Cold sensing in grapevine-Which signals are upstream of the microtubular "thermometer". *Plant Cell Environ* 40: 2844–2857

Wang R, Duan D, Metzger C, Zhu X, Riemann M, Pla M, Nick P (2022) Aluminum can activate grapevine defense through actin remodeling. *Hortic Res* 9

Weaver JC, Chizmadzhev Y (1996) Theory of electroporation: A review. *Bioelectrochemistry and Bioenergetics* 41: 135–160

Wheeler GL, Brownlee C (2008) Ca2+ signalling in plants and green algae--changing channels. *Trends in Plant Science* 13: 506–514

Yamamoto M, Fujishita M, Hirata A, Kawano S (2004) Regeneration and maturation of daughter cell walls in the autospore-forming green alga Chlorella vulgaris (Chlorophyta, Trebouxiophyceae). *J Plant Res* 117: 257–264

Yordanova ZP, Woltering EJ, Kapchina-Toteva VM, Iakimova ET (2013) Mastoparan-induced programmed cell death in the unicellular alga Chlamydomonas reinhardtii. *Ann Bot* 111: 191–205

Yoshikawa N, Belay A (2008) Single-Laboratory Validation of a Method for the Determination of c-Phycocyanin and Allophycocyanin in Spirulina (Arthrospira) Supplements and Raw Materials by Spectrophotometry. *J AOAC Int* 91: 524–529

Zhang Q, Barbosa-Cánovas GV, Swanson BG (1995) Engineering aspects of pulsed electric field pasteurization. *Journal of Food Engineering* 25: 261–281

Zhang Y, Zhu H, Zhang Q, Li M, Yan M, Wang R, Wang L, Welti R, Zhang W, Wang X (2009) Phospholipase dalpha1 and phosphatidic acid regulate NADPH oxidase activity and production of reactive oxygen species in ABA-mediated stomatal closure in Arabidopsis. *Plant Cell* 21: 2357–2377

Zuo Z, Zhu Y, Bai Y, Wang Y (2012) Acetic acid-induced programmed cell death and release of volatile organic compounds in Chlamydomonas reinhardtii. *Plant Physiol Biochem* 51: 175–184

Zuppini A, Gerotto C, Baldan B (2010) Programmed cell death and adaptation: two different types of abiotic stress response in a unicellular chlorophyte. *Plant Cell Physiol* 51: 884–895

Zuppini A, Gerotto C, Moscatiello R, Bergantino E, Baldan B (2009) Chlorella saccharophila cytochrome f and its involvement in the heat shock response. *J Exp Bot* 60: 4189–4200

Acknowledgments

Ich möchte mich zuerst bei meinem Betreuer am IHM, Christian Gusbeth, bedanken. Vielen Dank für deine anhaltende Unterstützung bei der praktischen Durchführung der Experimente, für die angeregten Diskussionen und zuletzt für die Korrektur meiner Thesis. Vielen Dank auch an das ganze Team Bioelektrik: Daniel, Sahar, Ioannis, Rüdiger, Natalja, Ralf, Wolfgang und Aude!

Ein großes Dankeschön geht auch an meine Professoren Georg Müller am IHM und Peter Nick in der Botanik. Vielen Dank, dass ihr den Rahmen geschaffen habt, der meine Arbeit ermöglicht hat.

Zuletzt möchte ich natürlich auch meinem persönlichen Umfeld danken: meinem Freund Simon und meiner Familie, die mich alle bei jedem Schritt stets unterstützt haben. Danke auch an Maike, die noch bis in die Nacht diese Arbeit auf Sprache korrigiert hat. Ihr seid die Besten!